Delayed bilateral teleoperation : a direct force-reflecting control approach

Delayed bilateral teleoperation

A direct force-reflecting control approach

Dennis Heck

The research reported in this thesis is part of the research program of the Dutch Institute of Systems and Control (DISC). The author has successfully completed the educational program of the Graduate School DISC.

This research is supported by the Dutch Technology Foundation STW, which is part of the Netherlands Organisation for Scientific Research (NWO) and partly funded by the Ministry of Economic Affairs (project number 12157).

The research was performed at Eindhoven University of Technology.

A catalogue record is available from the Eindhoven University of Technology Library.
ISBN: 978-90-386-3900-0

Printed by CPI - Koninklijke Wöhrmann, Zutphen, the Netherlands.

Delayed bilateral teleoperation
A direct force-reflecting control approach

PROEFSCHRIFT

ter verkrijging van de graad van doctor aan de
Technische Universiteit Eindhoven, op gezag van de
rector magnificus prof.dr.ir. F.P.T. Baaijens, voor een
commissie aangewezen door het College voor
Promoties, in het openbaar te verdedigen
op dinsdag 15 september 2015 om 16.00 uur

door

Dennis Johannes Franciscus Heck

geboren te Roosendaal

Dit proefschrift is goedgekeurd door de promotoren en de samenstelling van de promotiecommissie is als volgt:

voorzitter:	prof.dr. L.P.H. de Goey
1^{e} promotor:	prof.dr. H. Nijmeijer
copromotor:	dr.ir. A. Saccon
leden:	prof.dr.ir. W.P.M.H Heemels
	dr. R. Carloni (Universiteit Twente)
	prof.dr. F.C.T. van der Helm (Technische Universiteit Delft)
	prof. C. Melchiorri (Università di Bologna)
adviseur:	dr.ir. C.J.M. Heemskerk

Abstract

This thesis focusses on the design of control architectures for bilateral teleoperators interacting with a stiff environment, while the communication suffers from delays. In bilateral teleoperation, a human operator interacts with a haptic master device to operate a slave device inside a remote environment. The controller creates an artificial bilateral coupling between the master and slave device, such that the operator is presented with force information regarding the slave-environment interaction. A high quality of this haptic feedback is important to obtain good telepresence, but with existing control architectures the performance is not always satisfactory. Typically, the reflected environment is perceived too soft and in free motion a high physical operator effort is required, thereby making the teleoperator rather heavy to operate. To improve the quality of the haptic feedback, the following contributions are presented in this thesis.

The first contribution is the identification of the controller structure to achieve high-performance delayed bilateral teleoperation. It is observed that the majority of existing control architectures can be classified as either bilateral motion synchronization or direct force-reflection. In bilateral motion synchronization, both the master and slave controller synchronize the motion of the two devices. In contrast, only the slave controller is used for motion synchronization in direct force-reflection architectures, while the master controller reflects the slave-environment contact force directly. It is shown experimentally that the performance (in terms of motion synchronization and operator effort in free motion, and stiffness reflection in contact) of direct force-reflection architectures, especially with a Position/Force-Force controller, is less sensitive to delays. Therefore, a direct force-reflection-based architecture should be designed to obtain high performance bilateral teleoperators in the presence of delays.

The second contribution is related to the stability of the local slave-environment interaction. A common problem in both teleoperation and single manipulator

control is that after the impact the manipulator bounces back from the stiff environment. To guarantee a stable local interaction between the slave manipulator and the stiff environment, a novel analysis tool is developed to evaluate stability of the switched system, consisting of the environment, slave and its controller, while tracking arbitrary motion- and force profiles coming from the master system. With this tool, guidelines are derived to achieve exponentially stable impacts (the amplitude of the bouncing decreases exponentially over time), or even impacts without bounces. For a rigid slave impacting a stiff environment, these guidelines suggest that the controller should implement a considerable (and often unrealistic) amount of damping, resulting in inferior tracking performance. Therefore, the design of a compliant slave, created for instance by including a compliant wrist, is considered. Together with a model reduction technique of the compliant slave dynamics, the tool designed for the rigid slave is used to provide guidelines for both the controller parameters and compliant wrist design. In this way, the impact of the slave with the environment can occur without bounces, independently of the operator's input or communication delays.

The final contribution is the introduction of an energy-based controller to optimize the achievable performance of direct force-reflecting architectures. When using a direct force-reflecting architecture in the presence of delays, the master might recoil violently when the slave makes contact with the environment. Since this recoiling is accompanied with active behavior of the teleoperator, a novel energy-based architecture is designed to enforce passivity of the teleoperator from the operator and environment perspective. The controller is structured with an outer layer, called the performance layer, and an inner layer, called the passivity layer. In the performance layer, in principle any controller can be implemented to obtain high performance. In the passivity layer, the output of the performance layer is modified and a variable amount of damping is injected via an innovative logic that follows a principle of energy duplication (following the direct force-reflection philosophy) and takes into account the effects of the delays. Passivity of the teleoperator is formally proven and the tuning of the control parameters is elaborately discussed. Using a Position/Force-Force architecture in the performance layer, the effectiveness of the proposed controller to obtain low operator effort and high transparency, while making and breaking contact with a static and stiff environment, is demonstrated experimentally for a challenging round-trip communication delay of 100 ms.

Samenvatting

Dit proefschrift beschouwt het ontwerp van een regelaar voor een bilaterale teleoperator die contact maakt met harde objecten en waarbij de communicatie onderhevig is aan tijdsvertragingen. In bilaterale teleoperatie beweegt de operator (gebruiker) een haptisch master systeem, bijvoorbeeld een joystick, om de slave in een op afstand gelegen omgeving aan te sturen. Daarnaast wordt de interactiekracht tussen de slave en de omgeving door de regelaar teruggekoppeld naar de master om zo de operator het gevoel te geven zelf aanwezig te zijn in de omgeving van de slave. Een hoge kwaliteit van de teruggekoppelde kracht is noodzakelijk, maar met de huidige regelaars is de kwaliteit niet altijd voldoende. Vaak voelt de teruggekoppelde omgeving te zacht aan en is de master nogal zwaar, waardoor de operator een significante krachtsinspanning moet leveren om de master te bewegen. Daarom is in dit proefschrift onderzoek gedaan naar het verbeteren van de kwaliteit van de haptische terugkoppeling wanneer de communicatie onderhevig is aan tijdsvertragingen.

Allereerst is de meest geschikte structuur van een regelaar geïdentificeerd om met een bilaterale teleoperator, met tijdsvertragingen in de communicatie, hoogwaardige prestaties te verkrijgen. Het merendeel van de bestaande regelaars kan worden geclassificeerd als bilaterale bewegingssynchronisatie of directe krachtterugkoppeling. In bilaterale bewegingssynchronisatie dragen zowel de master- als slave regelaar bij aan de bewegingssynchronisatie van de twee systemen. Daarentegen wordt in regelaars met directe krachtterugkoppeling alleen de slave regelaar gebruikt voor bewegingssynchronisatie, terwijl de master regelaar de krachten van de interactie tussen de slave en omgeving direct terugkoppelt naar de operator. Door middel van experimenten zijn de prestaties van de verschillende regelaars geanalyseerd in termen van bewegingssynchronisatie en kracht geleverd door de operator gedurende een vrije beweging van de slave, en de teruggekoppelde stijfheid gedurende contact tussen de slave en de omgeving. Er is aangetoond dat de prestaties van directe kracht-terugkoppelende regelaars, en

vooral van een Positie/Kracht-Kracht regelaar, minder gevoelig zijn voor verandering in de tijdsvertraging. Daarom zou voor een bilaterale teleoperator met tijdsvertragingen in de communicatie een directe kracht-terugkoppelende regelaar ontworpen moeten worden om hoogwaardige prestaties te verkrijgen.

Ten tweede is de stabiliteit van de lokale interactie tussen de slave en de omgeving onderzocht. Een gemeenschappelijk probleem in zowel teleoperatie als bij het regelen van een enkele robotarm is dat na de botsing (impact) de slave of robotarm terug stuitert van de harde omgeving. Om een stabiele lokale interactie van de slave en de harde omgeving te garanderen, is er een nieuwe techniek ontwikkeld om stabiliteit van het geschakelde (switched) systeem te evalueren, terwijl er een willekeurig tijdsvarieërend referentie signaal gevolgd wordt. Het geschakelde systeem bestaat uit de omgeving, slave en regelaar, en het tijdsvarieërend referentie signaal wordt gegenereerd door de operator. Met deze techniek zijn vervolgens vuistregels afgeleid om exponentiële stabiliteit van de botsing (de amplitude van het stuiteren neemt exponentieel af over de tijd), en zelfs botsingen zonder terugstuiteren van de slave te garanderen. Voor een niet-flexibele slave is volgens deze vuistregels een aanzienlijke (en vaak onrealistische) hoeveelheid demping van de regelaar nodig om stabiele botsingen te garanderen. De vereiste demping zorgt voor een verminderd volggedrag van het referentie signaal. Daarom is naast de niet-flexibele slave ook een slave geanalyseerd met flexibiliteit, bijvoorbeeld mechanisch aangebracht in de pols van de robotarm. Een model reductie van de dynamica van de flexibele slave is gecombineerd met de ontwikkelde techniek voor de niet-flexibele slave. Hieruit zijn vuistregels afgeleid voor zowel de regelaar als het ontwerp van de flexibiliteit. Door het toepassen van deze vuistregels is het mogelijk om een willekeurig tijdsvariërend bewegings- en krachtsignaal te volgen, terwijl een botsing zonder terugstuiteren van de slave is gegarandeerd, onafhankelijk van de tijdsvertragingen of het door de operator gegenereerde referentie signaal.

Tenslotte is er een energie-gebaseerde regelaar geïntroduceerd, waarmee de te behalen prestaties van directe kracht-terugkoppelende regelaars geoptimaliseerd kan worden. Met tijdsvertragingen in de communicatie is een veelvoorkomend probleem van directe kracht-terugkoppelende regelaars dat de master hevig kan terugslaan nadat de slave contact heeft gemaakt met de harde omgeving. Deze terugslag gaat gepaard met actief gedrag van de teleoperator. Daarom is er een nieuwe energie-gebaseerde regelaar ontworpen om, vanuit het perspectief van de operator en de omgeving, passiviteit van de teleoperator af te dwingen. De regelaar is opgebouwd uit een buitenste laag, de prestatie-laag, en een binnenste laag, de passiviteits-laag. In de prestatie-laag kan in principe elke regelaar worden geïmplementeerd om de gewenste hoogwaardige prestaties te verkrijgen. In de passiviteits-laag wordt de output van de prestatie-laag aangepast en wordt er een variabele hoeveelheid demping toegevoegd. Hierdoor wordt passiviteit van

de teleoperator gegarandeerd, zelfs als er tijdsvertragingen in de communicatie aanwezig zijn. Volgens het principe van directe krachtterugkoppeling geschiedt de aanpassing van de output en de demping volgens een innovatieve logica volgend uit het dupliceren van energie. Passiviteit van de geregelde teleoperator is formeel bewezen en het tunen van de parameters van de regelaar is uitvoerig besproken. Voor een 100 ms gecombineerde vertraging van master naar slave en vice versa is, met een Positie/Kracht-Kracht regelaar in de prestatie-laag, experimenteel aangetoond dat met de nieuwe regelaar zowel een hoogwaardige krachtterugkoppeling als een makkelijk te bewegen teleoperator verkregen kan worden.

Societal Summary

To minimize health risks, maintenance in nuclear fusion or space applications is often performed remotely using a teleoperator. The teleoperator consists of a local interface, e.g. a joystick, called the master device, and a robotic manipulator, called the slave device, inside the hazardous remote environment. The human operator commands the slave via the master device and a control architecture makes the slave follow the master. Furthermore, the forces exerted by the slave on the environment are measured and reflected to the operator, via the master, to make him/her aware of the remote operation. Due to the resulting bi-directional information exchange, such a system is called a bilateral teleoperator.

If the master and slave sides are physically separated over a large distance, the information exchange suffers from communication delays. These delays affect the quality of the haptic feedback. Typically, the environment is perceived too soft, a high physical effort is required to operate the teleoperator, and the slave might bounce back from the environment.

In this PhD thesis, using a novel technique to analyze the slave-environment interaction, guidelines are presented for the controller and slave design to prevent that the slave bounces back from the environment after making contact. Furthermore, a novel control architecture is introduced for bilateral teleoperators subject to communication delays to obtain high-performance force feedback, while requiring low physical effort from the operator. Both solutions improve the performance of bilateral teleoperators. Ultimately, this could lead to reduced maintenance times, the prevention of damage of the slave and/or environment, and a reduction of the maintenance costs.

Contents

Nomenclature

Notation

In this thesis, the subscript $i \in \{m, s\}$ is used to indicate the master or slave device and $j \in \{m, s\}$ is used to indicate the other device, so that $j \neq i$, i.e. $j = s$ if $i = m$ or $j = m$ if $i = s$. For the sake of brevity, the explicit mention of time dependency is omitted, so a given signal x should be interpreted as $x(t)$. Furthermore, the notation x^T is used to denote the delayed version of x, so x^T should be interpreted as $x(t - T)$. The dependency of an integrand on the integration variable is usually omitted and, e.g., $\int_{t_0}^{t_1} x d\tau$ is used in place of $\int_{t_0}^{t_1} x(\tau) d\tau$.

Abbreviations

4C	4-channel architecture
BEP	Bounded Environment Passivity
DOF	Degree of Freedom
GUAS	Global Uniform Asymptotic Stability
GUES	Global Uniform Exponential Stability
HSC	Haptic Shared Control
ISS	Input-to-State Stable
LMI	Linear Matrix Inequality
LTI	Linear Time Invariant
P-F	Position-Force architecture
P-P	Position-Position architecture
PaL	Passivity Layer
PC	Passivity Controller
PDd	Proportional-derivative plus damping controller
Pd	Proportional plus damping controller

PeL	Performance Layer
PF-F	Position/Force-Force architecture
PO	Passivity Observer
RMS	Root Mean Square
TDPC	Time Domain Passivity Controller
TL	Transparency Layer
TLC	Tank Level Controller
W	Wave variable architecture
Wt	Wave variable architecture with position tracking

Letters and symbols

Symbol	**Description**	**Unit**
b	Viscous friction coefficient	
b_e	Damping coefficient environment	
$\hat{b}_e$	Estimated damping coefficient environment	
b_f	Damping coefficient force controller	Ns/m
b_h	Damping of human operator	
b_t	Damping of manipulator-tip connection	Ns/m
b_w	Characteristic wave impedance	
$f_i(q_i, \dot{q}_i)$	Joint space (nonlinear) friction vector	
$\bar{f}_i(x_i, \dot{x}_i)$	Cartesian space (nonlinear) friction vector	
$g_i(q_i)$	Gravity vector in joint space	
$\bar{g}_i(x_i)$	Gravity vector in Cartesian space	
k_{di}	Derivative gain in motion controller	
k_e	Stiffness of environment	
$\hat{k}_e$	Estimated stiffness of environment	
k_f	Proportional gain force controller	-
k_h	Stiffness of human operator	
k_{pi}	Proportional gain in motion controller	
k_t	Stiffness of manipulator-tip connection	N/m
m_h	Acceleration feedforward gain in operator model	
q_i	Degrees of freedom in the joint space	
t	Time	s
u_i	Wave variable from master to slave	$\sqrt{\text{W}}$
v	Eigenvector	
v_i	Wave variable from slave to master	$\sqrt{\text{W}}$
$w_f(t)$	Bounded perturbation	
x_i	End-effector degrees of freedom in Cartesian space	
$\overline{\dot{x}}_i$	Upper bound norm $\dot{x}_i$	m/s
z	Motion tracking error	

Symbol	Description	Unit
A_i	System matrix	
B_i	Local damping gain	
$C_i(q_i, \dot{q}_i)$	Coriolis' matrix in joint space	
$\bar{C}_i(x_i, \dot{x}_i)$	Coriolis' matrix in Cartesian space	
E_i	Energy of device i	J
E_{comm}	Total energy in communication channel	J
$E_{e,comm}$	Environment energy in communication channel	J
$E_{h,comm}$	Operator energy in communication channel	J
$E_{i,b\#}$	Constant energy level, $\# \in \{1, 2, 3\}$	J
$E_{i,bal}$	Total energy balance controller	J
$\underline{E}_{i,bal}$	Lower bound $E_{i,bal}$, measurable online	J
$E_{i,diff}$	Energy difference controller	J
$E_{i,harv}$	Energy to be harvested	J
F_e	Slave-environment interaction force	N
$\overline{F}_e$	Upper bound norm F_e	N
F_h	Operator-master interaction force	N
$\overline{F}_h$	Upper bound norm F_h	N
F_{ic}	Cartesian space control force/torque	
F_{ic}^*	Control force/torque of Passivity Layer	
$F_{i,harv}$	Harvesting force	N
$F_{i,rec}$	Recovery force	N
I	Identity matrix	
$J_i(q_i)$	Geometric manipulator Jacobian	
$LP(s)$	Lowpass filter	
M	Manipulator mass	kg
M_a	Estimated manipulator mass used for feedforward	kg
$M_i(q_i)$	Inertia matrix in joint space	
$\bar{M}_i(x_i)$	Inertia matrix in Cartesian space	
M_t	Mass of manipulator tip	kg
P	Power	W
P_{diss}	Dissipated power in Passivity Layer	W
P_e	Power exchange slave and environment	W
P_h	Power exchange operator and master	W
P_{ic}	Power exchange controller and device i	W
$P_{i,gen}$	Generated power	W
$\mathbb{R}$	Space containing real numbers	
$\mathcal{S}_1$	Free motion subspace of Σ^w	
$\mathcal{S}_2$	Contact subspace of Σ^w	
$\mathcal{T}_\#$	Time interval, $\# \in \{1, 2, 3, 4\}$	s

Symbol	Description	Unit
T_i	Communication delay	s
T_r	Round-trip communication delay	s
T_{samp}	Sampling time	s
V	Storage function or functional	
$\underline{V}$	Lower bound V	
α_i	Constant parameter appearing in $P_{i,diss}$	s^{-1}
β_i	Constant parameter appearing in $F_{i,harv}$	
γ_i	Constant parameter appearing in $F_{i,rec}$	
ε	Small constant	
λ_i	State-dependent variable gain between 0 and 1	-
μ_1	Motion scaling gain	
μ_2	Force scaling gain	
ν_i	Largest eigenvalue of $\bar{M}_i(x_i)$	
$\sigma(t)$	Switching sequence	
τ_e	Torque applied by slave on environment	Nm
τ_h	Torque applied by operator on master	Nm
$\tau_{h,RMS}$	RMS value operator effort	Nm
τ_{ic}	Joint space control force/torque	
τ_{id}	Force/torque used in wave transformations	
Δq_{RMS}	RMS value motion tracking error $q_m - q_s$	rad
$\Delta q_{RMS}^{T_m}$	RMS value motion tracking error $q_m^{T_m} - q_s$	rad
$\Delta\tau_{RMS}$	RMS value force tracking error	Nm
$\Delta\tau_{RMS,ss}$	RMS value force tracking error during steady-state	Nm
ΔS_{RMS}	RMS value stiffness reflection	Nm/rad
$\Delta S_{RMS,ss}$	RMS value stiffness reflection during steady-state	Nm/rad
Φ	State transition matrix	
$\Omega_1(t)$	Free motion subspace	
$\Omega_2(t)$	Contact subspace	
Σ^p	Perturbed switched system	
Σ^u	Unperturbed switched system	
Σ^w	Unperturbed system under worst-case switching	

Subscripts and superscripts

Symbol	Description
b	Bound
bal	Balance
com	Communication channel

Symbol	**Description**
d	Desired
$diff$	Difference
$diss$	Dissipated
e	Environment
gen	Generated
h	Human operator
$harv$	Harvested
l	Number of joint degrees of freedom
m	Master
n	Number of end-effector degrees of freedom
p	Perturbed
rec	Recovery
s	Slave
t	Tip
u	Unperturbed
w	Worst-case

Chapter 1

Introduction

1.1 Teleoperation

The word *teleoperation* literally means *operation at a distance*. By performing operations remotely, a teleoperator allows humans to safely and accurately perform critical tasks in otherwise inaccessible environments. The human operator uses a local interface, called the *master*, to command a robotic device, called the *slave*, inside the remote environment. Typical examples of teleoperators are depicted in Fig. 1.1. For instance, by commanding a robotic slave device inside a hot and radioactive nuclear reactor, an operator can perform the maintenance remotely without health risks. With a mobile teleoperator to dismantle explosives or to explore unknown areas, even in space, otherwise dangerous tasks can be executed safely by the human operator. Telerobotics can even be found in hospitals, where in minimally invasive surgery the knowledge of a surgeon to perform delicate operations is combined with the precision of robotic devices.

In all these applications, the human operator communicates his or her decisions via the local interface. At the remote side, the slave then executes the task set by the operator. In essence, the brain is separated from the body. Due to the unique combination of human skills to adapt to unknown and unstructured environments with the high precision that can safely be achieved with robotic devices, teleoperation has become a thriving research topic over the past decades.

1.1.1 Teleoperation and force feedback

One of the first teleoperators was designed by Goertz in the 1950s for radioactive material handling. The teleoperator was electrical and used on-off switches to

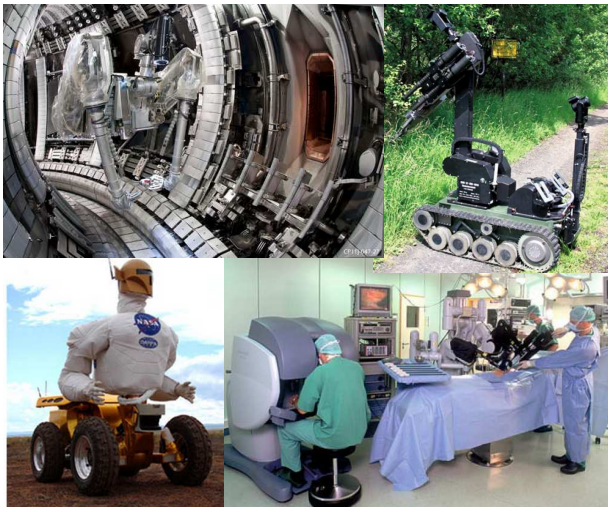

Fig. 1.1. Examples of teleoperators. From top left to bottom right: Maintenance in the Joint European Torus (JET) nuclear fusion reactor (picture taken from [57]); The telerobotic system tEODor for disarming explosives (picture taken from [122], Chapter 31); Robonaut, by NASA and DARPA, attached to Centaur 1 for surface exploration (picture taken from [86]); The da Vinci telerobotic system by Intuitive Surgical Inc. used in minimally invasive surgery (picture taken from [122], Chapter 31).

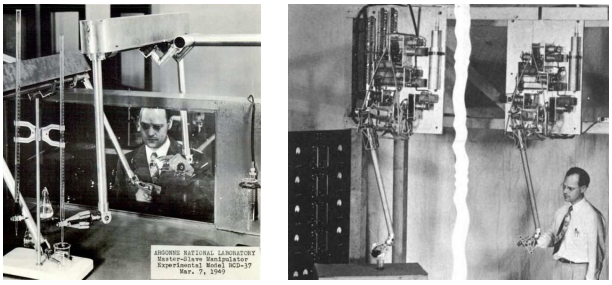

Fig. 1.2. Early bilateral teleoperators. Left: Mechanical master-slave teleoperator by Goertz (patent 1949). Right: The ANL Model E1: The first electric bilateral teleoperator by Goertz and Thompson (1954). Pictures taken from [38]

actuate various degrees of freedom of the slave. This device was slow and somewhat awkward to operate [90]. Therefore, Goertz build a mechanically linked master-slave system [45] (see Fig. 1.2) and observed that the bilaterally transmitted forces and vibrations improved the perception and task execution. The mechanical coupling limited the distance between the operator and environment and, initially, required kinematically identical devices. Goertz realized the value of an electrically coupled teleoperator to circumvent these issues. By combining force reflection with the electrically actuated teleoperator [46], he laid the foundations of modern bilateral teleoperation.

Since the 1980s, together with the increase in computational power, also control theory started to develop bilateral teleoperation. The main goal in the control design became to make the teleoperator transparant by mimicking the haptic sensation of directly performing the task. Achieving optimal transparency turned out to be very difficult due to the bilateral coupling of two nonlinear mechatronic devices, which often have different kinematics, inertia and degrees of freedom. These devices typically suffer from imperfections like measurement noise, encoder quantization, finite sampling time and nonlinear friction. On top of that, the human arm dynamics are nonlinear and time-varying. In combination with the transitions of the slave between free motion and contact with the uncertain and possibly stiff environment, the initial focus was on analyzing and proving stability using techniques from, e.g., passivity-, Lyapunov- or linear system theory. Only during the last two decades, the focus shifted more towards achieving acceptable performance.

1.1.2 Communication delays

One of the main advantages of the physical separation of the operator input from the task execution is that the distance between the local and remote side can be increased. Unfortunately, increasing the distance also leads to delays in the communication between both sides. These delays affect the closed-loop stability of teleoperator due to the bilateral coupling between the master and slave. To cope with the delays the first attempts in the 1960s were based on supervisory control, where only high-level commands were sent to the slave. Force feedback was absent. It was not until the late 1980s and early 1990s that engineers applied network- and transmission line theory to solve the stability issue in delayed bilateral teleoperation [10, 91]. Since then, fueled by the internet as a communication medium, the amount of publications addressing delayed bilateral teleoperation exploded.

Although some major improvements have been made over the years, control engineers are still struggling with the trade-off between stability and performance. Designing a high-performance teleoperator is even more challenging when the closed-loop response is affected by communication delays. To illustrate a typical problem, consider an example where the master and slave are controlled

to follow the (delayed) motion of the other device. Suppose that the slave is unobstructed by the environment and the operator starts to move the master. It takes a delay T_m from the master side to the slave side before the slave starts to follow the motion of the master. In turn, the response of the slave is reflected to the master with a delay T_s from the slave to the master side. This delayed slave response is used by the controller of the master to create force feedback. Hence, the action of the operator and reaction of the master controller are not applied simultaneously. The round-trip delay $T_m + T_s$ between the action and reaction could easily lead to instability, e.g., due to an out-of-phase motion of the master and slave device.

The stability issue described above would not exist if no force is reflected when the slave is in free motion. Using only force feedback when the slave is in contact with the environment solves the instability in free motion, but it shifts the problem to the contact phase. Once the master is moved past the virtual location of the environment, it takes a round-trip delay before the slave-environment impact force is reflected to the operator. As a result, the operator could move the master virtually inside the environment. If the slave is controlled to follow the master position, the slave controller builds up the slave-environment interaction force. In many cases, this force is too large for the operator to handle, the master recoils and the operator cannot keep the slave in contact with the environment. Although, in this example, the teleoperator is not necessarily unstable, it remains a challenge to prevent a recoiling of the master and provide good force feedback at the same time.

1.1.3 Performance

Many solutions have been proposed to stabilize the teleoperator in the presence of delays (see, e.g., [11, 55, 94, 105]), but there is still room to improve the accompanying performance. The main reason why the majority of the existing literature primarily focuses on stability is the diversity of destabilizing factors in a teleoperator. Apart from the delays, the control architectures must be robust for changing operator impedance (stiffness, damping, and inertia properties, possibly time-varying), the switch in the dynamics between free motion and contact with a possibly stiff environment and other disturbances typically present in mechatronic devices, such as friction and drive train flexibility. Including all these factors in the analysis to guarantee stability for even a worst-case operator input leads to a massive control problem. A typical approach to reduce the complexity is to overapproximate the different uncertainties, at the cost of obtaining conservative stability results. An example is to consider all teleoperator components independently and enforce passivity of all individual elements. The analysis becomes manageable, but the introduced conservatism typically leads to high levels of local damping injection [96] or a significant reduction of the coupling strength between the master and slave [65, 139].

An interesting challenge in obtaining high-performance teleoperators is that there does not exist a unique measure to quantify performance. The general believe is that good task performance will follow directly if a realistic haptic sensation is created by making the teleoperator transparent, i.e. by matching the master and slave positions and the forces applied by the operator and environment on the teleoperator [69]. In the absence of alternatives, performance metrics like transparency are often translated directly from the delay-free to the delayed case. However, creating, e.g., the highly transparent teleoperator of the delay-free case is in general not possible in the presence of delays. Trying to do so typically leads to high efforts to operate the device. Should the controllers then purely be designed to achieve transparency? A basic level of transparency might still be favorable, but achieving optimal transparency seems pointless. Hence, already in the design of a teleoperator with high performance, other performance criteria, like operator effort, should be included.

Once it is clear how to quantify performance, another interesting question is how to obtain it. Clearly, not every controller is affected by the delay in the same way. For instance, the examples of the previous section illustrate that the delay affects the free motion phase in only one of the two controllers. Apart from a few approaches like model-mediated teleoperation [81], the general approach in control design for delayed bilateral teleoperation is to take a controller that was originally designed to yield sufficient performance in the delay-free case. If, consequently, concessions must be made to guarantee stability in the delayed case, the intended performance is lost. It is better to design a controller specifically for the delayed teleoperator. But in order to do so, a clear understanding is required on how certain properties or characteristics of a controller affect the performance metrics *as a function of the delay.* Such a valuable comparison is missing in the literature. Only a few articles, like [11], address this issue theoretically, but with all imperfections of mechatronic devices, it is at the least questionable if the theoretical performance can be achieved in practice.

1.2 Motivation and objectives

In remote handling applications for the International Thermonuclear Experimental Reactor (ITER), or in search and rescue operations, a high performance bilateral teleoperator is required to perform remote operations accurately and fast. Existing control architectures designed for delayed bilateral teleoperation provide a reasonable performance, but there is still room for improvement. For example, depending on the size of the delay, the haptic feedback is characterized by a heavy teleoperator and/or a spongy feeling of the hard environment. Such a distortion of the perception is undesired as it could affect the accuracy of the operations and an increase in the task completion time. Therefore, this thesis focuses on the design of a high performance control architecture for delayed bilateral teleoperation. The research objective can be summarized as follows.

Develop and experimentally validate a control architecture for bilateral teleoperation with communication delays, trading off stability and performance, but paying particular attention to low physical operator effort and high transparency when interacting with a stiff environment.

In order to obtain this high performance teleoperator, the research objective is split in stability- and performance-related objectives. However, instead of focussing on stability first and then optimizing for performance, the order is reversed: First the focus is on obtaining high performance and then on achieving stability.

Performance-related objectives

Regarding performance, the first objectives involve the analysis of current architectures to identify bottlenecks in achieving high performance. Consequently, a performance-optimized architecture could be obtained by combining the benefits of several controllers and eliminating their drawbacks. The performance-based objectives are:

1. Identify how existing controllers, and methods to analyze stability, affect the performance that can theoretically be achieved.

2. Identify, as a function of the delay, how specific components of the control architectures affect the performance that can be achieved in practice.

From these objectives, the structure of a control architecture to achieve high performance can be identified.

Stability-related objectives

After the identification of a high performance control architecture, the next step is to guarantee stability, without compromising the achievable performance. This requires a nonconservative analysis method to combine the required stability with the desired high performance. To this end, the stability of the slave-environment interaction is considered separately from the stability of the bilateral connection. The stability-based objectives are:

3. Guarantee stability of the interaction between the slave and the stiff environment, independent of the input coming from the operator.

4. Design a control architecture and analysis method to achieve a stable bilateral teleoperator with high performance.

1.3 Contributions

The main contributions presented in this thesis are the following:

- *A proposed paradigm shift in delayed bilateral teleoperation controller design* – The first contribution is the explicit mention that in the research literature (as well as in common practice) there are two design philosophies to control bilateral teleoperators with delays. Those philosophies are referred to as *bilateral motion synchronization* and *direct force reflection*. The common approach in the literature is to design a bilateral motion synchronizing architecture, but, instead, this thesis focuses on direct force-reflecting controller designs to achieve high transparency and low operator effort. The motivation is given below.

  In the literature, the majority of the approaches treat the delayed case as an extension of the delay-free teleoperator. Supported by the favorable properties of, e.g., passivity theory to analyze stability, most architectures use virtual springs and dampers to create a mechanical coupling between the master and slave. Since both controllers synchronize the motion of the master and slave, these architectures are denoted as bilateral motion synchronizing controllers. A strong coupling is required to synchronize the motion of the master and slave, but such a connection is highly sensible to delays. Stability can only be guaranteed by reducing the coupling strength or using high damping gains. Both solutions contribute to a softer perception of the environment and, in free motion, the operator requires high effort to move the teleoperator.

  Therefore, a shift in the design philosophy is advised if the bilateral communication is subject to delays. Unlike bilateral motion synchronization, the slave controller should be tasked with tracking of the motion of the master device and the master controller should reflect the environment to the operator. These architectures are termed *direct force-reflection* controllers. The slave controller mimics the operator and the master controller mimics the environment. The bilateral teleoperation control problem, and the difference between bilateral motion synchronization and direct force-reflection are illustrated in Fig. 1.3. With both types of architectures, a similar performance can be achieved if delays are not present. However, the analysis and experimental work presented in this thesis suggest that, from a performance perspective, direct force-reflection architectures are more robust to delays and could potentially result in lower operator efforts and higher transparency. Therefore, the use of a direct force-reflection philosophy is strongly recommended to design high performance bilateral controllers for delayed teleoperation.

- *Novel experimental performance comparison* – A novel experimental design is developed to directly compare several existing bilateral motion synchro-

(a) Control problem: How to connect the tool of the operator (master) with the tool (slave) in the remote environment?

(b) Bilateral motion synchronization: the environment is reflected to the operator by a stiff master-slave connection.

(c) Direct force-reflection: the slave controller mimics the operator and the master controller represents a copy of the environment.

Fig. 1.3. The bilateral teleoperation control problem depicted in (a) and the two controller design philosophies shown in (b) and (c).

nizing and direct force-reflecting architectures on the achievable performance. To make the comparison fair and repeatable, a virtual human operator is used. Clear quantitative performance metrics are designed to capture the motion tracking accuracy, the quality of the force reflection and stiffness perception, and the physical operator effort. Using this comparison, the most favorable controller structure is identified to achieve high performance in terms of the considered metrics. By performing the comparison experimentally, the performance during dynamic and static tasks in both free motion and contact is identified under realistic operating conditions. This makes the obtained results highly representative for a broad range of maintenance operations.

- *Novel stability method for the slave-environment interaction* – For the interaction of a single manipulator with a stiff environment, a novel method is designed to analyze stability, while tracking a time-varying hybrid motion-force trajectory. The focus is on the one degree-of-freedom contact case. Sufficient conditions are presented to guarantee input-to-state stability of the switching closed-loop system with respect to perturbations related to the time-varying desired motion-force profile. The switching occurs when the manipulator makes or breaks contact with the environment. The analysis shows that to guarantee closed-loop stability while tracking arbitrary time-varying motion-force profiles, the controller should implement a considerable (and often unrealistic) amount of damping, resulting in inferior tracking performance. Therefore, it is proposed to mechanically redesign the manipulator by including a compliant wrist. Using the novel analysis method, guidelines are provided for the design of the compliant wrist while employing the designed switching control strategy, such that stable tracking of a motion-force reference trajectory can be achieved and bouncing of the manipulator while making contact with the stiff environment can be avoided.

- *Novel controller for delayed bilateral teleoperation* – A novel two-layer control architecture is proposed for bilateral teleoperation with constant communication delays. The controller is structured with an outer layer, called the performance layer, and an inner layer, called the passivity layer. In the performance layer, any controller can be implemented to obtain high performance. In the passivity layer, the output of the performance layer is modified to guarantee that, from the operator and environment perspective, the overall teleoperator is passive. Passivity is ensured by modulating the performance layer outputs and by injecting a variable amount of damping via an innovative energy-based logic that follows a principle of energy duplication and takes into account the effects of the delays. In contrast to bilateral motion synchronizing controllers, where the master and slave controllers implement an as-stiff-as-possible coupling between the master and

slave devices, the proposed scheme is specifically designed for direct force-reflection. The tuning of the control parameters is elaborately discussed and illustrated by means of several simulation examples. Furthermore, the effectiveness of the proposed controller to obtain low operator effort and high transparency, while making and breaking contact with a static environment, is demonstrated experimentally for a challenging round-trip communication delay of 100 ms.

1.4 Outline of the thesis

The performance- and stability-related objectives presented in Section 1.2 are considered one by one in chapters 2 to 5. Consequently, this thesis is organized as follows.

Chapter 2 contains a review of the literature. It introduces in detail the components of the teleoperator and addresses existing issues in modeling, controller design, stability analysis and achieving high performance. In particular, a more detailed motivation and discussion is presented for the paradigm shift from bilateral motion synchronization to direct force-reflection when designing controllers for delayed bilateral teleoperation.

In Chapter 3, several bilateral motion synchronization and direct force-reflection architectures are compared experimentally. Clear quantitative performance metrics are used to measure the performance of each architecture as a function of the delay. The results do not only support the proposed change in the design philosophy, but also illustrate explicitly the performance that can be expected in practice. Furthermore, the setup used for all experiments presented in this thesis is introduced here in detail.

The design of a control law and the accompanying analysis method for the tracking of a time-varying motion-force profile of a manipulator while making and breaking contact with a stiff environment, is discussed in Chapter 4. In particular, guidelines are provided for the design of the compliancy in the manipulator to guarantee stable and even bounceless impact of the manipulator with the environment for any operator input.

The design and passivity analysis of a novel 2-layer control architecture are presented in Chapter 5. The architecture consists of a Performance Layer and Passivity Layer and is developed according to the direct force-reflection design philosophy to obtain good performance in the presence of delays. It is illustrated both numerically and experimentally that because the control action of the Performance Layer is only modified when passivity tends to get lost, both a high transparency and a low operator effort in free motion can be achieved.

Chapter 2

Literature review

This chapter provides a brief overview of control architectures proposed for bilateral teleoperation with delays in the communication channel. In particular, the focus is on the bilateral motion synchronization and direct force-reflection architectures, which have been introduced previously in Section 1.3. For these architectures, the methods to analyze stability are addressed, together with the effect of these methods on the trade-off between guaranteeing stability and obtaining good performance.

This chapter is organized as follows. First, in Section 2.1, a detailed description of all components of the teleoperator is presented. Section 2.2 focusses on bilateral motion synchronization and Section 2.3 addresses direct force-reflection architectures. The effect on the performance of existing approaches to guarantee stability of the teleoperator is briefly discussed in Section 2.4. Furthermore, Section 2.5 presents in the form of Haptic Shared Control an alternative approach to improve the task performance. Finally, Section 2.6 concludes on the most promising control architectures and stability techniques to achieve high performance in the form of a low operator effort and high transparency in delayed bilateral teleoperation.

2.1 Modeling of bilateral teleoperators

In bilateral teleoperation, an operator interacts with a remote environment via a local interface that is connected to a remote slave device. This is shown schematically in the block diagram of Fig. 2.1. The local interface is called a haptic master, since it presents the operator with force feedback regarding the slave-environment interaction. The connection between the master and slave is obtained by exchanging motion and force information over a communication

Fig. 2.1. Block diagram of a bilateral teleoperator.

network. A local controller on each side uses this information to create a bilateral coupling such that the operator can both actuate the slave device and receive force feedback from the remote side. This bilateral coupling should create a form of *telepresence*, i.e. the operator is given the feeling that he is present at the remote side. The following sections describe the different components of the bilateral teleoperator in more detail.

2.1.1 Master and slave dynamics

Both the master and slave device are considered as a robotic manipulator, consisting of multiple degrees of freedom (DOF), and having either a serial or parallel configuration. The devices are typically equipped with position sensors to measure the joint displacement, and sometimes with force sensors to measure the interaction with the operator or environment. The operator controls the master device, while a controller computes torques and forces that are simultaneously applied on the device. The slave device is operated by the slave controller and using it's end-effector it can interact with the remote environment. In this thesis, it is considered that the links of the manipulators are rigid and the joints feature no flexibility. As a result, the dynamics of the devices can be obtained via standard modeling techniques, such as described in [123, 125]. Indicating with $q_i \in \mathbb{R}^l$, with l the number of joints and $i \in \{m, s\}$, the joint position of the master (m) and slave (s) device respectively, the nonlinear dynamics in joint space are represented by

$$M_m(q_m)\ddot{q}_m + C_m(q_m, \dot{q}_m)\dot{q}_m + g_m(q_m) + f_m(q_m, \dot{q}_m) = \tau_{mc} + J_m^\top(q_m)F_h, \quad (2.1)$$

$$M_s(q_s)\ddot{q}_s + C_s(q_s, \dot{q}_s)\dot{q}_s + g_s(q_s) + f_s(q_s, \dot{q}_s) = \tau_{sc} - J_s^\top(q_s)F_e, \quad (2.2)$$

where the inertia matrix is denoted by $M_i \in \mathbb{R}^{l\times l}$, $C_i \in \mathbb{R}^{l\times l}$ are the Coriolis' matrices, $g_i \in \mathbb{R}^l$ is the gravity vector, $f_i(q_i, \dot{q}_i) \in \mathbb{R}^l$ the (nonlinear) friction terms, $J_i \in \mathbb{R}^{n\times l}$ the geometric manipulator Jacobian, with n the number of Cartesian DOFs, and $\tau_{ic} \in \mathbb{R}^l$ are the control torques of device i. It is assumed that the operator and environment only interact with the end-effectors of the master and slave device, respectively. As a result, $F_h \in \mathbb{R}^n$ represents the forces and torques exerted by the operator on the end-effector of the master, and $F_e \in \mathbb{R}^n$ represents the forces and torques exerted by the end-effector of the slave on the environment (hence the minus sign).

Since the operator and environment interact on end-effector level with the master and slave, respectively, and because the configuration and dimensions of

the master and slave might differ, the dynamics (2.1), (2.2) are often transformed to the Cartesian space representation

$$\bar{M}_m(x_m)\ddot{x}_m + \bar{C}_m(x_m, \dot{x}_m)\dot{x}_m + \bar{g}_m(x_m) + \bar{f}_m(x_m, \dot{x}_m) = F_{mc} + F_h, \quad (2.3)$$

$$\bar{M}_s(x_s)\ddot{x}_s + \bar{C}_s(x_s, \dot{x}_s)\dot{x}_s + \bar{g}_s(x_s) + \bar{f}_s(x_s, \dot{x}_s) = F_{sc} - F_e, \quad (2.4)$$

where $\bar{M}_i \in \mathbb{R}^{n\times n}$, $\bar{C}_i \in \mathbb{R}^{n\times n}$, $\bar{g}_i \in \mathbb{R}^n$ and $\bar{f}_i \in \mathbb{R}^n$ are the equivalent Cartesian space matrices and vectors, and $x_i \in \mathbb{R}^n$ denotes the end-effector position and orientation of device i. The control forces and torques on end-effector level $F_{ic} \in \mathbb{R}^n$ are related to the joint torques τ_{ic} by $\tau_{ic} = J_i^\top(q_i)F_{ic}$. For more background material regarding the transformation from (2.1), (2.2) to (2.3), (2.4), the interested reader is referred to [125].

A widely used property of the manipulator is that, with the control force and torque considered as input and the velocity as output, the dynamics are passive. The interested reader is referred to [125, Chapter 7] for more background material and [59, Chapter 6] or [119, Chapter 2] for a definition of passivity.

2.1.2 Environment

Environments typically present in remote handling and maintenance applications for nuclear fusion and space applications are characterized by hard materials. Establishing a proper interaction between the slave and environment, a key requirement in these applications, is one of the major problems in bilateral teleoperation, especially in combination with communication delays. A good understanding of this interaction is therefore crucial to guarantee a stable impact, preferably without bounces of the slave against the environment.

The approaches taken in the literature can roughly be categorized in approaches that either do or do not use a model of the environment. When a model of the environment is used, this model usually describes the force as a function of the penetration of the environment by means of a flexible contact model. The most commonly encountered contact models are the Hertz contact model, the Kelvin-Voigt model and the Hunt-Crossley model [56]. For further reading on contact models, the interested reader is referred to [44]. An alternative to the flexible contact model, although rarely used in bilateral teleoperation literature, is to model the manipulator-environment interaction with a nonsmooth mechanics approach [20].

In many applications, the remote environment is static and can be represented by a passive velocity-to-force map, i.e. there exists a finite constant $E_e(t_0)$, depending on the initial condition at time t_0, representing the initially stored energy of the environment, such that the energy of the environment $E_e(t)$ satisfies [119, Chapter 2]

$$-E_e(t_0) \leq E_e(t) - E_e(t_0) \leq \int_{t_0}^{t} F_e^\top \dot{x}_s d\sigma \quad (2.5)$$

where $\dot{x}_s$ and F_e represent the input and output of the environment. Note that the maximally extractable energy is bounded from below. By using (2.5), explicit modeling of the slave-environment interaction is circumvented. The disadvantage is that extra conservatism is introduced in the analysis, since stability must be guaranteed for *any* passive environment, e.g., for any value of the impedance.

It must be stressed that in teleoperation the interaction of the slave with the environment is of a hybrid nature: The environment model switches from zero applied force in free motion to nonzero applied force when the slave is in contact with the environment. Stability of the teleoperator can therefore not be concluded from stability of the free motion and contact situations alone. Also transitions from free motion to contact, and viceversa, must be included in order to analyze and prevent contact instability, i.e. bouncing of the slave against the environment with increasing amplitude. Ideally, the teleoperator achieves bounceless contact, so only one transition from free motion to contact after impact. Despite the often mentioned and experienced contact instabilities (see, e.g., [36,69,78]), the contact transitions are rarely included in the stability analysis. Only a few articles, among which are [88, 89], analyze stability during the transitions by using a multiple Lyapunov function approach.

2.1.3 Operator

The operator is responsible for the execution of the task. The teleoperator should thus be designed in such a way that it becomes intuitive to use for the operator. A good understanding of the behavior of the operator for a certain task is crucial for the design of a stable and high performance teleoperator.

Interestingly, the human actuation and perception bandwidths are not identical, but asymmetric [22, 36, 128]. Several maximum bandwidths are reported in [22] for different types of actuation: 1-2 Hz for unexpected signals, 2-5 Hz for periodic signals, approximately 5 Hz for internally generated or learned trajectories, and approximately 10 Hz for reflexive actions. The perception bandwidths are much higher: "Sensation of mechanical vibration of the skin has been reported as high as 10.000 Hz, but the ability to discriminate one signal from another declines above 320 Hz" [22].

Modeling the interaction between the operator and the master device is difficult due to, e.g., the need to capture the operator's intention in both free motion and contact tasks. In the unconstrained directions, the operator controls the motion of the slave device, but in the constrained directions, the operator controls the interaction force between the slave and the environment [36]. Furthermore, the characteristics of a human arm (such as the stiffness level due to muscle contraction) are time-varying and vary even between operators.

Several authors have identified models for certain tasks performed by operators. For example, the human behavior can be modeled as a hybrid dynamical system deterministically as in [100] or stochastically as in [140], but these mod-

els have to be trained with a sufficient amount of data sets and are relatively complex for the stability analysis. A more simple model for point-to-point motion is the minimum jerk model (with a bell-shaped velocity profile) [39], related to a minimum effort approach employed by operators. This model is restricted to unconstrained motion only. The most frequently used model to represent the operator in both free motion and contact, due to its simplicity, is based on a mass-spring-damper model, and is sometimes extended with a lowpass filter to include the operator's limited actuation bandwidth (see e.g. [77, 134]). The mass, damping and stiffness characteristics of the human arm, representing the operator's arm impedance, are taken into account explicitly. To simplify the stability analysis, these parameter values are usually considered constant, resulting in a Linear Time Invariant (LTI) operator model. Such a modeling approach is also taken in the simulations of Chapter 5. In contrast, a range of impedance parameters is identified in [76, 77] for both free motion and contact tasks and the parameters are considered to be time-varying within bounded sets.

To circumvent explicit modeling, the operator is often assumed to be characterized by a passive velocity-to-force map (see [55,94] and the references therein). Passivity of the human operator is based on the work of Hogan, who concludes that "the muscular actuators and neural feedback driving the arm would surely constitute an active system, yet experiments to date indicate that the impedance at the hand appears indistinguishable from that of a passive object" [54]. However, assuming a passive operator might lead to conservative analyses. The operator can change his stiffness within a bounded set of parameter values, but the set of dynamics covered by passive systems, containing stiffness values from zero to infinity, is much larger than the set of dynamics the operator can show.

In more recent publications there is an ongoing discussion regarding passivity of the operator. Depending on the system boundary, the operator can display nonpassive behavior in certain tasks, (see e.g. [108], [106]). Consider, for example, the force applied by the human hand on the master as the input and the resulting motion of the hand as the output. When controlling the unstable equilibrium of a pendulum, the operator must inject energy to swing up the pendulum. Instead of focusing on passivity, Burdet et al. [23] report that a human operator tends to stabilize a manipulated object in the presence of external forces by learning an internal model of the dynamics.

2.1.4 Controller design

Due to the physical distance between the master and slave side, the control architecture is distributed over a network, such as the internet, and the information exchange suffers from delays. The delay can be either constant or time-varying and the values can range from a few milliseconds for short distance teleoperation to a few hundred milliseconds for global communication [9], or even multiple seconds in space applications [120]. Moreover, the information exchange could

suffer from lost packets or even a complete communication blackout. This thesis focusses on constant delays up to a few hundred milliseconds. Although highly interesting, the literature discussed here does not include the time-varying delay case or dropouts explicitly. Note that a small variation of the delay can be removed at the cost of additional constant delay by using a buffer and releasing the received packages at a fixed rate.

The control architecture ensures a bilateral connection between the master and slave. The goal of the bilateral coupling is to make the slave device follow the motion of the master, induced by the operator, and provide the operator with haptic feedback regarding the progress of the task. This feedback must be sufficiently intuitive for the operator. A 'good feedback' is difficult to quantify since it is a subjective measure that varies between operators and tasks. Control engineers have attempted to capture the performance requirements in several criteria that can be measured and used to design and evaluate controllers. The most popular criteria are listed below.

- *Transparency* – This is the most frequently used performance metric. Transparency implies that the operator can feel through the teleoperator as if s/he is interacting with the environment directly. Perfect transparency is achieved when $F_h(t) = -F_e(t)$ and $x_m(t) = x_s(t)$ [69], and requires the teleoperator to be massless and infinitively stiff. Partly due to the inherent trade-off between stability and transparency this is hard, if not impossible, to obtain in practice. Moreover, several studies, among which are [17,137], report that the improvement in task performance saturates for increasing levels transparency. Hence, perfect transparency is not required, but only a basic (task- and operator dependent) level is sufficient.

- *Z-width* – The Z-width represents the range of impedances that can be reflected to the operator [34]. The two extremes of the range are obtained by calculating the reflected impedance in free motion and in contact with an infinitely stiff environment. Note that a teleoperator with a larger Z-width does not necessarily result in a better perception of the remote environment than one with a smaller Z-width: When interacting with soft environments, the reflection of high stiffnesses is not required.

- *Fidelity* – This is a variant of transparency proposed specifically for telesurgery [26]. Instead of focusing on the transmission of the environment impedance, fidelity incorporates the human perceptual capabilities and describes how well changes in the compliancy of the environment can be felt by the operator.

- *Operator and task performance* – Apart from teleoperator performance, also the operator effort and quality of the task execution are of importance. Examples of task performances metrics include the task execution time and targeting accuracy. The operator effort consists of a physical component,

which is related to the energy the operator needs to perform the task, and the mental load, which is related to how intuitive the teleoperator is to work with. Several examples of task and operator related metrics are reported in [67]. Although rarely used in comparative studies, these metrics could potentially offer more insight on how to improve control architectures. In this thesis, the physical operator effort is considered as one of the key performance metrics.

Obtaining good performance is important, but even proving stability is already a difficult task due to the communication delays, the interaction and impact with hard environments, the time-varying operator characteristics, possible active behavior of the operator and the bilateral coupling. In fact, one should analyze switched nonlinear time-varying delay differential equations, but employ nonconservative stability techniques to obtain good performance. These techniques do not yet exist for these differential equations, so the current focus in the literature is on solving subproblems like delay-stability or impact of the slave with the environment.

Controller classification

Control architectures for bilateral teleoperation are often classified by the number of signals that are transmitted over the communication channel. For example, a 2-channel P-F architecture, where 'P' stands for *position* and 'F' for *force*, transmits position information from master to slave, and force information from slave to master. In a P-P architecture only position information is exchanged. An example of a 3-channel architecture is the P-PF architecture, where compared to P-P additional force information of the environment is transmitted to the master. A 4-channel architecture is also known as a PF-PF controller. With this classification, a total of 9 different architectures can be distinguished for bilateral teleoperation.

Several articles, see e.g. [11, 55, 80, 94, 105, 126], present an overview of proposed architectures for delayed bilateral teleoperation. A classification is made on whether the analysis is based on passivity or not [55], schemes that either do or do not use wave variables [94], or schemes that explicitly use available information about the operator, environment or task at hand [105].

In this thesis, architectures are classified on their primary goal: either *bilateral motion synchronization* (see Fig. 2.2(a) and Fig. 1.3(b)) or *direct force-reflection* (see Fig. 2.2(b) and Fig. 1.3(c)). In bilateral motion synchronization, *both* the master and slave controller aim at motion synchronization, resulting in a series connection of the teleoperator components. The environment force is reflected indirectly by creating a *tight* coupling between the master and slave, using e.g. a virtual spring and damper, like the classical P-P controller. In direct force-reflection, the slave controller acts as a *virtual* operator, and the master controller acts as a *virtual* environment, specifically aiming to reflect the

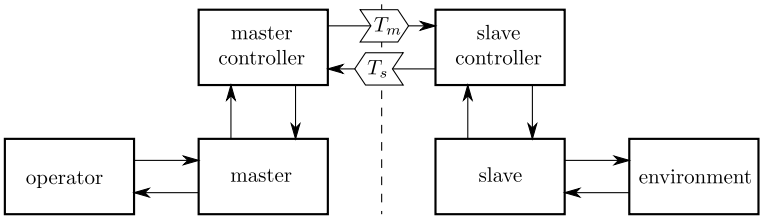

(a) Bilateral motion synchronization.

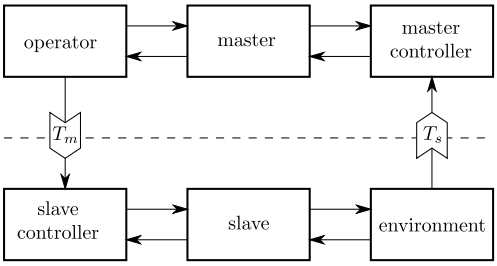

(b) Direct force-reflection.

Fig. 2.2. Block diagrams of the two different control approaches for bilateral teleoperation, as already illustrated in Fig. 1.3. Arrows represent information flows and T_m and T_s represent, respectively, the communication delays from master to slave and viceversa.

slave-environment contact force. A typical example is the P-F architecture. Sections 2.2 and 2.3 address the two classes of control architectures in more detail.

2.2 Bilateral motion synchronization

In bilateral motion synchronization, both the master and slave controller aim at motion synchronization with the other device. This is achieved by measuring and transmitting position (and/or velocity) information. Furthermore, the architectures PF-P, P-PF and PF-PF (the 4-channel controller) use also the force applied by the operator and/or environment to improve motion synchronization. The P-P architecture is easier to implement in practice, because expensive force sensors, suffering from noisy measurement signals and requiring calibration, are not required.

This section first discusses the effect of the communication delay and environment perception via the P-P architecture. Then, the three extensions of this architecture are addressed and their effect on the operator effort and perception of the environment is elaborated.

2.2.1 Position-Position control

The P-P architecture originates from the delay-free case and consists of two local controllers to minimize the master-slave motion tracking error. Due to its simplicity, it is the most popular architecture to achieve bilateral teleoperation. Furthermore, stability is often analyzed in the joint space. Apart from feedforward terms and local compensation of the dynamics like gravity, inertia and friction, originating from single manipulator control [125], each controller achieves synchronization by using a feedback controller. Due to its mechanical equivalence to a spring and damper the feedback term usually consists of a proportional-derivative controller

$$\tau_{mc} = k_{pm}(q_s - q_m) + k_{dm}(\dot{q}_s - \dot{q}_m), \tag{2.6a}$$
$$\tau_{sc} = k_{ps}(q_m - q_s) + k_{ds}(\dot{q}_m - \dot{q}_s). \tag{2.6b}$$

The positive gains k_{pi} and k_{di}, with $i \in \{m, s\}$, represent the proportional and derivative gain. These gains are typically selected as $k_{pm} = k_{ps}$ and $k_{dm} = k_{ds}$ to prevent scaling, resulting in a virtual spring-damper coupling between the master and slave. Unfortunately, even in the undelayed situation the P-P controller has two major drawbacks: the slave dynamics are reflected to the operator and the reflection of the environment stiffness is poor. The explanation of these drawbacks is given in the next paragraphs by considering

$$\begin{aligned} M_m(q_m)\ddot{q}_m + M_s(q_s)\ddot{q}_s + C_m(q_m, \dot{q}_m)\dot{q}_m + C_s(q_s, \dot{q}_s)\dot{q}_s + g_m(q_m) \\ + g_s(q_s) + f_m(q_m, \dot{q}_m) + f_s(q_s, \dot{q}_s) = J_m^\top(q_m)F_h - J_s^\top(q_s)F_e, \end{aligned} \tag{2.7}$$

which is obtained by using (2.6) in the master and slave dynamics (2.1)-(2.2).

Reflection slave dynamics

The reflection of the slave dynamics follows directly from (2.7), since apart from the environment force F_e the operator must also overcome all dynamics on the left-hand side. Reflecting the slave dynamics is undesired since it distorts perception and increases fatigue, especially for heavy teleoperators. Therefore, the master and slave should be designed either very lightweight or the dynamics must be compensated by the controller with, e.g, an inverse dynamics approach. Due to difficulties in the identification, especially the friction components that can be nonlinear, position dependent and time-varying, and due to the absence of velocity and acceleration measurements, accurate online compensation of the dynamics is hard to achieve in practice.

Stiffness perception

Even when the master and slave are identical, such that $J_m = J_s$, (2.7) reveals that the perception of F_e is distorted due to the master and slave dynamics.

Only when the master and slave are in rest, i.e. when $\ddot{q}_i = \dot{q}_i = 0$, the gravity and friction terms are compensated, and the master and slave configurations are identical, i.e. $q_m = q_s$ such that $J_m(q_m) = J_s(q_s)$, the closed-loop dynamics (2.7) reduce to $F_h = F_e$. In this situation, using (2.6a) in (2.1) and (2.6b) in (2.2), the master and slave dynamics reduce to

$$\begin{aligned} J_m^\top(q_m)F_h &= -\tau_{mc}, \\ J_s^\top(q_s)F_e &= \tau_{sc}. \end{aligned} \tag{2.8}$$

Without force scaling, $k_{pm} = k_{ps}$, such that $\tau_{mc} = -\tau_{sc}$, (2.8) reduces to

$$J_m^\top(q_m)F_h = k_{pi}(q_s - q_m) = J_s^\top(q_s)F_e. \tag{2.9}$$

Hence, the synchronization error $q_s - q_m$ increases proportionally with F_e. A very large value of k_{pi} is required to create a tight coupling between the master and slave, something that can rarely be obtained. A limited value of k_{pi} does not reduce the reflection of F_e (in steady-state), but due to a position difference between the master and slave, the environment is perceived softer: the teleoperator represents a spring connected in series with the environment stiffness.

An interesting approach to improve the transparency is presented in [88, 89]. Here, Ni and Wang propose a gain-switching controller, based on the following observation: "Intuitively, there should be no force feedback to the operator when the slave manipulator is in free motion, which indicates that the master controller should have gains as low as possible; otherwise, the system would feel sluggish due to the position error. The slave controller should have high gains for good position tracking performance in free motion. When the slave manipulator has a hard contact, the master controller should have high gains to make the operator sensitive to the collision happening at the remote site; while the slave controller should have low gains in order to soften the collision" [88]. Remarkably, Ni and Wang hint at mimicking a bilateral motion synchronization controller with a direct force-reflection architecture. Asynchronous switching is proposed in [88] and, in combination with a multiple Lyapunov function approach to include the switching nature of the environment and controller gains, a switching control law is derived that guarantees stable contact in a setpoint regulation problem. However, using different gains in the master and slave controller results in a scaling of the reflected force, thereby still affecting the operator's perception of the remote environment stiffness.

Effect of delays

When using the P-P architecture in delayed teleoperation, assuming constant delays for simplicity and illustrative purposes, the transmitted master and slave positions q_m and q_s arrive T_m and T_s seconds later, respectively, at the other side. Defining the delayed master and slave positions as $q_i^{T_i} := q_i(t - T_i)$, the

controllers (2.6) become

$$\tau_{mc} = k_{pm}(q_s^{T_s} - q_m) + k_{dm}(\dot{q}_s^{T_s} - \dot{q}_m), \tag{2.10a}$$
$$\tau_{sc} = k_{ps}(q_m^{T_m} - q_s) + k_{ds}(\dot{q}_m^{T_m} - \dot{q}_s). \tag{2.10b}$$

Hence, the controllers synchronize the motion of their device with the delayed motion of the other device. Clearly, at time t, the master and slave have a different motion tracking error, since $q_s^{T_s} - q_m \neq -(q_m^{T_m} - q_s)$. So although the controllers try to synchronize with the remote device, the two local controllers have different goals. Apart from the destabilizing effect of the delay on the closed-loop dynamics, this can result in undesired oscillations with a frequency related to the round-trip delay $T_r := T_m + T_s$.

Another drawback of the P-P architecture is that it results in 'delay-induced forces' that are reflected to the operator. To illustrate this, rewrite (2.10a) as

$$\tau_{mc} = k_{pm}(q_s - q_m) + k_{dm}(\dot{q}_s - \dot{q}_m) \underbrace{+ k_{pm}(q_s^{T_s} - q_s) + k_{dm}(\dot{q}_s^{T_s} - \dot{q}_s)}_{\text{Delay induced forces}}. \tag{2.11}$$

The first two terms on the right hand side are identical to the control action (2.6a) of the undelayed situation. The last two terms on the right hand side are caused by the delay and represent a spring-damper connection between the current position and velocity of the slave and the position and velocity T_s seconds ago. High gains k_{pm} and k_{dm} or fast motion of the slave will result in additional forces reflected to the operator. "This makes the system feel sluggish in free space motion, since the lags between master and slave position movements cause large reaction forces to be supplied to the operator" [69].

Several methods have been proposed to guarantee stability of the delayed teleoperator under bilateral motion synchronizing and attempt to approach the performance level of the undelayed case. These methods include the use of scattering or wave variables, damping injection, additional force information and the use of predictors. In the remainder of this section, these methods are briefly discused.

2.2.2 Scattering and wave variables

The first solution to guarantee stability in delayed bilateral synchronization originates from passivity theory. Denote the teleoperator by the 2-port system consisting of the master, slave, controllers and communication channel. Since the master and slave dynamics are passive 2-port systems and the two PD-controllers (2.6) represent passive components in the undelayed situation, it suffices to make the communication network passive to guarantee passivity of the teleoperator. When transmitting power variables over a network subject to delays, the communication network is not passive [10,91], i.e. "specific choices of the input variables ... will produce energy which can drive the overal system unstable" [91].

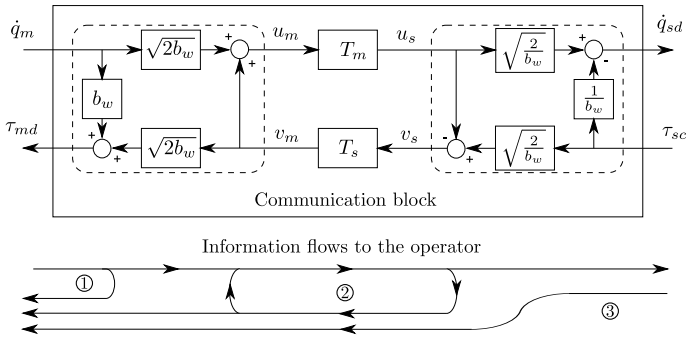

Fig. 2.3. Wave variable transformations and information flows.

Based on results from transmission line theory, Anderson and Spong [10] introduced the *scattering transformation* to create a lossless communication block. Niemeyer and Slotine presented in [91] an equivalent formulation which they call the *wave variable transformation*. With u the forward wave transmitted from master to slave and v the backward wave transmitted from slave to master, the wave variables are defined as

$$\begin{aligned} u_m &= \tfrac{1}{\sqrt{2b_w}}(\tau_{md} + b_w\dot{q}_m), \qquad & u_s &= \tfrac{1}{\sqrt{2b_w}}(\tau_{sc} - b_w\dot{q}_{sd}), \\ v_m &= \tfrac{1}{\sqrt{2b_w}}(\tau_{md} - b_w\dot{q}_m), \qquad & u_s &= \tfrac{1}{\sqrt{2b_w}}(\tau_{sc} + b_w\dot{q}_{sd}). \end{aligned} \tag{2.12}$$

The wave variables u_i and v_i have the unit $\sqrt{W}$, such that $u_m^T v_m$ and $v_s^T u_s$ represent the power exchanged with the master and slave respectively. The constant $b_w > 0$ is the *characteristic wave impedance* that can be tuned to trade-off speed of motion with levels of force [92] to achieve the desired performance. In practice, the upper bound of the wave impedance is limited by non-idealities such as encoder resolution, amplifier bandwidth and servo delay [129, 130].

An example of the encoding and decoding of the power variables is illustrated in Fig. 2.3. The power variables $\dot{q}_m$ and τ_{sc} are first encoded into wave variables. The latter quantities are then transmitted over the network, such that

$$u_s = u_m^{T_m}, \qquad v_m = v_s^{T_s}. \tag{2.13}$$

The wave variables received from the remote side are decoded into the desired signals $\dot{q}_{sd}$ and τ_{md}, which are used in the controllers. Due to the interaction between the forward and backward transmissions, the communication block is rendered passive for *any constant* delay value [91]: The energy of the communication block satisfies

$$\begin{aligned} E_{comm} &= \int_{t_0}^{t} \tau_{md}^\top(\sigma)\dot{q}_m(\sigma) - \tau_{sc}^\top(\sigma)\dot{q}_{sd}(\sigma)d\sigma \\ &= \frac{1}{2}\left(\int_{t-T_m}^{t} u_m^2(\sigma)d\sigma + \int_{t-T_s}^{t} v_s^2(\sigma)d\sigma\right) \geq 0. \end{aligned} \tag{2.14}$$

In its classical form, the wave variable approach introduces two significant transparency issues. The first issue is that position tracking cannot be guaranteed due to the transmission of only velocity signals. The second issue is the distortion of the reflected force. This is illustrated in the bottom part of Fig. 2.3, where it can be seen that the force reflected to the operator consists of three components [92]. Via path ① the operator receives a viscous friction term with damping constant b_w. The forces reflected via path ② result from the loop in the wave domain and include the communication delays. This loop, which is the result of the connection between the forward and backward transmission paths, results in wave reflections: oscillations with a frequency equal to $(T_m + T_s)^{-1}$. Only the information reflected via path ③ contains the useful information that was initially transmitted to the operator.

For a good force reflection, the information of paths ① and ② must be attenuated or eliminated. The viscous friction term of path ① could be reduced by selecting a small wave impedance b_w, but that is not always desired. Using *impedance matching* [33,91,92], *wave filtering* [91,92,128] or *wave shaping* [128], the wave reflections can be reduced or even eliminated. In impedance matching, the wave impedance b_w is matched with the impedance of the controllers, i.e. the derivative gains k_{di}. In wave filtering, a lowpass- or Notch filter is applied in the wave domain to attenuate the oscillations. Wave shaping, suitable for delays larger than 100 ms, is presented as a "filter that automatically tunes itself to the wave reflection resonance" [128].

Wave variables and position tracking

Since velocity signals are used in the wave variable transformation (2.12), the positions of the master and slave might drift apart. The drift is the result of discrete sampling, numerical errors and data loss. Popular solutions to guarantee position tracking include the use of *wave integrals* [92, 93, 95], the encoding of both position and velocity via $q_i + \lambda \dot{q}_i$, with $\lambda > 0$ a constant parameter, in the wave transformation (2.12) [31,33,114] and the use of proportional terms outside the wave domain [32, 85, 94]. For the sake of brevity, only the latter solution is discussed here briefly. For more background information, the interested reader is referred to [126].

In [32, 85, 94], the position commands are transmitted explicitly outside the wave domain. This action is not passive, so stability of a 1-DOF linear teleoperator is analyzed with a positive definite Lyapunov-like functional

$$\begin{aligned} V(X) \;=\; & \frac{1}{2}\left(M_m(q_m)\dot{q}_m^2 + M_s(q_s)\dot{q}_s^2 + k_p(q_m - q_s)^2\right) \\ & + \int_{t_0}^{t} \left(\tau_e \dot{q}_s - \tau_h \dot{q}_m\right) d\sigma + \int_{t-T_m}^{t} u_m^2 d\sigma + \int_{t-T_s}^{t} v_s^2 d\sigma. \end{aligned} \tag{2.15}$$

The state $X := [q_m - q_s, \dot{q}_{i,[0,t]}, u_{m,[-T_m,t]}, v_{s,[-T_s,t]}]$. The evaluation of a signal $x_i(t)$ over the time interval $[a, b]$, with $a < b$, is denoted by $x_{i,[a,b]}$. The first three

terms on the right-hand side of (2.15) are related to the kinetic and potential energy of the teleoperator; the latter for the delay-free situation. The first integral on the right hand side is nonnegative and represents the passive operator and environment (a crucial assumption). The last two integrals result from integrating (2.14) and represent the energy in the communication block. Using local damping injection terms $B_i\dot{q}_i$ in each controller, with B_i a positive damping constant, the authors prove that if the inequality

$$k_{pm}k_{ps}(T_m^2 + T_s^2) < 4B_mB_s \tag{2.16}$$

is satisfied, the velocities $\dot{q}_i$ asymptotically converge to zero, the tracking error $q_m - q_s$ remains bounded and only converges to zero asymptotically when $\tau_e = 0$. Asymptotic convergence of the tracking error to zero for only $\tau_e = 0$ is inherent to *bilateral motion synchronization* architectures, as illustrated in (2.9). The bound (2.16) states that the proportional gain is limited by the delay and the amount of injected damping. A large value of k_{pi} implies much local damping injection, resulting in a sluggish (i.e. strongly damped) feeling in free motion. A low value of k_{pi} allows for a small B_i, but this reduces motion tracking and a poor stiffness reflection. A trade-off between these two extremes is inevitable, hence performance is sacrificed at the cost of position tracking.

Performance improvements for wave-variable-based architectures

A *generalized scattering* transformation is introduced in [51, 52, 134] to extend the wave transformation (2.12) for better performance. In [8, 84, 95], extensions of (2.12) are presented for systems with multiple DOF. An interesting approach to improve performance is to make the wave impedance time-varying. This is done in [129] by switching between two values depending a free motion or contact situation of the slave. In [112, 114] the wave impedance is varied continuously.

Finally, Munir and Book [84] (see [83] for time-varying delays) modify a Smith predictor in combination with a Kalman estimator and an energy regulator in the wave domain to predict the reflected wave in a passive way. By predicting the reflected wave, the effect of the time delay on the performance, e.g. the delay induced force illustrated in (2.11), are reduced.

2.2.3 Damping injection schemes

In [94], the authors compare several of the wave variable-based synchronization architectures with architectures that do not use wave variables. The stability analyses for the latter are based on Lyaponov-like functionals and have a similar structure as presented in [32, 85], i.e. of the form (2.15). The proposed schemes include Pd-control [96, 98] and PDd-control [70, 96, 97, 136] (with 'd' implying damping). In [29, 30, 74, 99], several extensions are presented that use adaptive terms to compensate for parametric uncertainties, similar to single manipulator

control [125]. All these architectures require a minimum amount of damping injection to guarantee stability, as illustrated below.

For constant delays, and ignoring gravity terms and friction, the following PDd-controllers are proposed in [96] to synchronize the master and slave motion

$$\tau_{mc} = k_{pm}(q_s^{T_s} - q_m) + k_{dm}(\dot{q}_s^{T_s} - \dot{q}_m) - B_m\dot{q}_m, \tag{2.17a}$$
$$\tau_{sc} = k_{ps}(q_m^{T_m} - q_s) + k_{ds}(\dot{q}_m^{T_m} - \dot{q}_s) - B_s\dot{q}_s \tag{2.17b}$$

with B_i the local amount of injected damping. Selecting $k_{dm} = k_{ds} = 0$ results in the Pd-controller presented in [98]. Stability of the closed-loop system is analyzed with the following storage functional

$$\begin{aligned} V(q_m - q_s, \dot{q}_{i,[-T_i,t]}) = \frac{1}{2}\left(\dot{q}_m^\top M_m(q_m)\dot{q}_m + \dot{q}_s^\top M_s(q_s)\dot{q}_s + k_p(q_m - q_s)^2\right) \\ + \int_{t_0}^{t}\left(\tau_e^\top \dot{q}_s - \tau_h^\top \dot{q}_m\right)d\sigma + E_e(t_0) + E_h(t_0) \\ + \frac{k_d}{2}\int_{t-T_m}^{t}(\dot{q}_m(\sigma))^2 d\sigma + \frac{k_d}{2}\int_{t-T_s}^{t}(\dot{q}_s(\sigma))^2 d\sigma, \end{aligned} \tag{2.18}$$

where for the sake of brevity $k_p := k_{pm} = k_{ps}$ and $k_d := k_{dm} = k_{ds}$. The first three terms on the right-hand side represent the kinetic energy of the master and slave, and the potential energy of the coupling in the undelayed situation. The first integral is nonnegative due to the assumed passivity of the environment and operator (a crucial assumption), and $E_e(t_0)$ and $E_h(t_0)$ represent the initially stored energy of the environment and operator, respectively. The last two integrals are functionals to guarantee that V decreases over time. Using a storage functional like (2.18) usually results in a delay-independent result, but the authors of [96] obtained a delay-dependent result by exploiting the inequality (see also [85] for a proof)

$$-2\int_0^t x^\top(\sigma)\int_{-T}^{0} y(\sigma+\theta)d\theta d\sigma \leq \alpha\|x(t)\|_2^2 + \frac{T^2}{\alpha}\|y(t)\|_2^2, \tag{2.19}$$

where $x(\cdot) : \mathbb{T} \to \mathbb{R}^n$ and $y(\cdot) : \mathbb{T} \to \mathbb{R}^n$ are two arbitrary vector signals and the constant $\alpha > 0$. The velocities $\dot{q}_i$ converge to zero asymptotically, and the tracking error $q_m - q_s$ remains bounded if (2.16) is satisfied. Due to the spring-connection, $q_m - q_s$ only converges to zero when $\tau_e = 0$, as illustrated in (2.9). Equation (2.16) implies a trade-off between k_{pi} and the required damping injection to guarantee stability for *all* passive operators and environments.

Adding damping could eventually contribute to position tracking by reducing the velocity of both devices. But when damping is added in free motion, the impact of the slave with the environment is perceived softer by human operators [15]. Furthermore, when the damping gains are selected too large, the operator

is no longer able to move the teleoperator. Although the position error might converge to zero, the fact that the operator cannot move the device is clearly not desired. The trade-off between high B_i and k_{pi}, the latter required for good motion tracking *and* force reflection, and low B_i and k_{pi} must be considered with care.

2.2.4 3- and 4-channel bilateral motion synchronization

To improve the performance, the traditional P-P architectures can be extended with the forces applied by the operator and environment on the teleoperator. Using LTI techniques, in [14] a P-PF and PF-P architecture are compared on both stability and theoretical performance in the presence of delays. It is concluded that PF-P is more suitable for teleoperators with a heavy slave, whereas the P-PF is recommended for teleoperators with a heavy master. In [5], the authors propose to use a P-PF architectures for the interaction with soft tissues.

Most of the work on 4-channel control originates from Lawrence's 4-channel architecture [69], presented for linear systems. 3- and 2-channel architectures can be derived from the 4-channel architecture by setting certain control terms to zero. Especially in the delay-free case the 4-channel controller can provide the best transparency of all architectures. In free motion, the use of F_h in the slave controller improves motion tracking. Combined with the use of F_e in the slave, this architecture results in the best stiffness reflection of all bilateral motion synchronization architectures. But for nonzero delay values, the 4-channel architectures also suffers from delay-induced forces. For more background material on 4-channel control, the interested reader is referred to the overview papers [55, 126], the references therein, and [48] for an analysis on impedance and admittance type master and slave devices.

2.2.5 Predictors

To reduce or eliminate the delay-induced forces, the master and slave controllers need information of the *current* position of the remote device. This can be achieved by using predictors. Unfortunately, it is hard, if not impossible, to predict the interaction with the operator, due to the changing impedance characteristics of the human arm and the operator's intention, and environment, due to the uncertainties in the environment properties and location. Despite these problems, several authors propose schemes with predictors to (partially) compensate for the delay-induced forces. For an overview up to 2006, the reader is referred to the introduction of [124] and the references therein.

The benefits of a predictor in the wave domain include better motion and force tracking, while passivity can still be analyzed [91]. One of the first attempts to use a predictor in the wave domain is by Munir and Book [84]. In [83] and [28]

the control scheme is extended to compensate for position drift due to variable delays, drop outs or initial position errors.

In [104], it is shown (both theoretically and in simulation) that using accurate models of the master and slave dynamics in a predictor, together with a good operator and environment model that includes perfect predictions of the exogenous inputs, yields significant improvements in motion and force tracking. A perfect prediction of the exogenous operator and environment inputs, however, is rarely available. In [141] the authors extend the adaptive architecture of [31] with two predictors to predict the motion of the remote device. It is assumed that the forces of operator and environment do not change during the delay interval, such that the delayed information can be used in both predictors. Finally, [87] considers the effect of the delay on the teleoperator as a disturbance and the authors design a communication disturbance observer. The master and slave are modeled as simple masses or inertias and the response of the slave is predicted on the master side. In contrast to the previously mentioned methods, this scheme does not require knowledge of the delay value.

Despite (partially) compensating for the delay-induced forces by incorporating predictors, the fundamental problems inherent to bilateral motion synchronization, such as the reflection of the slave dynamics and poor reflection of high stiffnesses, remain. These issues are absent in the majority of the direct force-reflecting architectures discussed in the next section.

2.3 Direct force-reflecting teleoperation

In direct force-reflection architectures the master and slave controller are designed to, respectively, reflect the environment to the operator and synchronize the motion of the slave with that of the master. From the 5 possible architectures P-F, F-P, F-F, PF-F and F-PF, both F-P and F-PF are rarely addressed in the literature, because these controllers suffer from delay-induced forces. Delay-induced forces are absent in the P-F, F-F and PF-F controllers, since the master controller does not directly contribute to motion synchronization. From these three controllers, only the P-F and PF-F architectures received significant attention in the literature, since the F-F controller lacks position tracking.

It will be shown in this section that, compared to bilateral motion synchronization, direct force-reflecting architectures like P-F and PF-F have more potential to obtain good motion tracking and force reflection, especially in delayed teleoperation. Unfortunately, these architectures are known to have drawbacks like contact instability, bouncing of the slave against the environment and a poor stiffness reflection (see e.g. [36,69,78]). Unlike bilateral motion synchronization, these schemes are not passive (see, e.g., [138]), such that direct force-reflection architectures have not been explored as extensively as bilateral motion synchronization.

Existing problems with direct force-reflection architectures are illustrated below using the P-F architecture. Subsequently, two proposed solutions are addressed to guarantee a stable teleoperator. This section is concluded with a brief discussion on the PF-F architecture.

2.3.1 Position-Force control

In contrast to bilateral motion synchronization, direct force-reflection is most frequently used in the task-space since the slave interacts with the environment via its end-effector. Therefore, the force reflecting architectures are presented in the task-space. The manipulator dynamics are then given by (2.3), (2.4).

Without communication delays, the P-F architecture is given by

$$F_{mc} = -\mu_2 F_e \tag{2.20a}$$
$$F_{sc} = k_{ps}(\mu_1 x_m - x_s) + k_{ds}(\mu_1 \dot{x}_m - \dot{x}_s), \tag{2.20b}$$

where $\mu_1 > 0$ and $\mu_2 > 0$ are the motion and force scaling gains. When the slave is in free motion, $F_e = 0$ and therefore also $F_{mc} = 0$, such that the control architecture is unilateral. For unilateral synchronization stability can be concluded, independent of the delay, by analyzing stability of the master and slave subsystems separately. In contact, however, $F_e \neq 0$ and thus $F_{mc} \neq 0$ and the controller *switches* to a bilateral architecture. In the static case, thus $\ddot{x}_m = \ddot{x}_s$ and $\dot{x}_m = \dot{x}_s$, ignoring friction and gravity, the dynamics (2.3), (2.4) with controller (2.20) reduce to

$$F_h = -F_{mc} = \mu_2 F_e, \tag{2.21a}$$
$$F_e = F_{sc} = k_{ps}(\mu_1 x_m - x_s). \tag{2.21b}$$

Selecting $\mu_2 = 1$ implies $F_h = F_e$, so that the operator perceives an exact copy of the environment force. However, even when $\mu_1 = 1$, the tracking error $x_m - x_s = F_e/k_{ps}$. So, similar to bilateral motion synchronization, a high proportional gain k_{ps} is required to accurately transmit the stiffness of the environment.

A frequently reported problem of P-F architectures is unstable behavior when interacting with stiff environments [64, 69]. This instability can have multiple causes. The first and most trivial one is unstable dynamics of the teleoperator, including the operator dynamics, in the contact phase.

The second cause of instability is due to the impact of the slave with the environment. Both the environment and controller have switching dynamics. Unstable switching between free motion and contact is known as contact instability and is characterized by bouncing of the slave against the environment with increasing amplitudes. To prevent contact instability, also the switching behavior must be included in the analysis. This is not done in the Bounded Environment Passivity (BEP) approach of [138], since the 1-port teleoperator-environment system is considered to be LTI (see [35]). Standard Lyapunov- and

passivity-based approaches include the switch between free motion and contact in the analysis. But the impact itself is not modeled and can therefore not be analyzed directly. *Stable* bouncing can thus not be analyzed or excluded.

A common problem in direct force-reflection, due to the switching between a unilateral and bilateral scheme, is that "the direct feeding back of contact forces usually results in the master recoiling violently when the slave is contacted with a stiff environment. To stabilize the system, the magnitude of reflected forces must be attenuated significantly" [36]. As reported in e.g. [62, 64], this implies that either the product $\mu_1\mu_2$, or the proportional gain k_{ps} must be considerably reduced. Both solutions contribute to the "spongy" or "mushy" feeling that human operators find unsatisfactory [69], giving these architectures a bad name.

Effect of delays

When the communication channel suffers from constant delays, (2.20) becomes

$$F_{mc}(t) = -\mu_2 F_e^{T_s} \tag{2.22a}$$

$$F_{sc}(t) = k_{ps}(\mu_1 x_m^{T_m} - x_s) + k_{ds}(\mu_1 \dot{x}_m^{T_m} - \dot{x}_s). \tag{2.22b}$$

In free motion of the slave the scheme is unilateral and stability is *not* affected by the delay. This is a clear advantage over bilateral motion synchronization schemes. But when the slave makes contact with the environment, two additional problems arise compared to the undelayed case.

The first problem is that the teleoperator itself might become unstable when interacting with the environment. This instability can come from either the unstable in-contact dynamics, which include also the master and operator, or from the transitions between free motion and contact. Stability can be analyzed with, for example, Llewellyn's absolute stability criterium for LTI systems, or with Lyapunov-like functionals such as (2.18) for nonlinear systems, but these methods are delay-independent are therefore conservative. To the best of the author's knowledge, only [61] considers a delay-dependent method, using Linear Matrix Inequalities (LMIs), to analyze stability of the switched teleoperator.

The second problem is that the operator is not able to bring the slave in contact with the environment. Using Fig. 2.4, this can be explained as follows. Denote the time when the master position passes the position of the environment $x_e = 0$ by t_1. Assuming perfect motion tracking, the slave makes contact at $t_2 = t_1 + T_m$, and the force $F_{mc} = -\lambda F_e^{T_s}$ of (2.22a) is applied on the master device at $t_3 = t_1 + T_r$. During the interval $[t_1, t_1 + T_r]$, the master moved *virtually* inside the environment. Meanwhile, the slave controller (2.22b) attempts to follow x_m, thereby creating large forces F_{sc} and F_e. Later on, the operator is presented with this unexpected large environment force and usually cannot react to it immediately, such that the master is pushed back and reaches position x_e at time t_4. At time $t_5 = t_4 + T_s$ also the slave detaches, such that the force $F_e = 0$ arrives on the master side at $t_6 = t_4 + T_r$. So, during the interval $[t_4, t_4 + T_r)$,

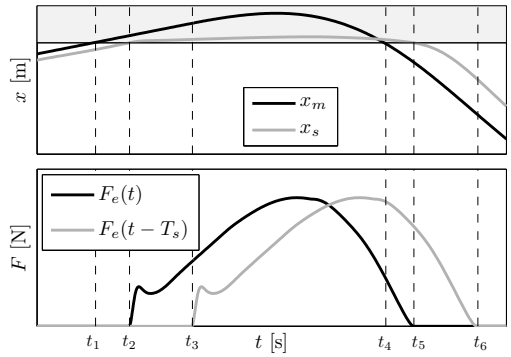

Fig. 2.4. Response of the master and slave with a P-F architecture and $T_s = 2T_m$ to illustrate that the operator is not able to keep the slave in contact with the environment.

the master receives a significant force $F_e \neq 0$ and is accelerated away from the environment. If the operator still tries to make contact with the environment, the same pattern repeats itself, usually with increasing amplitude. This phenomena is often described when performing physical experiments, but cannot be analyzed when the operator and environment dynamics are not explicitly included in the analysis, e.g., when they are considered as passive 1-port systems.

Induced master motion

An interesting analysis of the recoiling of the master device, termed *induced master motion*, is presented by Kuchenbecker and Niemeyer [64, 65]. Their analysis focusses on LTI systems without delays. Induced master motion is the motion of the master device caused by force feedback (thus by F_{mc}) rather than user intention. It "compromises the stability of a telerobot by allowing the force feedback signal to influence the slave's commanded position, creating an internal control loop that is unstable under high gain" [64]. To cancel the induced master motion, the authors propose to subtract the movement caused by F_{mc} from the originally transmitted master motion x_m. This subtraction is based on a superposition principle and is therefore only applicable to linear systems.

Based on the principle of induced master motion, Polushin et al. [107–109] developed a projection-based force reflection algorithm that can be used for nonlinear systems with communication delays and bounded activity of the operator. Their approach uses a small gain analysis and is based on the following question: "which forces does the human operator actually feel when (s)he interacts with a master device? The answer is almost tautological: the human operator feels the interaction forces between his/her arm and the master device. Specifically, the

force felt by the human operator is exactly the component of the external forces that is compensated during the interaction with the human hand. It is important to notice that, since this component of the external force is compensated, it does not generate the induced master motion" [108]. The authors propose to "decompose the reflected force into "interaction"and "momentum-generating" components, and attenuate the latter while applying the former in full." This is achieved by e.g. *projecting* the reflected force, i.e. F_e, on the applied operator force F_h and only implement on the master side the projected force

$$F_{mc} = -\operatorname*{sat}_{[0,1]} \left(\frac{F_e^\top F_h}{\max\left(|F_h|^2, \varepsilon\right)} \right) F_h. \tag{2.23}$$

The saturation prevents that the reflected force is larger in magnitude than the operator force, and ε is a small constant to prevent division by zero. Hence, using (2.23) prevents a recoiling of the master since the control force is limited by the applied operator force.

A drawback of the projection-based method of the form (2.23) is an odd perception of the environment. It is claimed that forces in other directions than the direction of F_h are "not immediately felt by the human operator" [108]. Components of the forces in directions tangential to the operator force are therefore not presented to the operator. This last step is a remarkable way of thinking. Instead of reflecting F_e in full, where the operator's applied force is a reaction to the reflected force, now the reflected force is a reaction to the operator's force. In other words, the teleoperator does not inform the operator, but the operator informs the teleoperator in which directions to inform him.

2.3.2 Position/Force-Force control

An interesting extension of the P-F architecture, at least in the undelayed situation, is the 3-channel PF-F architecture, where additionally also the operator force is transmitted to the slave side. This extra force signal can be interpreted as a feedforward signal when the slave is in free motion, while in the contact case it improves the reflected environment stiffness. Compared to the P-F architecture, it is shown in [139] using the LTI BEP approach that the PF-F architecture, without delays, has a larger range of system parameters that leads to stable in-contact operation. In the delayed case, stability of the PF-F architecture is analyzed in e.g. [5, 49], albeit for LTI systems that do not include transitions from free motion to contact. It is concluded in [5] that the PF-F architecture is best suited for heavy environments with large impedances, i.e. environments that can typically be found, e.g., in remote maintenance applications for nuclear fusion. Unfortunately, also the PF-F architecture can suffer from a recoiling of the master device when the slave makes contact with the environment.

An interesting form of the PF-F architecture, specifically proposed for larger delays, is considered in the *model mediated telemanipulation* architecture of [81]. Here, the master is connected to a proxy, a copy of the slave, and interacts with a virtual, possibly simplified, version of the remote environment. By interacting with the proxy, a violent recoiling of the master due to the delay can be prevented by designing a suitable update of the virtual environment. However, building and using a local model of the remote environment is only possible in well known and structured environments with limited moving components.

2.4 Stability and performance

The previous sections already addressed several techniques to analyze and guarantee stability of the teleoperator. Ideally, stability is analyzed for the delayed bilateral connection of the two (nonlinear) teleoperators, the presence of delays, the interaction of the slave with the (stiff) environment, the time-varying characteristics of the human arm, and the possibly active behavior of the human operator. Unfortunately, each of the techniques considered in the addressed literature focuses on only a few of these properties.

For example, one of the most popular analysis techniques for linear teleoperators is Llewellyn's two-port absolute stability criterium [75], which analyzes unconditional stability of the linear time-invariant (LTI) master-communication-slave 2-port system. The environment is only considered as a passive 1-port system, such that the impact of the slave with the environment cannot be analyzed. The BEP method [138] does include an environment model to reduce conservatism, but it assumes that the 1-port master-communication-slave-environment system is LTI (see [35]), therefore ignoring contact transitions. These transitions are included in [76], together with a range of operator and environment stiffnesses. The authors solve numerically a set of LMIs to obtain a robust 4-channel controller. Unfortunately, delays are not considered in this work.

Popular analysis techniques for nonlinear teleoperators, such as the Lyapunov-like functionals (2.15) and (2.18), used in the references mentioned in [94], also assume passivity of the environment. Transitions between free motion and contact are not included in the model, so persistent bouncing of the slave manipulator against the environment cannot be analyzed.

Apart from not addressing all properties affecting the stability and performance, some techniques consider a too large class of uncertainty. For example, if the operator and environment are considered as passive systems, then stability is analyzed for *any* passive system, including both infinitively stiff and very soft systems. Other examples are guaranteeing delay-independent stability and including all possible operator motions. The result is that the stability analysis becomes too conservative. The consequence is a reduction in performance, for example, due to a reduced strength of the bilateral coupling and/or the injection of a significant amount of local damping. An alternative and less conservative

approach is to monitor the amount of activity online and adapt the amount of injected damping based on the current need. This approach is known as Time Domain Passivity Control (TDPC).

Time-domain passivity control

The original TDPC was proposed to create a passive interaction with virtual environments [47]. In [117], this approach was applied to bilateral teleoperation. A Passivity Observer (PO) is used to monitor the incoming and outgoing energy flows of components of the teleoperator. Passivity is guaranteed by means of variable damping injection with a so-called Passivity Controller (PC). The advantage of this approach is that damping is only injected when passivity tends to get lost. As a result, performance is improved compared to schemes that require constant damping injection.

The approach was extended to include time delays in [12] by incorporating an energy reference algorithm. This algorithm uses a forward and backward PO to determine the energy present in the communication channel. Two local PCs are responsible for maintaining passivity according to the PO at the local side. Two other extensions of the TDPC are the passive coupling between the continuous and discrete domains [13], and the separation of the energy interaction into an incoming and outgoing energy flow [118]. In the latter case, energy packets are send to the other side, making the approach robust to time-varying delays. The combination of all these approaches can be found in the algorithm described in [116]. An extension towards a 4-channel architecture is presented in [111].

Two-layer architecture

With the TDPC approach passivity is guaranteed independent of the control architecture used to achieve performance. The PO and PC monitor and regulate passivity of the teleoperator. Using a two-layer approach, in combination with energy storage tanks to represent the energy available for the controllers, the separation between passivity and transparency is made explicit by Franken et al. in [40, 41].

In the hierarchical top layer, called the Transparency Layer (TL), an algorithm is implemented that is responsible for achieving the desired performance. This could be any of the architectures discussed in the previous sections (e.g., P-P, P-F, or wave variable schemes). In the lower layer, called the Passivity Layer (PaL), passivity of the teleoperator is enforced. The main difference of this approach with the TDPC is the explicit use of energy tanks to guarantee passivity. The energy tanks represent the amount of stored energy that can be used to apply the control action coming from the TL. When a tank is empty, there is no energy to implement the required local control action coming from the TL and the control action is cut-off. The energy to fill *both* tanks is obtained from the operator by injecting a variable amount of damping on the master side.

The amount of energy subtracted from the operator is regulated by the Tank Level Control (TLC) and depends on a desired energy level in the tanks, and the energy protocol used to distribute (synchronize) the energy over the two tanks. The distribution of energy is required, since the operator is considered as the only active element of the teleoperator system, and therefore needs to provide *both* tanks with energy.

It must be stressed that while both online energy control concepts offer a less conservative technique to stabilize the delayed teleoperator, they do not directly offer a solution for bouncing behavior of the slave against the environment, contact instability, or recoiling of the master device. Nevertheless, it is experimentally shown in [40] that using the variable damping gain contributes to stabilizing and the impact by significantly reducing the impact oscillations.

2.5 Haptic shared control

All previously mentioned architectures focus on obtaining optimal transparency. This is mainly because for transparency clear performance metrics exist to help control engineers in designing controllers. But perfect transparency is not always required for the operator to complete a task. In [69], Lawrence already rose the question "What degree of transparency is necessary to accomplish a given set of teleoperation tasks?" As mentioned in Section 2.1.4, [17,137] report a saturation effect on the task performance for increasing levels of transparency.

A completely different approach, which does not focus on achieving transparency, but instead on improving task performance, is Haptic Shared Control (HSC) [101]. In HSC, the goal is to improve the *task performance* by presenting the operator with additional haptic cues. These cues are obtained by processing information coming from different sensors and assist the operator in performing tasks like obstacle avoidance and guiding the operator in a peg-in-hole task.

HSC has been developed for various tasks, such as car driving [1], subsea robotics [66] and nuclear maintenance [18], and can be designed separately from the architecture used to provide transparent forces. HSC can be classified in passive and active guidance [2]. An example of passive guidance are virtual fixtures, as presented in e.g. [3, 115]. These virtual fixtures can be designed as forbidden regions, e.g., a virtual wall through which the master is not allowed to penetrate, or haptic potential fields around obstacles. Active guidance is presented in e.g. [4], where the operator is presented with guiding forces that actively push the master towards an optimal path. Both types of HSC depend on the available knowledge of the operator, environment and task at hand. Erroneous information could lead to wrong guidance to the operator, so when designing HSC it is important that the HSC forces can be overruled by the operator.

2.6 Discussion

Controlling a bilateral teleoperator is a challenging task due to the nonlinear manipulator dynamics, the need to interact with (stiff) environments, transitions between the free motion and contact phases, the time-varying operator dynamics and the active behavior of the operator. When the communication channel is subject to delays, this affects the stability of the teleoperator and, with current approaches, the performance is sacrificed drastically.

After separating bilateral motion synchronization and direct force reflection architectures it is observed that the majority of the approaches reported in the literature focuses on the former approach. In bilateral motion synchronization, the coupling strength depends on the gains of both motion feedback controllers. These architectures suffer from a reflection of the slave dynamics and a limited reflection of the environment stiffness. The communication delay affects stability in bilateral motion synchronization in both free motion and contact. Achieving position tracking, using either wave variables or damping injection schemes, results in a trade-off between a reduction in the reflected stiffness or a constant amount of damping injection. Both influence the performance significantly.

Surprisingly, almost all of the existing literature on bilateral motion synchronization focus on solving position tracking problems and reducing the amount of damping, but reducing the delay-induced forces is almost never addressed. It seems that these delay-induced forces can only be reduced with the use of predictors. But complete elimination is not possible, since that would require exact knowledge of the future interaction of the operator and environment with the teleoperator, such that the delay-induced forces remain.

For good force reflection, a stiff connection between master and slave is required. But if this comes at the price of significant delay-induced forces, it is at least questionable if a bilateral motion synchronization approach must be considered at all!

Direct force-reflection has received much less attention, especially in delayed teleoperation. These architectures do not suffer from delay induced forces, since only the environment force is reflected and usually no motion feedback terms are present in the master controller. Even in the delay case, stability in free motion of the slave is guaranteed due to the unilateral structure of the architecture. In contact, the scheme switches to a bilateral architecture and the environment properties are directly reflected to the operator. But since the dynamics between free motion and contact differ significantly, controlling the impact of the slave with the environment is more crucial compared to bilateral synchronization schemes. When affected by communication delays, a commonly reported drawback of the force reflection schemes is a ‘violent recoiling’ of the master device that usually results in the operator being unable to keep the slave in contact with the environment.

To deal with this problem, an often proposed solution is to reduce the force reflection gain. This results in a poor perception of the environment and therefore this reduced-force-reflection scheme is reported to give poor performance. The author of this thesis is of the opinion that a lack of (nonconservative) analysis tools and a proper understanding of the switching behavior in the context of bilateral teleoperation is the main reason for the poor performance. A surprisingly limited amount of publications for bilateral teleoperation take the switching into account explicitly and are able to analyze the bouncing of the slave against the environment. Such an analysis is key in providing stable and even bounceless impact with the environment.

Thus, after comparing bilateral motion synchronization with direct force reflecting teleoperation, the author believes that a direct force-reflecting architecture has more potential for delayed bilateral teleoperation. The latter scheme does not suffer from delay-induced forces or reflection of the slave dynamics, and in free motion of the slave, the delay does not affect stability. The often observed impact instability and recoiling of the master need to be acknowledged as caused by the switching of the dynamics between free motion and contact. Nonconservative tools are required for delay-dependent stability of switched systems, such that the full potential of these architecture can be exploited. These analytical tools are not yet fully developed. Therefore, a good alternative is to separate the performance- from stability requirements. A performance-oriented controller can be implemented in one layer of the controller and, by monitoring online the energy exchange between components of the teleoperator, active behavior can be detected and passivity can be guaranteed in a second layer by injecting a variable amount of damping based on the actual need. Additionally, Haptic Shared Control forces can be implemented to assist the operator and improve the task performance.

In the next chapter, several bilateral motion synchronizing and direct force-reflecting architectures are implemented on an experimental setup to compare, as a function of the delay, the transparency and operator effort that can be achieved in practice.

Chapter 3

An experimental comparison of control architectures for delayed bilateral teleoperation

3.1 Introduction

In the previous chapter, an overview of different control architectures for delayed bilateral teleoperation was presented. There, a distinction was made between architectures aiming at either bilateral motion synchronization (Section 2.2) or direct force-reflection (Section 2.3). In the presence of delays, the former architectures suffer from delay-induced forces in free motion, whereas in the latter schemes the master can recoil when the slave makes contact with a stiff environment. In general, the stability of the teleoperator is affected more for increasing values of the delay. For both type of architectures, the common approach to guarantee stability is to locally inject damping, lower the controller gains, or apply both options at the same time. Both injecting damping and lowering the controller gains have a negative effect on the performance (measured in terms of, e.g., accuracy in the motion synchronization and force reflection). However, for increasing values of the delays the amount and kind of loss in performance are different for each architecture. A good understanding on how the performance is affected by the delays is therefore key when designing high performance controllers. Obtaining this understanding is the purpose of this chapter.

The comparison between different control architectures for teleoperation, presented in this chapter, is not new. Several researchers have compared different architectures using ad hoc performance criteria designed to quantitatively capture several aspects of performance. In [69], Lawrence analytically compared a

P-P, P-F and a 4-channel architecture on transparency (i.e. force tracking and impedance reflection in the contact phase). Considering the trade-off between stability and passivity, it was concluded that for the delay-free case "a proper use" of all 4 channels provides the best performance "in the sense of accurate transmission of task impedances to the operator" [69]. In [48], an analysis is presented in which the effect of communication delays is investigated. Several 2-channel architectures are compared with the 4-channel controller on the transmittable range of impedances (Z-width). It was concluded that the 2-channel architectures suffer less from a performance degradation for increasing delays than a 4-channel controller, but the use of both position and force information yields the best performance. In [11], ten different controllers are compared on motion tracking, perceived inertia and damping in free motion, and reflected stiffness and position drift in the contact phase. Each architecture was thoroughly analyzed, both analytically and in simulation, but the authors did not arrive at a specific conclusion.

A general drawback of analytical studies is that they do not include the practical limitations such as measurement noise, limited encoder resolution, sampling time and drive-train imperfections, such as friction (both static and dynamic) and compliancy. These limitations also affect the performance that can be achieved in practice and should therefore be included in the analysis, as done in, e.g., [7,14,113,121]. In [121], it is illustrated that, in a palpation task with soft tissue, a P-F architecture yields a better sensitivity of the transmitted impedance to changes in the environment (called fidelity) than a P-P controller. In [7], a P-P, P-F and a 4-channel architecture are compared. There, the 4-channel controller performs best in terms of free motion position tracking, impedance reflection and force tracking, thereby confirming Lawrence's analytical results. Unfortunately, delays are not included in the analysis of [7, 121]. Delays are instead included in the comparison of 2-channel architectures presented in [14]. The authors conclude that the use of force data improves the transparency of the teleoperator. Rodríguez-Seda et al. [113] use 18 subjects to analyze the effect of data loss on the stability and transparency for both constant and time-varying delays. They conclude that loss of data is less critical compared to the effect of time delays. However, only bilateral motion synchronizing architectures (mainly using wave variables) are analyzed and schemes that use force information explicitly are not included. To the best of the author's knowledge, an extensive experimental comparison of both bilateral motion synchronization and direct force-reflection architectures, as a function of the communication delays, has not yet been reported.

In this chapter, six architectures are compared experimentally on a variety of performance metrics using a 1-DOF setup. The selected architectures cover both bilateral motion synchronization and direct force-reflecting architectures, thus representing a broad range of existing controllers. Considering the inherent trade-off between stability and performance, the main goal of this chapter is to

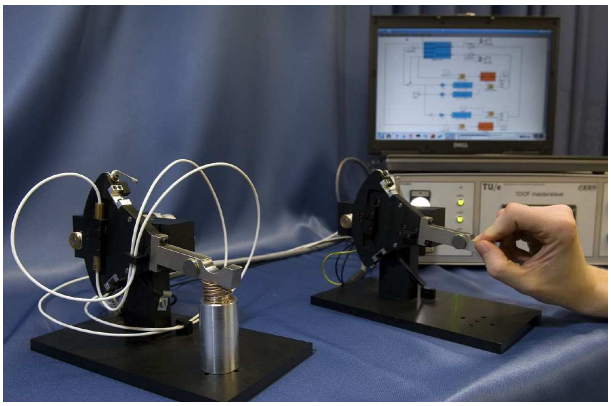

Fig. 3.1. 1-DOF experimental setup (image taken from [50]).

illustrate the differences in behavior and performance that can be achieved, as a function of the delay, with bilateral motion synchronization and direct force-reflection architectures. It is not the author's intention to compare advanced controllers on optimal performance, but rather to provide insight in the consequences of specific controller design choices.

The experimental comparison is performed, similar to the above mentioned studies, for the free motion and contact phase considered separately. In free motion of the slave, the analyzed performance criteria are motion tracking and operator effort. In contact of the slave with a stiff environment, the force tracking and reflected stiffness are analyzed. Using these metrics, a clear distinction in performance is obtained for the two classes of controllers. Specifically, under the conditions studied, direct force-reflecting architectures suffer less from a performance degradation caused by communication delays.

This chapter is organized as follows. Section 3.2 introduces the 1-DOF setup on which the comparison is performed. Section 3.3 discusses the experimental design and performance metrics used in the analysis. The considered controllers and tuning of their parameters are discussed in Section 3.4. The results are presented and analyzed in Section 3.5 and a discussion follows in Section 3.6.

3.2 The experimental 1-DOF setup

The experiments conducted in this work are performed on the two identical 1-DOF revolute master and slave devices, depicted in Fig. 3.1. A schematic drawing is shown in Fig. 3.2. Each device is actuated with a Maxon RE 35 DC servo motor ①, which drives the rotational segment ③ of the device with a capstan drive ②. The rotation of the motor is measured with an incremental encoder, having a resolution of $2.1 \cdot 10^{-5}$ rad. The capstan drive has a reduction

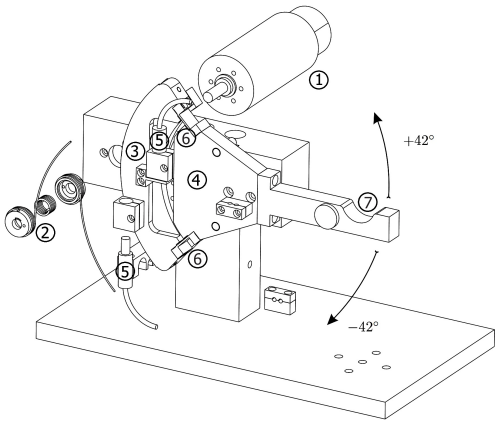

Fig. 3.2. Schematic drawing of the 1-DOF experimental setup (picture taken from [50]).

of 1/10 and results in a resolution of $2.1{\cdot}10^{-6}$ rad for the rotational segment ③. This rotational segment has an operating range from -42° to 42 °, with 0° being the horizontal configuration. The operator or environment can interact with the end-effector ⑦, which is located at 7.5 cm from the point of rotation on the other side of this segment. The torque applied by the motor on the end-effector is limited to 1.5 Nm.

The rotational segment is split in two concentric parts, i.e. ③ and ④ in Fig. 3.2. These are connected by two short and thick leaf springs ⑥, having a nominal torsional stiffness of $3.5{\cdot}10^{3}$ Nm/rad [50]. The torque transmitted through the leaf springs is measured indirectly with two inductive sensors ⑤ that measure the relative rotation between the inner and outer segment. The maximum difference in rotation is in the order of 100 μm. The resolution of the torque measurements is $5.25 \cdot 10^{-4}$ Nm.

All experiments performed in this chapter are sampled at 2 kHz. The position measurements are filtered with a first-order lowpass filter with a cut-off frequency of 80 Hz. Velocity signals are obtained by numerically differentiating the filtered position signals. The torque signals are filtered with a first-order lowpass filter with a cut-off frequency of 30 Hz to reduce the measurement noise.

Terminology. Although the setup considered in this study consists of two devices with only revolute joints, in this chapter the *rotations and torques* are usually denoted by *positions and forces*. No confusion should occur, since in this chapter all quantities are in rotational units.

3.3 Experimental design and evaluation

This section first describes the design of the experiments and then the metrics used to analyze the performance of the controllers.

3.3.1 Experimental design

In total, 6 different control architectures (described, later on, in Section 3.4) are compared for 6 different communication delays. The delays between the master and slave devices are selected as $T_m = T_s \in \{0, 5, 10, 20, 35, 50\}$ ms. The 50 ms delay (100 ms round-trip delay) corresponds to a delay between the Netherlands and Japan over a backbone internet connection.

The evaluation of the performance of a specific controller-task-delay combination is highly affected by the manipulation capabilities of the human operator. For a fair comparison of the *controller* performance it is required that each of the 36 conditions is performed with an identical operator input. To cancel out variations in the results due to, e.g., learning effects, operator fatigue, variability between trials and variability between operators, it is decided not to perform the comparison with human operators. Instead, a *virtual* operator is modeled and implemented in software to achieve the desired consistency in the results.

The main goal of this comparison is to analyze the effect of communication delays on the controller performance. To this end, two sets of experiments are conducted to analyze the performance of the free motion and contact phases considered separately. The description of these experiments is discussed in detail below.

Free motion

During free motion, the virtual operator performs a positioning task by moving the master device according to a desired profile $q_d(t)$. Based on an identification in [77] of the interaction between a human operator and the 1-DOF setup described in Section 3.2, the virtual operator is modeled as

$$\tau_h = LP(s)\left(k_h(q_d(t) - q_m) + b_h(\dot{q}_d(t) - \dot{q}_m)\right) + m_h\ddot{q}_d(t), \tag{3.1}$$

where $k_h = 8$ Nm/rad and $b_h = 0.12$ Nms/rad correspond to a slightly firm grasp. The acceleration feedforward term $m_h\ddot{q}_d(t)$ represents the operator's internal model of the system. Consequently, m_h is selected as $m_h = 18 \cdot 10^{-3}$ kg/m^2. This value is close to the identified inertia of $20 \cdot 10^{-3}$ kg/m^2. The low-pass filter $LP(s)$, having a cut-off frequency of 10 Hz, represents to operator's limited capabilities to apply a high frequency force profile despite his intention and sensing capabilities.

The free motion task considered in this comparison consists of a sine-sweep with 0.3 rad amplitude and frequencies going from 0.1 to 1 Hz. The resulting

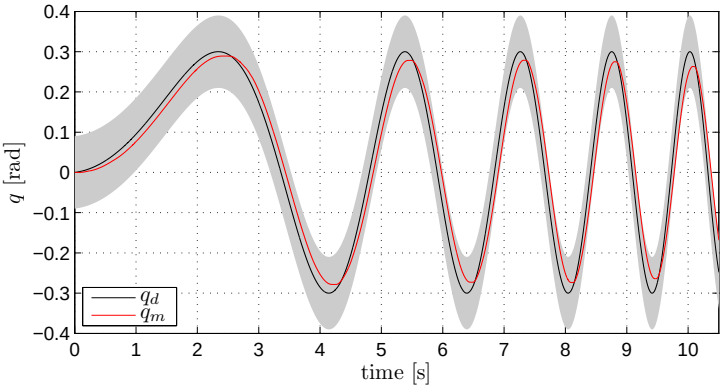

Fig. 3.3. Free motion desired operator trajectory $q_d(t)$ and the master position q_m (red line) from experiments with a PDd controller and $T_m = T_s = 50$ ms delay. The band of 0.09 rad (30% of the largest amplitude of $q_d(t)$) on both sides of $q_d(t)$ is indicated with the grey area.

desired operator trajectory $q_d(t)$, used in the operator model (3.1), is shown in Fig. 3.3. During all free motion experiments, the virtual operator torque τ_h, computed by (3.1), is added to the torque measured by the torque sensor.

Contact

During the contact experiments, the slave is positioned against an aluminium cylinder and does not break contact. The stiffness of the environment is much higher than the total stiffness of the drive-train of the setup. The contact task consists of an applied torque profile, which increases from 0 Nm to about 0.7 Nm in 3 s, followed by a 6 s constant torque phase and a decrease of the torque back to 0 Nm in 4 s. This torque profile, which is depicted in Fig. 3.4, is recorded from a contact experiment performed by a human operator. It is used as the torque applied by the virtual operator during all contact experiments and the profile is added to the measured operator torque.

3.3.2 Performance metrics

Many different metrics are used in the literature to evaluate the performance of controllers for bilateral teleoperation. The metrics used in this comparison are similar to the ones used in [7,11,113] to evaluate performance in the free motion and in contact phase.

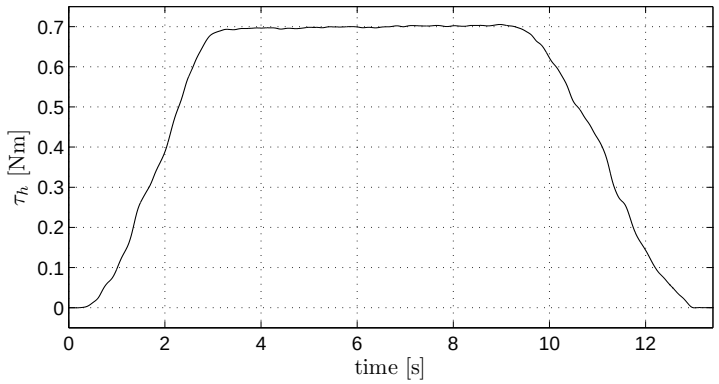

Fig. 3.4. Applied operator torque τ_h during the contact experiments.

Free motion

In free motion, the main goal of the controller is to make the slave follow the motion of the master. The position tracking is typically described by the motion tracking error $q_m(t) - q_s(t)$. For comparison purposes it is easier to describe the tracking performance by a single metric. This is achieved by computing the root mean square (RMS) value of the tracking error, i.e.

$$\Delta q_{RMS} := \sqrt{\frac{T_{samp}}{t_f - t_0} \sum_{k=t_0}^{t_f} \Big(|q_m(k) - q_s(k)|^2 \Big)} \tag{3.2}$$

with $T_{samp} = 5 \cdot 10^{-4}$ s the sampling time, t_0 the start of the experiment and t_f the end of the experiment.

In the presence of delays, the position of the master q_m is transmitted to the slave controller at time t, but arrives T_m seconds later. Because q_m is not directly available on the slave side, a second motion tracking metric is defined related to the motion tracking error $q_m^{T_m} - q_s$ present in the slave controller

$$\Delta q_{RMS}^{T_m} := \sqrt{\frac{T_{samp}}{t_f - t_0} \sum_{k=t_0}^{t_f} \Big(|q_m(k - T_m) - q_s(k)|^2 \Big)}. \tag{3.3}$$

Although interesting, as the results in Section 3.5 illustrate, this metric, to the best of the author's knowledge, has not been used explicitly in previously reported comparison studies.

Apart from motion tracking, it is important to include in the performance evaluation the operator's effort to manipulate the teleoperator. If the effort to

move the teleoperator is too high, this could lead to fatigue. Moreover, the operator might not feel the impact of the slave with the environment. For the free motion experiments, the operator effort is described by the RMS value of the torque τ_h applied by the operator

$$\tau_{h,RMS} := \sqrt{\frac{T_{samp}}{t_f - t_0} \sum_{k=t_0}^{t_f} \Big(|\tau_h(k)|^2 \Big)}. \tag{3.4}$$

Remark 3.1. This metric is related to the evaluated unconstrained movement impedance in [7] and the damping and inertia perceived in free motion in [11]. The operator effort was not analyzed in the experimental comparison performed in [113].

Contact

A key requirement for a transparent teleoperator (see Section 2.1 for a definition of transparency) is that the operator torque τ_h is applied on the environment, and that the environment torque τ_e is reflected to the operator. Therefore, the torque tracking error $\tau_h + \tau_e$ is evaluated (note the plus-sign, which corresponds to the sign definition of τ_e presented in Section 2.1). The contact task consists of parts where the torque applied by the virtual operator increases or decreases (the dynamic part), and a part where it is kept constant (the static part). Consequently, two metrics are used to analyze the torque tracking error $\tau_h + \tau_e$, namely

$$\Delta\tau_{RMS} := \sqrt{\frac{T_{samp}}{t_f - t_0} \sum_{k=t_0}^{t_f} \Big(|\tau_h(k) + \tau_e(k)|^2 \Big)}, \tag{3.5}$$

$$\Delta\tau_{RMS,ss} := \sqrt{\frac{T_{samp}}{t_{f,ss} - t_{0,ss}} \sum_{k=t_0}^{t_f} \Big(|\tau_h(k) + \tau_e(k)|^2 \Big)}. \tag{3.6}$$

The former metric evaluates the performance over the whole contact experiment. Using $t_{0,ss} = 6$ s and $t_{f,ss} = 9$ s, which represent the start and end of the steady-state window of the static interval, $\Delta\tau_{RMS,ss}$ describes the performance during the static phase only. Unlike the metrics (3.2) and (3.3), no difference was observed when using either τ_h or $\tau_h^{T_m}$ in (3.5) or (3.6). Therefore, only metrics with τ_h are considered here.

Apart from synchronizing τ_h and τ_e, the controller should properly reflect the stiffness of the environment to the operator. For contact with a rigid environment, the stiffness reflected to the operator is similar to the stiffness of the teleoperator. The performance metric of the teleoperator stiffness is the RMS value of the ratio of the applied operator torque τ_h and the position difference

$q_m - q_s$ between the master and slave. Similar to the torque synchronization, the reflected stiffness is analyzed for both the whole experiment (S_{RMS}) and the static part only ($S_{RMS,ss}$)

$$S_{RMS} := \sqrt{\frac{T_{samp}}{t_f - t_0} \sum_{k=t_0}^{t_f} \left(\left| \frac{\tau_h(k)}{q_m(k) - q_s(k)} \right|^2 \right)}, \tag{3.7}$$

$$S_{RMS,ss} := \sqrt{\frac{T_{samp}}{t_{f,ss} - t_{0,ss}} \sum_{k=t_0}^{t_f} \left(\left| \frac{\tau_h(k)}{q_m(k) - q_s(k)} \right|^2 \right)}. \tag{3.8}$$

Remark 3.2. Although the end-effector of the slave remained constant during the experiments, a position difference of $14{\cdot}10^{-4}$ rad (corresponding to about 190 encoder ticks) is measured by the encoder on the motor shaft due to the finite stiffness of the slave.

3.4 Control Architectures

The six controllers used in the experimental comparison are introduced in this section. They are selected to cover a wide range of architectures that have been proposed in the literature. For example, four controllers aim at bilateral motion synchronization, whereas two are direct force-reflecting architectures. Furthermore, three of the schemes use only motion information of the master and slave, whereas the other three use also torque information regarding the interaction of the teleoperator with the environment and operator. Finally, two of the schemes use wave variables to guarantee passivity of the teleoperator, whereas the other four require the injection of damping in the presence of delays. The following subsections introduce the selected controllers in more detail.

Proportional-derivative-plus-damping architecture (PDd)

The bilateral motion synchronizing PD-plus-damping (PDd) architecture, proposed in, e.g., [96], is extensively discussed in Section 2.2.3. The controller is

$$\tau_{ic} = k_{pi}(q_j^{T_j} - q_i) + k_{di}(\dot{q}_j^{T_j} - \dot{q}_i) - B_i\dot{q}_i \tag{3.9a}$$

with $i \in \{m, s\}$, $j \in \{m, s\}$, $j \neq i$, k_{pi} the proportional gain, k_{di} the derivative gain and B_i the local damping gain. According to [96], these gains should satisfy the inequality (2.16) to guarantee stability.

Wave variable architecture (W)

Many wave variable (W) architectures have been proposed in the literature. Here, the original symmetric architecture with impedance matching, to eliminate

wave reflections, is considered. This bilateral motion synchronizing scheme is extensively discussed in, e.g., [91, 92]. The master and slave controller are

$$\tau_{ic} = k_{pi} \int_{t_0}^{t} (\dot{q}_{id} - \dot{q}_i)\, d\sigma + k_{di}(\dot{q}_{id} - \dot{q}_i). \tag{3.10}$$

The desired velocity signals $\dot{q}_{id}$ are decoded from the wave variables as

$$\dot{q}_{md} = \frac{1}{b_w}\tau_{mc} - \sqrt{2b_w}v_m, \qquad \dot{q}_{sd} = \sqrt{2b_w}u_s - \frac{1}{b_w}\tau_{sc}, \tag{3.11}$$

where b_w is the wave impedance, and v_m and u_s are the wave variables received at the master and slave side. These are related via (2.13) to the transmitted wave variables

$$u_m = \sqrt{2b_w}\tau_{mc} - v_m, \qquad v_s = \sqrt{2b_w}\tau_{sc} - u_s. \tag{3.12}$$

Note that due to the transmission of velocities no position information is used in the controller. The scheme is stable for any delay, but asymptotic position tracking is not guaranteed. Wave reflections are eliminated by selecting $b_w = k_{di}$, which, after rewriting the above equations, results in [85]

$$\dot{q}_{id} = \frac{1}{2}\left(\dot{q}_j^{T_j} + \dot{q}_i\right). \tag{3.13}$$

Thus, unlike the PDd controller, the desired velocity signal $\dot{q}_{id}$ used in the controller (3.10) is not equal to $\dot{q}_j^{T_j}$. Instead, half of the desired velocity $\dot{q}_{id}$ depends on $\dot{q}_i$, the current velocity of the same device.

Wave variable architecture with position tracking (Wt)

A symmetric wave variable architecture with asymptotic position tracking (Wt) is presented in, e.g., [85]. This scheme is a hybrid form of the PDd and W architectures and also aims at bilateral motion synchronization. Wave variables are used to transmit velocity signals only, whereas position commands are transmitted directly. Local damping injection is required to guarantee stability in the presence of delays. The controllers are given by

$$\tau_{ic} = k_{pi}(q_j^{T_j} - q_i) + \underbrace{k_{di}(\dot{q}_{id} - \dot{q}_i)}_{=:\tau_{ict}} - B_i\dot{q}_i. \tag{3.14}$$

The desired velocities $\dot{q}_{id}$ are obtained from

$$\dot{q}_{md} = \frac{1}{b_w}\tau_{mct} - \sqrt{2b_w}v_m, \qquad \dot{q}_{sd} = \sqrt{2b_w}u_s - \frac{1}{b_w}\tau_{sct}, \tag{3.15}$$

where v_m and u_s are obtained via (2.13) from the transmitted wave variables

$$u_m = \sqrt{2b_w}\tau_{mct} - v_m, \qquad v_s = \sqrt{2b_w}\tau_{sct} - u_s. \tag{3.16}$$

According to [32, 85, 94], stability is guaranteed if the control parameters satisfy the bound

$$k_{pm}k_{ps}(T_m^2 + T_s^2) < 2B_mB_s. \tag{3.17}$$

Position-Force architecture (P-F)

The P-F architecture is the most basic direct force-reflecting architecture. It is unilateral when the slave is in free motion, whereas in the contact phase the slave-environment interaction force is reflected directly. The corresponding controller is

$$\tau_{mc} = -\tau_e^{T_s} - B_m\dot{q}_m \tag{3.18a}$$
$$\tau_{sc} = k_{ps}(q_m^{T_m} - q_s) + k_{ds}(\dot{q}_m^{T_m} - \dot{q}_s) - B_s\dot{q}_s. \tag{3.18b}$$

The local damping term B_i is used to help prevent a recoiling of the master when the slave makes contact with the environment.

Position/Force-Force architecture(PF-F)

The PF-F architecture is an extension of the P-F architecture and is given by

$$\tau_{mc} = -\tau_e^{T_s} - B_m\dot{q}_m \tag{3.19a}$$
$$\tau_{sc} = \tau_h^{T_m} + k_{ps}(q_m^{T_m} - q_s) + k_{ds}(\dot{q}_m^{T_m} - \dot{q}_s) - B_s\dot{q}_s. \tag{3.19b}$$

Compared to (3.18), also the operator torque τ_h is transmitted to the slave side. This improves the motion tracking and reflected contact stiffness [139]. Similar to the P-F controller, the local damping term B_i is used to prevent a recoiling of the master.

4-Channel architecture (4C)

The last architecture is the 4-channel (4C) controller. This controller is given by

$$\tau_{mc} = -\tau_e^{T_s} + k_{pm}(q_s^{T_s} - q_m) + k_{dm}(\dot{q}_s^{T_s} - \dot{q}_m) - B_m\dot{q}_m \tag{3.20a}$$
$$\tau_{sc} = \tau_h^{T_m} + k_{ps}(q_m^{T_m} - q_s) + k_{ds}(\dot{q}_m^{T_m} - \dot{q}_s) - B_s\dot{q}_s. \tag{3.20b}$$

In the delay-free case this controller provides the best performance [69], but when subject to delays the 4-channel controller also suffers from delay-induced forces (see Section 2.2), thereby limiting the performance.

Tuning

A crucial requirement when designing and tuning a controller for bilateral teleoperation is that the teleoperator is stable in both free motion and contact.

Moreover, the torque applied by a human operator in free motion cannot be too high and he or she must be able to keep the slave in contact with the environment. Due to delay-induced forces, the free motion phase is the most critical for the PDd, Wt and 4C architectures, whereas the contact phase (in particular the impact and detachment phase) is the most crucial for the P-F and PF-F controllers.

The tuning of the controller parameters has a major influence on the performance that can be obtained. Recall that in this work it is by no means attempted to obtain optimal tuning for each presented controller-delay combination. Instead, the tuning illustrates the basic level of performance that can be achieved and highlights the differences between the considered architectures.

A strict procedure is maintained to tune the controller parameters of each architecture-delay combination. In this procedure, performance is sacrificed, if necessary, to guarantee stability during the free motion, impact and contact phases. In free motion, the operator effort is kept bounded by tuning the controllers for each delay such that for all t the master position q_m stays within 0.09 rad of the desired trajectory $q_d(t)$ (see the grey area in Fig. 3.3). Observe that 0.09 rad is 30% of the largest amplitude of $q_d(t)$. An example of a master position q_m that satisfies the requirement for the operator effort is shown in Fig. 3.3 for the PDd controller with $T_m = T_s = 50$ ms. Furthermore, all controllers are tuned such that, when operated by a human operator, the contact phase is stable and a recoiling of the master, due to the impact or detachment of the slave with the environment, does not occur.

In the tuning procedure, all architectures start with similar nominal parameter values for the delay-free case, namely $k_{pi} = 17$ Nm/rad, $k_{di} = 0.1$ and $B_i = 0$ Nms/rad. For the Wt architecture, the wave impedance $b_w = k_{di} = 0.1$ Nms/rad to eliminate wave reflections. Then, for increasing values of the delay, the parameters k_{pi} and B_i are adjusted to prevent instability, a high operator effort or a recoiling of the master. For each controller-delay combination, k_{pm} and k_{ps} are kept equal to prevent motion or force scaling. For each of the controllers, adjusting the parameters is done according to one of the following procedures.

a. The architectures PDd, Wt and 4C suffer from delay-induced forces in free motion. For increasing values of the delays, these architectures are tuned to limit the operator effort. Compared to the previous delay value, first the proportional gains k_{pi} are lowered such that q_m is within the 0.09 rad band of $q_d(t)$. The local damping gain is then selected to just satisfy (2.16) and (3.17) for the PDd- and Wt controller, respectively. For the 4C controller, the damping gains are tuned to guarantee stability during free motion, impact and contact.

b. The architectures P-F and P-FF require high damping gains to prevent a recoiling of the master. Using too high damping gains (larger than 0.3 Nms/rad for the 1-DOF setup) is not desired, so for all delays, even for $T_m = T_s = 0$ s,

Table 3.1. Control parameters used in the experimental comparison.

Scheme	Parameter	0 ms	5 ms	10 ms	20 ms	35 ms	50 ms
PDd	k_{pi} [Nm/rad]	17	17	13	7	4	3
	k_{di} [Nms/rad]	0.1	0.1	0.1	0.1	0.1	0.1
	B_i [Nms/rad]	0	0.032	0.055	0.061	0.061	0.068
W	k_{pi} [Nm/rad]	17	17	17	17	17	17
	k_{di} [Nms/rad]	0.1	0.1	0.1	0.1	0.1	0.1
	b_w [Nms/rad]	0.1	0.1	0.1	0.1	0.1	0.1
Wt	k_{pi} [Nm/rad]	17	15	11	5.5	3	2.5
	k_{di} [Nms/rad]	0.1	0.1	0.1	0.1	0.1	0.1
	b_w [Nms/rad]	0.1	0.1	0.1	0.1	0.1	0.1
	B_i [Nms/rad]	0	0.053	0.065	0.070	0.072	0.078
P-F & PF-F	k_{pi} [Nm/rad]	8	8	8	8	8	8
	k_{di} [Nms/rad]	0.1	0.1	0.1	0.1	0.1	0.1
	B_m [Nms/rad]	0	0.01	0.03	0.08	0.18	0.25
	B_s [Nms/rad]	0	0.01	0.01	0.02	0.06	0.10
4C	k_{pi} [Nm/rad]	17	17	17	17	11	8
	k_{di} [Nms/rad]	0.1	0.1	0.1	0.1	0.1	0.1
	B_m [Nms/rad]	0.01	0.01	0.01	0.01	0.01	0.01
	B_s [Nms/rad]	0.02	0.02	0.04	0.04	0.04	0.04

the proportional gains are selected as $k_{ps} = 8$ Nm/rad. The damping gains B_i are then tuned to prevent a recoiling when the teleoperator is operated by a real human.

c. The W architecture is less affected by delays. Therefore, $k_{pi} = 17$ Nm/rad is not altered.

The parameter values obtained from this tuning procedure for each controller-delay combination are presented in Table 3.1. For each combination, the same values are used in both the free motion and contact experiments.

3.5 Experimental results

The results of the free motion and contact experiments are presented in the following subsections. In both cases, first a few time plots are discussed to illustrate the differences in behavior before the actual performance metrics are

presented. After these results, conclusions are drawn regarding the experimental results.

3.5.1 Free motion

Time plots

An example of the desired operator signal $q_d(t)$, master position $q_m(t)$, slave position $q_s(t)$ and operator torque $\tau_h(t)$ of the free motion experiments are shown in Fig. 3.5 for the PDd, W, PF-F and 4C architectures and a delay of $T_m = T_s = 50$ ms. These plots illustrate the differences in behavior of the controllers on both motion tracking and operator effort. Only the first 7 seconds are shown to improve visibility. Obviously, the motion tracking decreases and the operator effort increases for the omitted higher accelerations of the last 3 s, compared to the first 7 s. In this plot, and all other time-plots, $q_d(t)$ is shown in black, the master position q_m and operator torque τ_h are depicted in red, and the slave position q_s and environment torque τ_e are presented in blue.

For the PDd architecture there is a visible lag between q_m and $q_d(t)$, and between q_s and q_m. This lag is mainly caused by relatively smal proportional gains k_{pi} due to the delay-induced forces resulting from the master PD-controller. Consequently, τ_h is relatively large and q_m and q_s have a smaller amplitude than $q_d(t)$. The response of the teleoperator with the Wt architecture is similar to the PDd results since the derivative action is small compared to the proportional action.

For $T_m = T_s = 50$ ms, the W architecture has the lowest operator torque since it does not suffer from delay-induced forces and the injection of damping injection not required. The slave position q_s clearly differs from the master position q_m around the position reversals. This is because in the W architecture velocity signals are used in the wave variables and, consequently, the controller lacks asymptotic position tracking properties. For low velocities the computed torques τ_{mc} and τ_{sc} are not large enough to overcome the static friction of the devices.

The operator torques for the P-F and PF-F profiles were identical, since in both cases τ_h is only affected by the injected damping. Due to τ_h in τ_{sc} of the PF-F controller, the slave follows the master motion accurately apart from the 50 ms delay. The motion tracking with the P-F architecture is not as good as with the PF-F scheme, but still better than with the PDd, W or Wt controllers.

The tracking error $q_m - q_s$ is the smallest for the 4C controller. Due to the use of τ_h in τ_{sc}, also q_s tracks the amplitude of $q_d(t)$ accurately, despite the high operator torques caused by the delay-induced forces. The operator torques look similar to those of the PDd and Wt controller, because for these architectures the controller gains were adjusted to bound the operator effort.

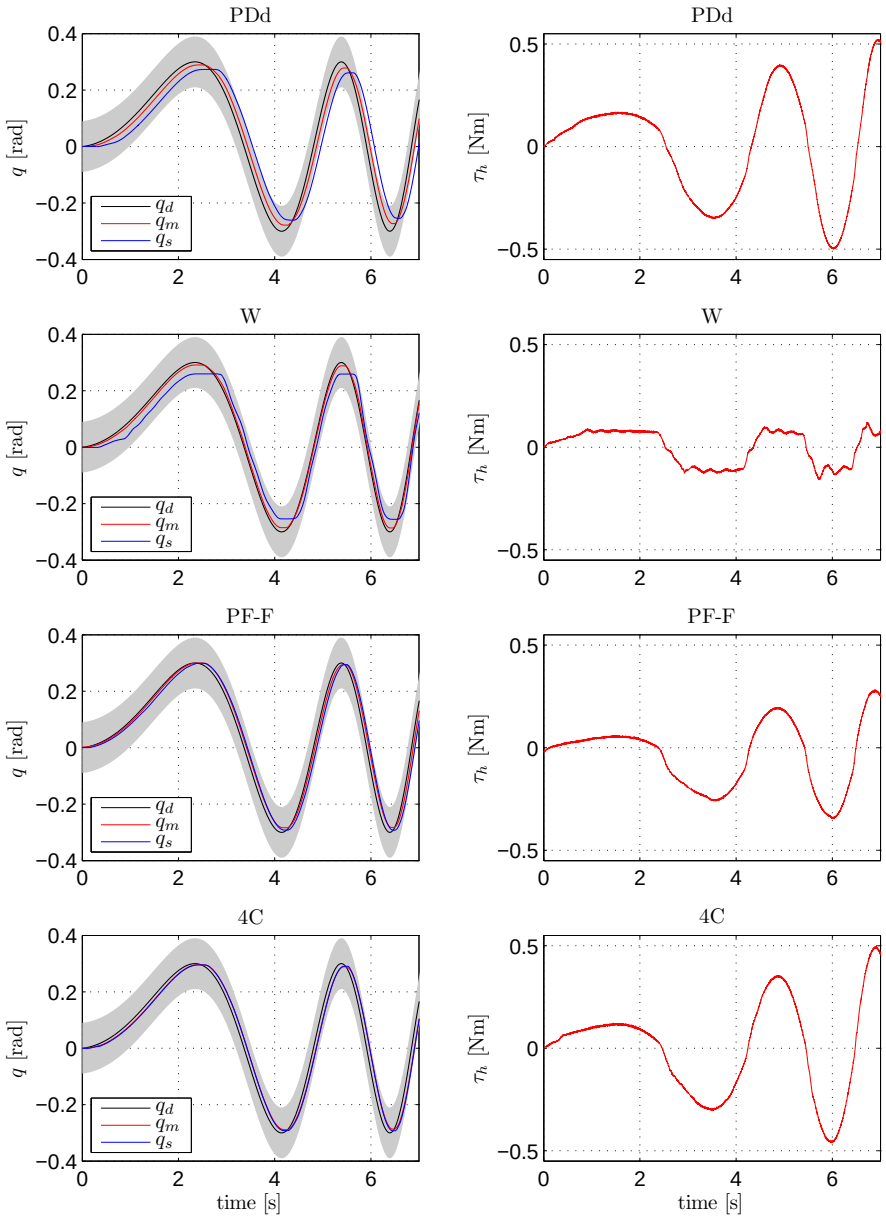

Fig. 3.5. Position and operator torque profiles of the PDd, W, PF-F and 4C architectures for the free motion experiments ($T_m = T_s = 50$ ms). The grey area represents the 30% band around $q_d(t)$.

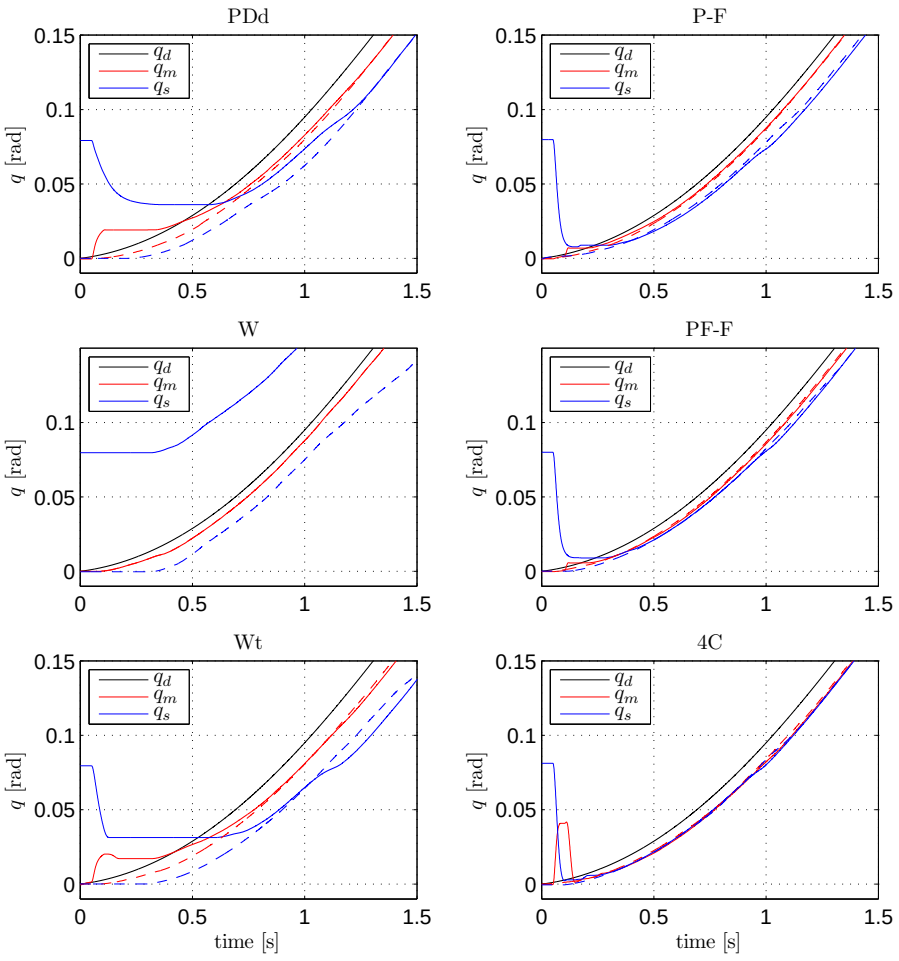

Fig. 3.6. Position profiles of two free motion experiments ($T_m = T_s = 50$ ms) with different initial positions for the slave.

For $T_m = T_s = 50$ ms, Fig. 3.6 shows the effect on the motion tracking and convergence of an initial offset in the master and slave positions. The dashed lines are obtained from experiments where the initial master and slave positions are identical, whereas for the solid lines the slave started with an offset of 0.08 rad compared to the master. In both experiments the same desired operator signal $q_d(t)$, defined in Fig. 3.3, is used. For the experiments with an initial position offset, the master position is initialized for the interval $\theta_i := [-T_i, 0)$ at $q_m(\theta_m) = 0$ rad, and the slave position is initialized at $q_s(\theta_s) = 0.08$ rad.

At time $t = 0$ s, the actual master and slave positions are transmitted. These signals arrive 50 ms later at the other side.

For all architectures except the W controller, which does not have asymptotic position tracking, do the master and slave positions converge to the same trajectories, independent of the initial positions. The convergence time is different per architecture and is related inversely proportional to k_{pi}.

For the PDd and Wt architectures, k_{pi} is relatively low, such that the convergence is relatively slow. Furthermore, the architectures PDd, Wt and 4C have motion feedback terms in both controllers. As a result, *both* the master and slave start to move to the *delayed* position of the other device after $t = 0.05$ s. Because the master device moves away from $q_d(t)$, the virtual operator reacts and increases τ_h to move q_m back to $q_d(t)$. In the 4C controller, this increased τ_h is transmitted to the slave and results in a larger initial slave movement compared to the PDd and Wt controllers. The master controllers of the P-F and PF-F controllers do not contain motion tracking terms. Therefore, the master position is barely affected by the initial position offset and the slave converges to the master position.

Motion tracking performance

Fig. 3.7 shows the performance results of the motion tracking errors of the 36 free motion experiments. The left plot depicts Δq_{RMS}, the RMS value of the tracking error $q_m - q_s$ computed by (3.2), whereas the right plots shows $\Delta q_{RMS}^{T_m}$, the RMS value of the tracking error $q_m^{T_m} - q_s$ computed by (3.3). In this plot, and all following figures showing RMS data, the blue lines represent the bilateral motion synchronizing architectures that do not use force information. The red lines represent the direct force-reflection schemes (plus 4C) that do use torque sensors. A solid line between two data points means that the controller gains are equal for the two subsequent delay cases, whereas a dashed line implies that the parameters are modified.

Both plots show that the motion tracking performance reduces (higher Δq_{RMS} and $\Delta q_{RMS}^{T_m}$) for increasing delays. This reduction is not only caused by the delay in receiving the position, torque or wave variables from the other side. For the PDd, Wt and, to a lesser extend, the 4C architecture the performance is also affected by the reduction of k_{pi} to prevent high operator efforts. For W the performance decrease is partly affected by the increasing difference of $\dot{q}_j^{T_j}$ and $\dot{q}_i$ in (3.13) for increasing delays. For the P-F and PF-F controllers the motion tracking performance is affected by the increase in injected damping for increasing delays.

When looking at Δq_{RMS}, it is observed that the 4C performs best, followed by PF-F. These architectures both use τ_h in the slave controller as a feedforward signal and this clearly improves the motion tracking performance. The performance of the 4C architecture seems most robust to delays, whereas the delays

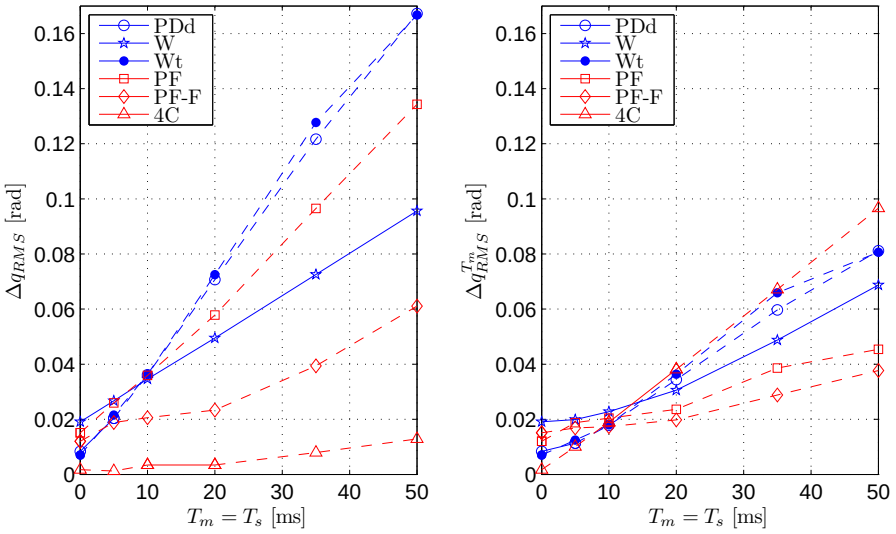

Fig. 3.7. RMS values of the free motion tracking errors as a function of the delay. The left plot shows Δq_{RMS}, defined in (3.2), whereas the right plot shows $\Delta q^{T_m}_{RMS}$, defined in (3.3).

affect the PDd and Wt the most.

When comparing the results of Δq_{RMS} with $\Delta q^{T_m}_{RMS}$, it is observed that the difference in performance of all controllers is smaller. The PDd and Wt controllers score better for $\Delta q^{T_m}_{RMS}$ due to the low gains k_{pi}. These gains are typically so low that the lag in tracking q_m by the slave is larger than T_m (see also Fig. 3.5), explaining the lower values of $\Delta q^{T_m}_{RMS}$. The W controller scores better for $\Delta q^{T_m}_{RMS}$, but the curve is no longer linear, which suggest that it might perform worse for even larger delays. The P-F and PF-F schemes perform best on $\Delta q^{T_m}_{RMS}$ since these are designed specifically to control the error $q^{T_m}_m - q_s$. Perhaps the most remarkable result is the performance of the 4C controller, since it is the worst of all architectures for 20 ms delay and higher. Adding motion synchronizing terms to the master controller, compared to the PF-F controller, clearly changes the goal of the controller, i.e. the motion tracking error that is controlled.

Operator effort

The RMS values $\tau_{h,RMS}$ of the operator effort are presented in Fig. 3.8. Apart from the W architecture the operator effort increases (higher $\tau_{h,RMS}$) for in-

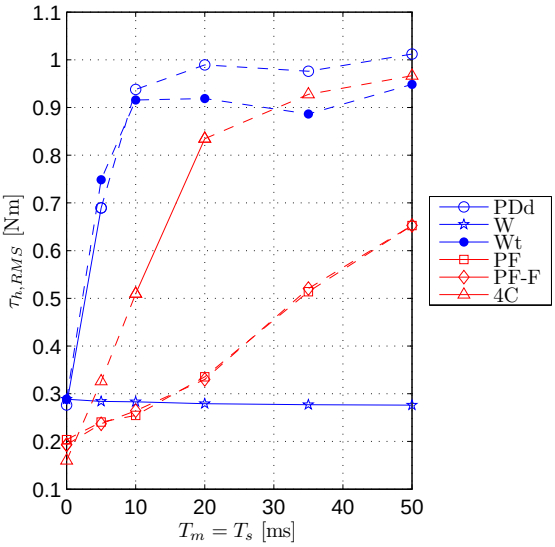

Fig. 3.8. RMS values of the free motion operator effort $\tau_{h,RMS}$, defined in (3.4), as a function of the delay.

creasing values of the delay. For the P-F and PF-F architectures the increase in operator effort is solely caused by the injected damping necessary to ensure stability. The master controllers are identical, such that, apart from measurement noise, the operator effort is identical.

For the PDd, Wt and 4C architectures the operator effort is mainly affected by the delay-induced forces. The saturation is the result of the tuning procedure: The gains k_{pi} are reduced to prevent that the master position exceeded the 0.09 rad band around $q_d(t)$. The saturated $\tau_{h,RMS}$ values represent the maximum allowable operator effort. Compared to PDd and Wt, the additional use of τ_h in τ_{sc} by the 4C controller reduces the motion tracking error and therefore also the operator effort. The difference in damping gains B_i has a smaller effect on the operator effort than the delay-induced forces. Lowering k_{pi} in the 4C controller reduces the delay-induced forces, but these forces would not vanish completely.

The operator effort for the W controller is unaffected by the delay. This controller does not have asymptotic position tracking properties. As a result, there are no delay-induced forces and the controllers gains could be kept equal for all W experiments.

3.5.2 Contact

Time plots

Examples of the experimental in-contact results are presented in Fig. 3.9 for $T_m = T_s = 50$ ms. The left column shows the measured master and slave positions, whereas the right column depicts the applied torque by the virtual operator and the interaction between the slave and environment. The response of the teleoperator for the omitted Wt and 4C architectures is similar to the response of the PDd and PF-F controllers, respectively. Theoretically, all architectures should be able to accurately reflect the environment torque to the operator during the static phase, i.e. $\tau_h = -\tau_e$. The observed deviation from $\tau_h = -\tau_e$ during the static phase and at the end of the experiments is of the same order for all architectures and is mainly caused by the static friction of the drive train. Therefore, the discussion below only focusses on the dynamic torque tracking and stiffness reflection.

The PDd controller has a lag larger than 50 ms of τ_e compared to τ_h. This is mainly caused by the relatively low gains k_{pi} and, to a lesser extend, by the injected damping. Since torque information is absent in the controllers, both τ_{mc} and τ_{sc} require a difference in the master and slave position to generate the requested torques. The maximum position difference of 0.225 rad for $\tau_h = 0.695$ Nm results in a perceived environment stiffness of 3.1 Nm/rad for the PDd controller. For the Wt architecture, the reflected stiffness equals 2.8 Nm/rad. In comparison, the reflected stiffness for $T_m = T_s = 0$ ms during the static part equaled 17 Nm/rad and 20.5 Nm/rad, respectively. These values are close to the proportional gains k_{pi}.

The torque tracking of the W architecture is comparable to that of the PDd and Wt controllers. The main distinction is the difference between the master and slave position in contact. The W controller has no asymptotic position synchronization, such that, despite the relatively high proportional gains k_{pi}, the reflected stiffness of 1.55 Nm/rad for $T_m = T_s = 50$ ms is the lowest of all architectures. Without delays, the reflected stiffness equals 8 Nm/rad.

For the P-F architecture, the reflected stiffness during the static phase equals 8.2 Nm/rad. This stiffness is independent of the delay, since $k_{ps} = 8$ Nm/rad for all delay cases. The most remarkable result is formed by the stairs in τ_e and q_m during the dynamic torque tracking. These stairs are not present in the zero delay case, but they increase in size for increasing values of the delay. The stairs are related to the start of a recoiling of the master due to a build-up of the slave-environment interaction force and the delay in the force reflection to the operator (see Section 2.3.1 for an elaborate description of the recoiling). The static friction in the slave device amplifies the sensitivity to the recoiling. However, a full recoiling is prevented by injecting a relatively high amount of damping.

For both the PF-F and 4C architectures, the torque tracking and reflected

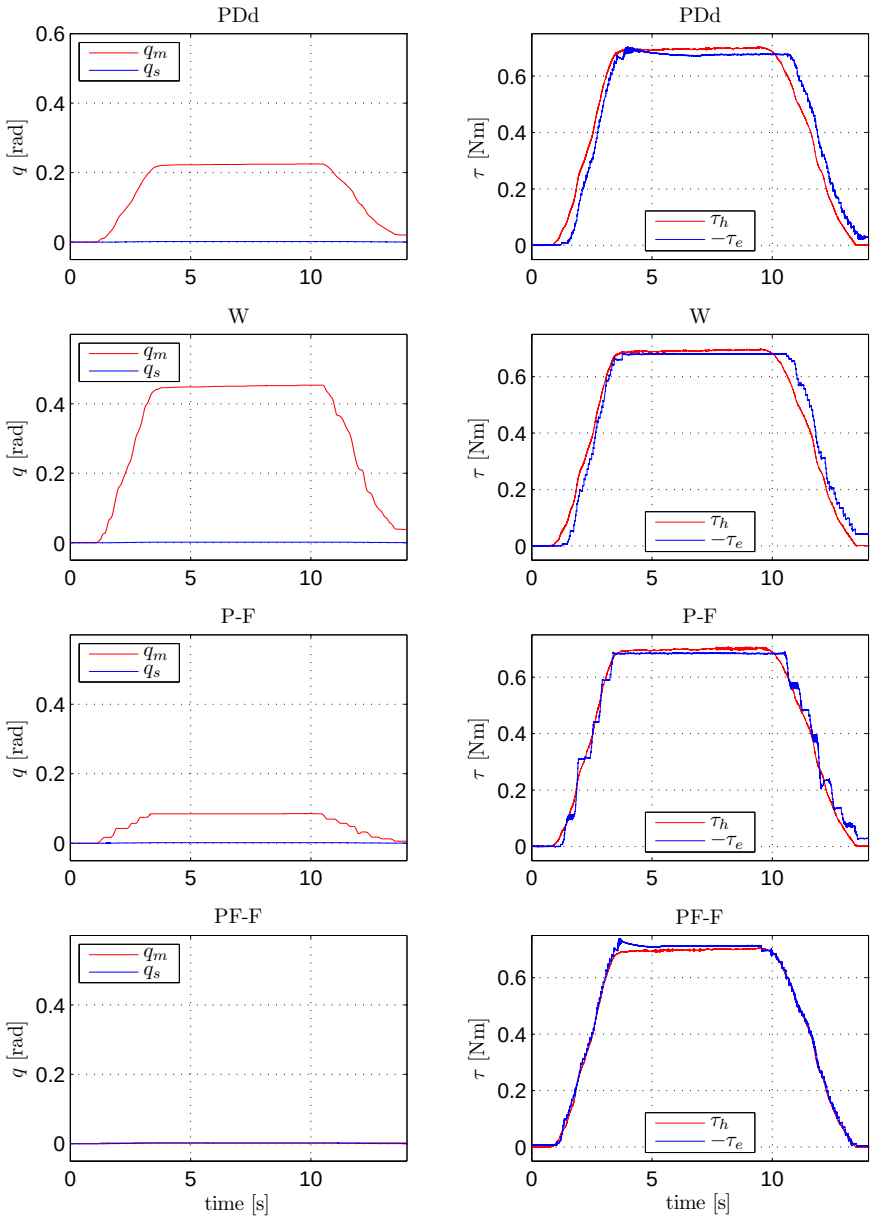

Fig. 3.9. Position and torque profiles of the PDd, W, P-F and PF-F architectures for the contact experiments ($T_m = T_s = 50$ ms).

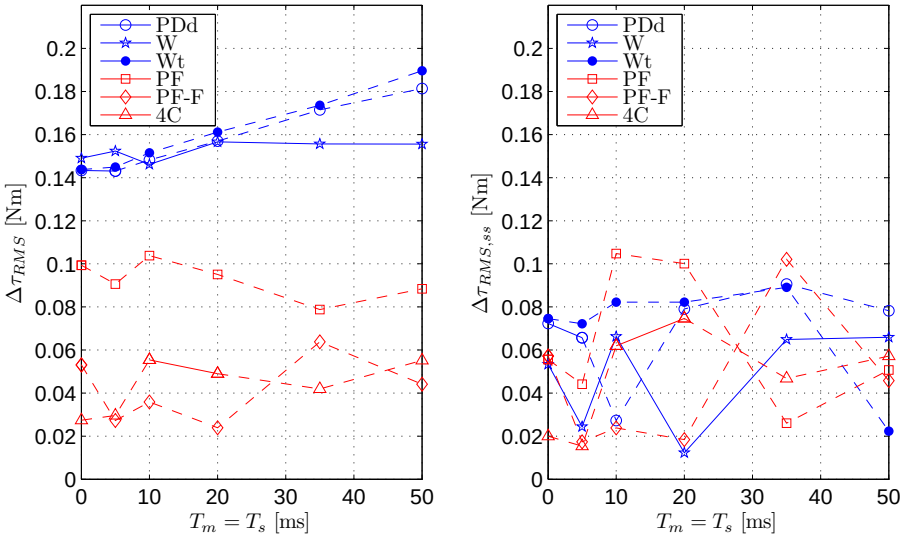

Fig. 3.10. RMS values of the torque tracking errors in contact as a function of the delay. The left plot shows the force tracking performance $\Delta\tau_{RMS}$ (defined in (3.5)) during the whole contact experiment, whereas the right plot only illustrates the performance $\Delta\tau_{RMS,ss}$ (defined in (3.6)) during steady-state.

stiffness are comparable. Due to the transmission of both τ_h and τ_e, these architectures have by far the best stiffness reflection and torque tracking during the dynamic part of the experiment. During the static phase, for both architectures a reflected stiffness of about 700 Nm/rad was achieved.

Torque tracking

The RMS values of the torque tracking error are shown in Fig. 3.10 for both the whole experiment, $\Delta\tau_{RMS}$, and for the static part considered separately, $\Delta\tau_{RMS,ss}$. Due to the static friction in the drive train, there are relatively large differences in $\Delta\tau_{RMS,ss}$ per controller for different delay values. As a result, no significant differences are observed in the steady-state torque tracking.

When looking at the torque tracking error for the whole experiment, a clear distinction is visible between the architectures with and without torque information. For the PDd and Wt architectures the dynamic torque tracking is the worst for delays larger than 5 ms due to the relatively low proportional gains k_{pi}. The value of $\Delta\tau_{RMS}$ increases proportional with the delay value due to the

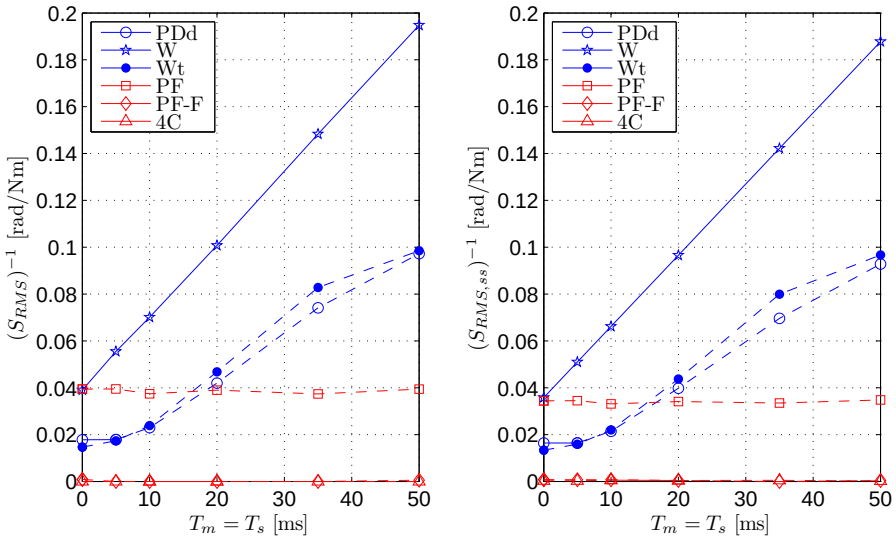

Fig. 3.11. RMS values of the reflected stiffness in contact as a function of the delay. The left plot shows $(S_{RMS})^{-1}$, the inverse of the reflected stiffness during the whole contact experiment, whereas the right plot shows $(S_{RMS,ss})^{-1}$, the inverse of the reflected stiffness during the steady-state phase.

applied tuning to bound the operator effort in free motion. For the W architecture, $\Delta\tau_{RMS}$ depends less on the delay and the torque tracking is better for higher delay values. The large difference between $\Delta\tau_{RMS}$ and $\Delta\tau_{RMS,ss}$ for the PDd, W and Wt controllers is the result of the relatively poor torque tracking during the dynamic parts.

Despite the steps in τ_e and q_m (see Fig. 3.9), the dynamic torque tracking performance of the P-F controller is better than with the architectures without torque information. Since k_{ps} is kept constant for all delay values, the dynamic torque tracking is independent of the delays (the variation for different delays is caused by the static phase). Finally, the PF-F and 4C controllers yield the best overal torque tracking performance due to the transmission of both τ_h and τ_e.

Reflected stiffness

Fig. 3.11 shows the performance of each architecture to reflect the environment impedance to the operator. In particular, the inverses of the reflected stiffnesses $S_{RMS,ss}$ and S_{RMS} are presented, such that, similar to the previously presented

results, a lower value represents a better performance. When comparing $S_{RMS,ss}$ and S_{RMS}, it is observed that for all architectures the performance of the reflected environment impedance is similar for both the static and dynamic part.

For the PDd, Wt and P-F controllers, the performance of reflecting the environment stiffness is proportionally related to k_{pi}, i.e. higher k_{pi} implies a better stiffness reflection. For the PDd and Wt controllers the proportional gains are reduced for increasing delays to bound the operator effort in free motion. This tuning clearly affects the environment stiffness perceived by the operator.

The W controller lacks asymptotic position tracking properties. Consequently, despite the highest k_{pi} values for all delays, the master position deviates from the slave position during the contact phase. The motion error $q_m - q_s$ increases proportionally with the delays, making this architecture the most sensitive to delays in terms of reflected environment impedance. These results show the importance of asymptotic position tracking in a bilateral motion synchronizing architecture.

The PF-F and 4C controllers provide by far the best stiffness reflection. Due to the use of τ_e and τ_h in the master and slave controllers, respectively, no position error between the master and slave is required to generate the requested torques. Despite the drive train imperfections, limited encoder resolution and measurement noise, the error $q_m - q_s$ never exceeded 0.001 rad during the contact experiments.

3.5.3 Conclusions

The results of the experimental comparison are combined in Tables 3.2 and 3.3. For each architecture, Table 3.2 describes per metric the relative performance for $T_m = T_s = 0$ ms. In the absence of delays, the 4C architecture performs best on all metrics, as already mentioned in [69]. Table 3.3 illustrates per metric in which way the performance is affected by the delay. For each metric, the performance is classified as a relatively large decay, a relatively small decay, or no decay for increasing delays. The distinction between a relatively small and large decay is determined by the mean of all nonzero decay rates. Overall, the PF-F architecture is affected least by the delays.

In general, for the bilateral motion synchronization architectures PDd, W and Wt, which lack direct force sensing, a performance loss due to the time delays is witnessed in both free motion and contact. In contrast, the 4C controller does exploit force information and, consequently, the performance is only affected in free motion in the form of a high operator effort. In the PDd, Wt and 4C architectures, the high operator effort is caused by the delay-induced forces. For the direct force-reflecting architectures P-F and PF-F only the free motion performance is affected due to injected damping necessary to ensure stability. In the presence of delays, the PF-F architecture gives the best performance, because, compared to the 4C controller, it does not suffer from delay-induced forces. As

Table 3.2. An overview of the performance per metric, at $T_m = T_s = 0$ s, relative to the architecture that performs worst (indicated with 100%). The 4C architecture performs best on all metrics.

	Metric	PDd	W	Wt	P-F	PF-F	4C
Free Motion	Δq_{RMS}	44%	100%	37%	79%	63%	9%
	$\Delta q_{RMS}^{T_m}$	44%	100%	37%	79%	63%	9%
	τ_{RMS}	96%	100%	100%	71%	67%	55%
Contact	$\Delta\tau_{RMS}$	96%	100%	96%	67%	36%	18%
	$\Delta\tau_{RMS,ss}$	-	-	-	-	-	-
	S_{RMS}^{-1}	45%	99%	37%	100%	2%	0%
	$S_{RMS,ss}^{-1}$	46%	100%	37%	96%	2%	1%

Table 3.3. An overview of the performance degradation for increasing values of the communication delay. The PF-F architecture has the smallest performance degradation.

	Metric	PDd	W	Wt	P-F	PF-F	4C
Free Motion	Δq_{RMS}	$\overline{\triangledown}$	$\overline{\triangledown}$	$\overline{\triangledown}$	$\overline{\triangledown}$	$\triangledown$	$\triangledown^*$
	$\Delta q_{RMS}^{T_m}$	$\overline{\triangledown}$	$\overline{\triangledown}$	$\overline{\triangledown}$	$\triangledown$	$\triangledown^*$	$\overline{\triangledown}$
	τ_{RMS}	$\overline{\triangledown}$	$\square^*$	$\overline{\triangledown}$	$\triangledown$	$\triangledown$	$\overline{\triangledown}$
Contact	$\Delta\tau_{RMS}$	$\triangledown$	$\square$	$\triangledown$	$\square$	$\square^*$	$\square^*$
	$\Delta\tau_{RMS,ss}$	-	-	-	-	-	-
	S_{RMS}^{-1}	$\triangledown$	$\overline{\triangledown}$	$\triangledown$	$\square$	$\square^*$	$\square^*$
	$S_{RMS,ss}^{-1}$	$\triangledown$	$\overline{\triangledown}$	$\triangledown$	$\square$	$\square^*$	$\square^*$

$\square$: Performance not affected by delays.
$\triangledown$: Relatively small performance decrease for increasing delays.
$\overline{\triangledown}$: Relatively large performance decrease for increasing delays.
*: Best performance for this metric.

anticipated in Sections 2.2 and 2.3, a direct force-reflection architecture yields the best performance in the presence of delays.

In general, using τ_h in the slave controller improves the motion tracking and stiffness reflection. The direct force-reflecting architectures P-F and PF-F are designed specifically to control the error $q_m^{T_m} - q_s$. In contrast, all other controllers have motion synchronizing terms in both the master and slave controller and seem to control the error $q_m - q_s$.

The operator effort rapidly increases for increasing delays when the master controller contains terms to asymptotically synchronize the master motion with that of the slave (PDd, Wt and 4C). These motion synchronizing terms result in undesired delay-induced forces. For both the PDd and Wt controller, limiting the operator effort in free motion by lowering k_{pi} results in a reduction of the reflected environment stiffness. The P-F, PF-F and W controllers do not suffer from delay-induced forces, but the direct force-reflecting architectures P-F and PF-F require high damping gains to guarantee stability during free motion to contact transitions. The operator effort of the W architecture is independent of the delay, but the motion tracking performance and stiffness reflection are significantly affected by the delays. Especially for reflecting the environment stiffness, asymptotic position tracking is key in bilateral motion synchronization architectures.

When comparing P-F and PF-F with 4C, it is clear that the delay-induced forces of the 4C controller are related to controlling the motion error $q_m - q_s$ to zero. When, instead, only the error $q_m^{T_m} - q_s$ is synchronized by the slave controller, as in P-F and PF-F, delay-induced force are absent. Even with the high damping gains B_m for P-F and PF-F the operator effort is smaller for larger delays, compared to the 4C controller, making the application of these two architecture more preferable for delayed bilateral teleoperation.

3.6 Discussion

In this work, the *controller* performance in both free motion and contact is analyzed for six architectures on four different performance metrics. The results show per criterium a clear relation between the different controller classes and obtained performance. An absolute threshold for a human operator for, e.g., operator effort or stiffness reflection are not included in the analysis. More work is required to obtain insight on, e.g., how much operator effort is allowed or how high the reflected stiffness must be in order to perceive the stiff environment as such. At this point, the author can only comment that when manually operating the devices, the delay-induced forces are strongly present and disturbing. In contact, the environment reflected with the PF-F and 4C controllers feels stiff, but soft with the other architectures.

The controllers considered in the experimental comparison are not necessarily the architectures that provide the best performance in the presence of delays.

They are merely selected as relatively simple representatives of different classes of control architectures. Obtaining optimal performance is not the goal of the tuning procedure described in Section 3.4, but the results illustrate how the performance is compromised for each architecture to guarantee stability in the presence of delays. For the P-F architecture, for example, the proportional gain k_{ps} was not altered for different delays. Consequently, the reflected stiffness was delay-independent. Lowering k_{ps} will reduce the reflected stiffness and motion tracking performance, but at the same time the operator effort will improve because less damping is required to guarantee stability. In contrast, such a trade-off in tuning k_{pi} is not possible for the PDd, Wt and 4C architectures due to the high operator effort caused by k_{pm} and the delay.

As a final remark, note that the injection of damping in free motion is not required for the P-F and PF-F architectures due to their unilateral nature. For zero injected damping, both $\Delta q_{RMS}^{T_m}$ and $\tau_{h,RMS}$ would be delay-independent and have a performance equal to their zero delay case. This makes the PF-F controller a very suitable architecture for high performance teleoperation when the communication suffers from delays. A time-domain passivity approach as presented in, e.g., [40] or Chapter 5 can be exploited to obtain low damping gains in free motion, while still being able to stabilize the contact phase and prevent a recoiling of the master.

Concluding, the experimental results illustrate that, despite practical limitations such as drive-train imperfections, limited encoder resolution and measurement noise, the overal performance improves when force information is included in the controllers. The design of an architecture with asymptotic motion tracking terms in the master controller should be avoided to prevent a high operator effort. In the presence of delays it is better to design a controller where only the slave controller is used for motion synchronization and, thus, to control $q_m^{T_m} - q_s$. In other words, direct force-reflection architectures have more potential than architectures aiming at bilateral motion synchronization when the communication suffers from delays. Even with the practical limitations, which especially affect architectures with force information, the obtained results support and extend this theory-based conclusion presented in Chapter 2.

Based on both the theoretical and experimental results of Chapters 2 and 3, the direct force-reflecting PF-F architecture seems the most promising to achieve high performance in the presence of delays. The purpose of the next two chapters is to guarantee a stable implementation, without compromising the achievable performance. Chapter 4 focuses on the local interaction between the slave and the environment, whereas Chapter 5 proposes a novel architecture to guarantee passivity of the teleoperator in the presence of delays. In particular, during free motion, high damping gains are absent, resulting in an improved operator effort that is superior to all architectures presented in the experimental comparison of this chapter.

Acknowledgement

The author greatly acknowledges the contribution of Ruud Beerens in designing the experiments and performing the pilot tests.

Chapter 4

Single manipulator switching control for tracking of a hybrid position-force trajectory

Achieving and guaranteeing a stable interaction of the slave with stiff environments is one of the main problems in bilateral teleoperation. For accomplishing the desired task the stability of transitions from free motion to constrained motion and from constrained motion to free motion is essential. Ensuring stability during these transitions is a challenge as the combined slave-environment dynamics switch abruptly at the moment of contact and detachment from the environment. This chapter focuses on achieving stable or even bounceless contacts of a manipulator interacting with a stiff environment. A *time-varying motion profile* should be tracked during free motion, whereas during constrained motion a *time-varying force profile* should be applied on the environment. Since the results presented here extend to any nonflexible manipulator interacting with the environment, such as, e.g., in automated assembly tasks and surface finishing, in this chapter the 'slave device' will be referred to as the 'manipulator'.

4.1 Introduction

Over the past decades, different control architectures have been proposed for motion-force control of a manipulator in contact with a stiff environment (for an overview, see, e.g., [122, Chapter 7]). The most studied and applied control schemes include stiffness, impedance and admittance control [24, 43, 53, 58, 135, 142], hybrid position-force control [60, 110], and parallel position-force con-

trol [27]. While these approaches usually exhibit sufficient robustness to be used in practice, a formal mathematical proof of stability is still lacking. Typically, the gains in these control schemes are tuned separately for free motion and constrained motion. Stability of the resulting closed-loop dynamics is analyzed using standard Lyapunov methods and guaranteed for free motion and constrained motion independently, but the contact and detachment transitions are not included in the analysis. Bouncing and unstable contact behavior might therefore still occur, and do still occur. As a practical solution, when implementing these control schemes on a physical manipulator, the manipulator is usually commanded to approach the environment with a very slow velocity to prevent the excitation of the unstable contact dynamics.

From an analysis perspective, only a few theoretical studies have addressed directly the instability resulting from bouncing of the manipulator against a stiff environment. In [37, 131], a switched position-force controller is considered, where the controller switches from motion to force control when contact with the environment is made. Using analysis techniques for switched systems, conditions for asymptotic stability are derived for a *constant* position or force setpoint regulation problem. Hysteresis switching is considered in [25] to prevent bouncing of the manipulator against the environment. In [103], the number of bounces is cleverly minimized by exploiting a transition controller, but then the contact force is controlled to a *constant* setpoint. In [68], nonlinear damping is proposed to minimize the force overshoot without compromising the settling time. In all these publications, tracking of desired *time-varying* motion and force profiles is not considered.

A popular approach to prevent unstable impacts is impedance control [6, 24, 58]. In the outer loop, the contact force is controlled by creating a desired impedance specified for the contact dynamics to compute a requested motion profile for the inner motion control loop. Consequently, the contact force is controlled indirectly, such that tuning the impedance parameters requires a trade-off between motion control, force control and stabilizing the effect of impacts. To alleviate the compromising effect of this trade-off on the tracking performance, the proportional gain is adapted online in [58], whereas in [24] the desired impedance is temporarily scaled during the transition phase. In [142], the impedance parameters are switched online to dissipate the kinetic energy engaged at impact. The proposed controller guarantees velocity regulation in free motion and tracking of a *constant* force setpoint in contact. For other forms of compliant control, such as variable impedance actuation, the interested reader is referred to [133]. To the best of the author's knowledge, a formal stability proof that includes in the analysis the free motion to contact transitions, while tracking arbitrary time-varying motion-force profiles, does not yet exist in the context of impedance and compliant control.

In the above mentioned papers, the manipulator-environment interaction is modeled using a flexible spring-damper contact model. The stiffness and damp-

ing properties of the environment are included explicitly and, as a consequence, the impact phase has a finite time duration. Such a modeling approach is also taken here.

Manipulator-environment interaction can also be modeled using tools from nonsmooth mechanics [20, 71]. In doing so, the time duration of the impact event is assumed to be zero and an impact law (e.g., Newton's law of restitution) is employed to characterize the collision. Stable tracking of specific force/position profiles using such nonsmooth mechanics modeling formalism has been addressed in this context. In [102], a discontinuous control scheme is proposed to ensure stable regulation on the surface of the unilateral constraint. A switched motion-force tracking controller for manipulators subject to unilateral constraints is considered in [19, 21, 82]. There, it is shown that the design of the desired trajectory in the transition phase is crucial for achieving stability. To the best of authors' knowledge, the problem of stable tracking of arbitrary force/position profiles as considered in this work has not been solved even in the framework of nonsmooth mechanics. The stability of the tracking controller cast in this framework is clearly of interest and deserves further investigation. This framework will not be addressed here because, as mentioned previously, a flexible (spring-damper) contact model is adopted.

In this chapter, a mathematical analysis is proposed that can help control engineers as well as mechanical designers to develop controlled manipulators that exhibit stable contact behavior with a stiff environment, while tracking a time-varying motion and force profile. Because in many tasks of practical interest the interaction of the robot end-effector with the environment occurs just in one direction, the contact stability problem is studied using a 1-DOF dynamic manipulator model. The remaining unconstrained DOFs can be controlled with standard motion control techniques (see [125]). For illustration purposes, a switched motion-force tracking control strategy is considered and stability of the resulting closed-loop dynamics is analyzed. The obtained stability conditions are given in Theorem 4.2 in Section 4.3. The stability analysis of the closed-loop system reveals that, due to the relatively stiff contact dynamics, the considered switched motion-force controller should implement a considerable amount of damping to guarantee stability while tracking an arbitrary time-varying motion-force profile. Because an excessive amount of damping limits the tracking performance due to a sluggish response, the contact dynamics are made compliant by using an alternative mechanical manipulator design that includes a compliant wrist. In this way, the resonance frequency of the impact and contact transients can be reduced and the associated energy can be dissipated in a passive way. The purpose of such a compliant energy absorbing component is similar to that of an impedance or compliant controller.

The main contributions of this chapter are as follows. First, a combination of the compliant wrist design with a switched motion-force controller is proposed for the tracking of time-varying motion and force profiles. Secondly, a stability

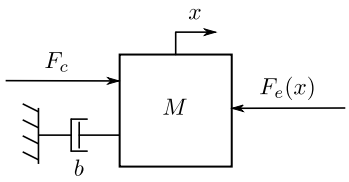

Fig. 4.1. 1-DOF manipulator.

analysis is proposed that provides design guidelines for both the compliant wrist and controller to guarantee stable contact while tracking arbitrary motion and force profiles. In particular, it is shown that for realistic system parameter values, the compliant model exhibits a clear distinction between fast and slow time-scale dynamics. Using model reduction, models of reduced order are obtained for the free motion and contact phase, respectively, representing only the slow dynamics. In combination with the stability analysis developed for the rigid manipulator, guidelines are obtained for the parametric design of the compliant wrist such that bouncing of the manipulator against the stiff environment can be prevented without the need of a considerable amount of damping from the controller.

This chapter is organized as follows. First, in Section 4.2, the manipulator and environment model are introduced and the controller design is proposed. The stability analysis is described in Section 4.3. Section 4.4 illustrates the obtained results by means of a simulation study. Section 4.5 discusses the benefits of additional (wrist-)compliance in the manipulator and illustrates how to tune the parameters of the controller and the compliant wrist. Finally, the conclusions are presented in Section 4.6.

Notation. The notation in this chapter differs from the notation used in the rest of this thesis. In particular, $i \in \{1, 2\}$ is used to indicate either the free motion ($i = 1$) or the contact subspace ($i = 2$).

4.2 System modeling and controller design

The primary goal is to make a manipulator track a desired time-varying motion-force profile. As explained in the introduction (Section 4.1), the focus is on a 1-DOF modeling of the manipulator-environment interaction.

Consider the decoupled contact DOF of the manipulator as depicted in Fig. 4.1. The Cartesian space dynamics are described by

$$M\ddot{x} + b\dot{x} = F_c - F_e, \tag{4.1}$$

where x represents the manipulator position, $M > 0$ the equivalent mass of the manipulator, $b > 0$ the viscous friction in the joint, F_c the control force and

F_e the force exchanged between the environment and the manipulator. The environment is modeled as a static wall at $x = 0$ and, without loss of generality, the manipulator is in contact with the environment for $x > 0$. In [37, 131], the environment is modeled as a piecewise linear spring. In this work, similarly to [25], an extended model, namely the Kelvin-Voigt contact model, is considered, which also includes damping and friction

$$F_e(x, \dot{x}) = \begin{cases} 0 & \text{for } x \leq 0 \\ k_e x + b_e \dot{x} & \text{for } x > 0 \end{cases} \tag{4.2}$$

with $k_e > 0$ and $b_e > 0$ the stiffness and damping properties of the environment, respectively. This model is nonlinear and non-smooth due to the abrupt change in F_e at $x = 0$.

In free motion, the manipulator is required to follow a bounded desired motion profile $x_d(t)$, whereas in contact, a desired force profile $F_d(t)$ should be applied to the environment. This work considers the following switched motion-force controller that switches between a resolved acceleration controller, e.g, mentioned in [125], in free motion and a proportional force controller, e.g. considered in [135], in the contact phase:

$$F_c = \begin{cases} M_a \ddot{x}_d(t) + k_d(\dot{x}_d(t) - \dot{x}) + k_p(x_d(t) - x), & \text{for } x \leq 0, \quad (4.3a) \\ F_d(t) + k_f(F_d(t) - F_e) - b_f \dot{x}, & \text{for } x > 0, \quad (4.3b) \end{cases}$$

such that both motion and force are controlled directly. Here, $k_p > 0$ and $k_d > 0$ are the proportional and derivative gains of the motion controller, respectively. The estimated mass of the manipulator $M_a > 0$ in (4.3a) might differ from the actual mass M in (4.1) due to uncertainties in the model parameter identification. The gain $k_f > 0$ represents the proportional term of the force controller and $b_f > 0$ is the damping gain, dissipating energy during the contact phase. For the controller (4.3), it is assumed that the contact force F_e, position x and velocity $\dot{x}$ can be measured. Although, in (4.3), the switching between motion control and force control is decided based on the actual position x of the manipulator, for a stiff environment, $k_e \gg b_e$, this is equivalent to switching based on the interaction force F_e. This implies that a perfect knowledge of the location of the environment is not necessary for the implementation of the controller defined by (4.3).

Remark 4.1. Compared to the controllers proposed in [19, 21, 82] obtained for systems modeled with nonsmooth mechanics, the considered controller (4.3) does not use a separate (third) controller for the transition phase from free motion to contact. Instead, the controller (4.3) uses the damping term $b_f \dot{x}$ during the whole contact phase.

In order to analyze stability of the system described by (4.1)-(4.3), the closed-loop dynamics are reformulated as a switching state-space model. A key idea

for the stability analysis, detailed in Section 4.3, is to express the force tracking error $F_d(t)-F_e$ in terms of the motion tracking error $x_d(t)-x$, such that both in free motion and in contact the goal is to make the tracking error $x_d(t)-x$ small. In contact, $x_d(t)$ then represents the 'virtual' desired trajectory, corresponding to the desired contact force $F_d(t)$. For the relationship between $F_d(t)$ and $x_d(t)$ during contact, $x \to x_d(t)$ and $\dot{x} \to \dot{x}_d(t)$ should also imply $F_e \to F_d(t)$. To this end, the following relationship is considered to deduce $x_d(t)$ from $F_d(t)$ in the contact phase:

$$\hat{k}_e x_d(t) + \hat{b}_e \dot{x}_d(t) = F_d(t), \quad \text{for } F_d(t) > 0, \tag{4.4}$$

where $\hat{k}_e$ and $\hat{b}_e$ are available estimates of k_e and b_e.

Assumption 4.1. *The desired position $x_d(t)$ and velocity $\dot{x}_d(t)$ trajectories are continuous, and the desired acceleration $\ddot{x}_d(t)$ is piecewise-continuous and bounded.*

Two separate user-defined motion and force profiles can be glued together to satisfy Assumption 4.1 by using the design procedure detailed in Appendix A.1.

In terms of the exact parameters k_e and b_e, (4.4) can be rewritten as

$$k_e x_d(t) + b_e \dot{x}_d(t) + w_f(t) = F_d(t), \quad \text{for } F_d(t) > 0, \tag{4.5}$$

with $w_f(t) := (\hat{k}_e - k_e)x_d(t) + (\hat{b}_e - b_e)\dot{x}_d(t)$ a bounded – due to Assumption 4.1 – perturbation. When the estimates $\hat{k}_e$ and $\hat{b}_e$ are exact, $w_f(t) = 0$ and $x - x_d(t) \to 0$ implies that $F_e - F_d(t) \to 0$. When $\hat{k}_e \neq k_e$ and/or $\hat{b}_e \neq b_e$, $w_f(t) \neq 0$ and acts as a perturbation in the stability analysis. Since the mapping (4.5) is only used for the stability analysis and not in the controller (4.3), the lack of exact knowledge of k_e and b_e will not affect the stability or tracking of the system described by (4.1)-(4.3).

After using (4.5), the goal of the controller is to make the errors $x_d(t) - x \to 0$ and $\dot{x}_d(t) - \dot{x} \to 0$. Hence, the tracking error

$$z = \begin{bmatrix} z_1 \\ z_2 \end{bmatrix} := \begin{bmatrix} x_d(t) - x \\ \dot{x}_d(t) - \dot{x} \end{bmatrix} \tag{4.6}$$

can be used to rewrite the closed-loop system dynamics (4.1)-(4.3) and (4.5) as the following perturbed switched system

$$\begin{aligned} \Sigma^p : \quad \dot{z} = A_i z + N w_i(t) = \begin{bmatrix} 0 & 1 \\ -K_i & -B_i \end{bmatrix} z + N w_i(t), \\ z \in \Omega_i(t), i \in \{1, 2\}, \end{aligned} \tag{4.7}$$

where $N = [0\ 1]^T$ and

$$K_1 := \frac{k_p}{M}, \quad B_1 := \frac{k_d + b}{M}, \tag{4.8a}$$

$$K_2 := \frac{(1 + k_f)k_e}{M}, \quad B_2 := \frac{(1 + k_f)b_e + b_f + b}{M}, \tag{4.8b}$$

$$w_1(t) := \frac{M - M_a}{M}\ddot{x}_d(t) + \frac{b}{M}\dot{x}_d(t), \tag{4.8c}$$

$$w_2(t) := \ddot{x}_d(t) + \frac{b_f + b}{M}\dot{x}_d(t) - \frac{1}{M}w_f(t), \tag{4.8d}$$

with w_f as in (4.5). The perturbations $w_i(t)$, $i = \{1, 2\}$, are bounded due to Assumption 4.1. All system parameters are positive, implying that in (4.7), for $i \in \{1, 2\}$, $K_i, B_i > 0$ and A_i is Hurwitz. The environment is located at $x = 0$, so switching occurs at $x = x_d(t) - z_1 = 0$. Expressed in the z-coordinates, the free motion and contact subspaces, respectively denoted by Ω_1 and Ω_2, are time-varying: $\Omega_1(t) := \{z \in \mathbb{R}^2 | x_d(t) - z_1 \leq 0\}$ and $\Omega_2(t) := \{z \in \mathbb{R}^2 | x_d(t) - z_1 > 0\}$. Note that for all t, $\Omega_1(t) \cup \Omega_2(t) = \mathbb{R}^2$ and $\Omega_1(t) \cap \Omega_2(t) = \emptyset$.

The environment stiffness k_e is typically much higher than the control gain k_p. Furthermore, the true value of k_e and b_e are usually unknown and therefore the control parameters cannot be selected to result in $K_1 = K_2$ and $B_1 = B_2$ in (4.7). Thus, in general, Σ^p in (4.7) represents a switched system. The stability of Σ^p does not follow from the stability of each of the two continuous subsystems (corresponding to free motion and contact) taken separately, as shown, e.g., in [27, 110] (see also [73] in the scope of generic switched systems). Hence, the switching between the two subsystems, corresponding to making and breaking contact, must also be taken into account. This is the purpose of the next section.

Remark 4.2. Note that the switched controller (4.3) is not the only controller that results a switched closed-loop system of the form Σ^p in (4.7). Also for other controllers, such as, e.g., the impedance controllers presented in [142], the resulting closed-loop dynamics can be expressed in the form Σ^p. Hence, the stability analysis presented in the next section has more generic applicability and can be used to guarantee stability of both the switched controller (4.3) and such impedance controllers while tracking arbitrary time-varying motion-force profiles.

4.3 Input-to-State Stability of a switched system

In this section, sufficient conditions are provided under which Σ^p in (4.7) is input-to-state stable (ISS) with respect to the input $w_i(t)$, $i = \{1, 2\}$. Note that $w_i(t)$ depends on $x_d(t)$, thereby encoding the information of $F_d(t)$ during the contact phases.

The following definitions, taken from [16], are required for the stability analysis.

Definition 4.1. *Consider a region $\mathcal{T}_i \subset \mathbb{R}^2$. If $z \in \mathcal{T}_i$ implies $cz \in \mathcal{T}_i$, $\forall c \in (0, \infty)$ and $\mathcal{T}_i \backslash \{0\}$ is connected, then $\mathcal{T}_i$ is a **cone**.*

Definition 4.2. *Let $\dot{z} = A_i z$ be the dynamics on an open cone $\mathcal{T}_i \subset \mathbb{R}^2$, $i = 1, ..., m$. An **eigenvector** of A_i is **visible** if it lies in $\overline{\mathcal{T}}_i$, the closure of $\mathcal{T}_i$.*

As a stepping stone towards proving ISS of (4.7), first sufficient conditions for the global uniform exponential stability (GUES) of the origin of Σ^p when $w_i \equiv 0$ are provided. This corresponds to studying the unperturbed system

$$\Sigma^u : \quad \dot{z} = A_i z, \quad \text{for } z \in \Omega_i(t). \tag{4.9}$$

The GUES of the origin of Σ^u for any $x_d(t)$ satisfying Assumption 4.1 can be concluded by considering the worst-case switching sequence [73, 79]. In this way, the time-invariant system Σ^w, defined below, with state-based switching is obtained, that represents the worst-case switching sequence for Σ^u in (4.9). The worst-case switching sequence is defined as the switching sequence that results in the slowest convergence (or fastest divergence) of the solution of Σ^u towards (or from) the origin. Denote with $\sigma(t) : \mathbb{R} \to \{1, 2\}$ the switching sequence corresponding to $i \in \{1, 2\}$ in (4.9). Note that $\sigma(t)$ depends on the initial condition $z(t_0) = z_0$. Then, the solution of Σ^u starting from z_0 at t_0 will be denoted by $z(t) = \Phi_u(t, t_0; \sigma) z_0$, with $\Phi_u(t, t_0; \sigma)$ the state transition matrix associated with the switching sequence $\sigma(t)$. For $K_2 > K_1$, representing a manipulator interacting with a stiff environment, the worst-case dynamical system Σ^w, associated with the *state-dependent* worst-case switching sequence σ^w of the system Σ^u for a given z_0, is characterized by the following lemma.

Lemma 4.1. *Consider the switched system*

$$\Sigma^w : \quad \dot{z} = A_i z, \qquad \forall z \in \mathcal{S}_i, \tag{4.10}$$

with A_1 and A_2 as in (4.7). Assume $K_2 > K_1$ and let

$$\mathcal{S}_1 = \{z \in \mathbb{R}^2 | z_2((K_1 - K_2)z_1 + (B_1 - B_2)z_2) \leq 0\},$$
$$\mathcal{S}_2 = \{z \in \mathbb{R}^2 | z_2((K_1 - K_2)z_1 + (B_1 - B_2)z_2) > 0\}.$$

For the solution of Σ^u in (4.9) corresponding to an arbitrary switching signal $\sigma(t)$ and initial condition z_0, $\|\Phi_u(t, t_0; \sigma) z_0\| \leq \|\Phi_w(t, t_0; \sigma^w) z_0\|$ for $t \geq t_0$, where Φ_w is the state transition matrix of the linear time-varying system $\dot{z} = A_{\sigma^w(t)} z$ with $\sigma^w(t)$ the switching sequence corresponding to $z(t_0) = z_0$ in (4.10). In this sense, $\Phi_w(t, t_0; \sigma^w) z_0$, $t \geq t_0$, is referred to as the worst-case response of Σ^u with initial condition z_0.

Proof. Let $\dot{z} = A_{\sigma(t)} z$ denote the time-varying vector field associated with the switching signal $\sigma(t) \in \{1, 2\}$ $\forall t$ corresponding to an arbitrary $x_d(t)$ satisfying Assumption 4.1. Let $V = \frac{1}{2} z^T z$ be a positive definite comparison function, with time derivative $\dot{V} = z^T \dot{z} = z^T A_{\sigma(t)} z$. Let us define $\dot{V}_i := z^T A_i z$ for $i = \{1, 2\}$. Then it holds that $\dot{V} = z^T A_{\sigma(t)} z \leq \max\left(\dot{V}_1, \dot{V}_2\right)$. From the structure of A_1 and A_2 in (4.7), with $K_2 > K_1$, it follows that $\dot{V}_1 > \dot{V}_2$ if $z_2((K_1 - K_2)z_1 + (B_1 - B_2)z_2) < 0$ and vice versa, such that the switching logic $\sigma^w(t) =$

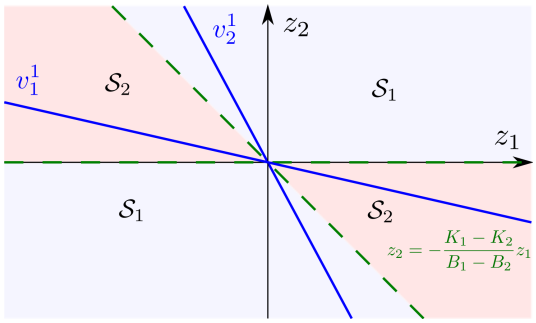

Fig. 4.2. Switching surfaces and domains of Σ^w for $K_2 > K_1$ and $B_2 > B_1$. The vectors v_1^1 and v_2^1 represent the real eigenvectors of A_1 in (4.14).

$\text{argmax}_{j\in\{1,2\}} \dot{V}_j$, which can be interpreted as the worst-case switching sequence of (4.9), is equivalent with the one in (4.10). For equal initial conditions z_0, it follows that $V(\Phi_u(t,t_0;\sigma)) \leq V(\Phi_w(t,t_0;\sigma^w))$. Since $V(z) = \frac{1}{2}\|z\|^2$, it follows that $\|\Phi_u(t,t_0;\sigma)\| \leq \|\Phi_w(t,t_0;\sigma^w)\|$ and Σ^w generates the worst-case response of Σ^u. □

From the definition of $\mathcal{S}_1$ and $\mathcal{S}_2$ given in Lemma 4.1, the two switching surfaces $z_2 = 0$ and $(K_1-K_2)z_1+(B_1-B_2)z_2 = 0$ are obtained that characterize the worst-case switching. These switching surfaces and the subsystems of Σ^w that are active between the switching surfaces are visualized in Fig. 4.2 for $K_2 > K_1$ and $B_2 > B_1$.

In Theorem 4.2 below, necessary and sufficient conditions for the global uniform asymptotic stability (GUAS) of Σ^w are given. Then, in Lemma 4.3, it is shown that GUAS of Σ^w implies GUES of Σ^u and this, in turn, implies ISS of Σ^p w.r.t. w_i for an arbitrary $x_d(t)$ satisfying Assumption 4.1. This result is given in Theorem 4.4 at the end of this section and, together with Theorem 4.2, constitutes the main result presented in this chapter.

The interested reader is referred to Appendix A.2 for further details about the background material used to obtain the following results.

Theorem 4.2. *Let $K_i, B_i > 0$, $\Delta K := K_1 - K_2 < 0$ and $\Delta B := B_1 - B_2$. The origin of the unperturbed, conewise linear system Σ^w is GUAS if and only if at least one of the following conditions is satisfied:*

i. Σ^w has a visible eigenvector associated with an eigenvalue $\lambda < 0$; in other words, one of the following two conditions is satisfied:

(a) a visible eigenvector exists in $\mathcal{S}_1$, i.e., $\Delta B < 0$, $B_1^2 \geq 4K_1$ and
$$\frac{\Delta K}{\Delta B} < \frac{2K_1}{B_1 - \sqrt{B_1^2 - 4K_1}}$$

(b) *a visible eigenvector exists in* $\mathcal{S}_2$*, i.e.,* $B_2^2 \geq 4K_2$ *and one of the following conditions is satisfied:*

1) $\Delta B < 0$ *and* $\dfrac{\Delta K}{\Delta B} > \dfrac{2K_2}{B_2 + \sqrt{B_2^2 - 4K_2}}$*, or*

2) $\Delta B \geq 0$.

ii. Σ^w *has no visible eigenvectors and* $\Lambda_1\Lambda_2 < 1$*, where* Λ_i*,* $i = \{1, 2\}$*, are given by:*

1) if $B_i^2 < 4K_i$*,*

$$\Lambda_i = \left(\frac{K_i}{\omega_i} \left(\frac{(\Delta K)^2}{L^2} + \frac{Q^2}{4\omega_i^2 L^2} \right)^{-1/2} \right)^{(-1)^i} e^{-\frac{B_i}{2\omega_i}\varphi_i} \tag{4.11}$$

with $\varphi_i := \mod\left(-\arctan(\frac{(-1)^i 2\omega_i \Delta K}{Q}), \pi\right)$, $Q := B_i\Delta K - 2K_i\Delta B$, $\omega_i := \frac{1}{2}\sqrt{4K_i - B_i^2}$ *and* $L := \sqrt{(\Delta K)^2 + (\Delta B)^2}$.

2) if $B_i^2 = 4K_i$*,*

$$\Lambda_i = \left| \frac{B_i L}{2\Delta K - B_i \Delta B} \right| e^{\left((-1)^i \frac{2\Delta K}{2\Delta K - B_i \Delta B}\right)}. \tag{4.12}$$

3) if $B_i^2 > 4K_i$*,*

$$\begin{aligned} \Lambda_i \;=\; & \left| \frac{\Delta K \lambda_{bi} + K_i \Delta B}{K_i L} \right|^{\left((-1)^i \frac{\lambda_{ai}}{\lambda_{bi} - \lambda_{ai}}\right)} \\ & \cdot \left| \frac{\Delta K \lambda_{ai} + K_i \Delta B}{K_i L} \right|^{\left((-1)^i \frac{\lambda_{bi}}{\lambda_{ai} - \lambda_{bi}}\right)} \end{aligned} \tag{4.13}$$

with $\lambda_{ai} := \frac{-B_i - \sqrt{B_i^2 - 4K_i}}{2}$ *and* $\lambda_{bi} := \frac{-B_i + \sqrt{B_i^2 - 4K_i}}{2}$.

Proof. From Lemma A.1 in Appendix A.2 it follows that Σ^w in (4.10) has no sliding modes on the switching surfaces. Therefore, Theorem A.4 can be applied to conclude GUAS of the origin of Σ^w. To this end, consider the conditions under points *i* and *ii* sequentially:

i. Since $K_i, B_i > 0$, both A_1 and A_2 are Hurwitz, such that $\Re(\lambda_{1,2}^i) < 0$, with $\lambda_{1,2}^i = \frac{-B_i \pm \sqrt{B_i^2 - 4K_i}}{2}$ being the eigenvalues of A_i. An eigenvector is visible in $\mathcal{S}_i$ if the eigenvalues $\lambda_{1,2}^i$ of A_i are real and for at least one of the corresponding eigenvectors

$$v_1^i := \begin{bmatrix} \frac{-B_i + \sqrt{B_i^2 - 4K_i}}{2K_i} \\ 1 \end{bmatrix}, \qquad v_2^i := \begin{bmatrix} \frac{-B_i - \sqrt{B_i^2 - 4K_i}}{2K_i} \\ 1 \end{bmatrix} \tag{4.14}$$

it holds that $v_j^i \in \mathcal{S}_i$, with $j = 1$ or $j = 2$. These eigenvectors lie in the second and fourth quadrant of the phase portrait. For $j = 1$, Fig. 4.2 shows the eigenvectors v_1^1 and v_2^1 and switching surfaces $z_2 = 0$ and $z_2 = -\frac{K_1-K_2}{B_1-B_2}z_1$. The subsystem active in $\mathcal{S}_1$ has a visible eigenvector if $\Delta B < 0$ (switching surface in second and fourth quadrant) and the slope of the corresponding real eigenvector with the steepest slope, i.e. v_1^1, is steeper than $z_2 = -\frac{K_1-K_2}{B_1-B_2}z_1$, i.e. the inequalities of condition *i.(a)* of the theorem hold.

Similarly, it follows that the subsystem active in $\mathcal{S}_2$ has a visible eigenvector if either 1) $\Delta B < 0$ (switching surface in second and fourth quadrant) and $z_2 = -\frac{K_1-K_2}{B_1-B_2}z_1$ has a steeper slope than the real eigenvector of $\mathcal{S}_2$ with the least steep slope, i.e. v_2^2, or 2) $\Delta B \geq 0$ (switching surface in first and third quadrant, hence $\mathcal{S}_2$ spans at least the whole second and fourth quadrant). These two cases hold when conditions 1) and 2) of condition *i.(b)* of the theorem are satisfied. For both cases, GUAS of the origin follows from case *(i)* of Theorem A.4 in Appendix A.2.

ii. In case no visible eigenvectors exist, case *(ii)* of Theorem A.4, provided in Appendix A.2, must hold with $\Lambda := \Lambda_1^2\Lambda_2^2 < 1$, or equivalently, $\Lambda_1\Lambda_2 < 1$ in order for the origin of Σ^w to be GUAS. The expressions (4.11)-(4.13) follow from the three cases (A.3)-(A.5) of part *(ii)* of Theorem A.4, with the following vectors and matrices

$$\rho_{12}^1 = -\rho_{12}^2 = \begin{bmatrix} 1 \\ 0 \end{bmatrix}, \quad \rho_{21}^1 = \rho_{21}^2 = \frac{1}{L}\begin{bmatrix} \Delta B \\ -\Delta K \end{bmatrix},$$

$$1)\ P_i = \begin{bmatrix} \frac{-K_i}{\omega_i} & \frac{-B_i}{2\omega_i} \\ 0 & 1 \end{bmatrix},\ 2)\ P_i = \begin{bmatrix} -\frac{2}{B_i} & -\frac{4}{B_i^2} \\ 1 & 0 \end{bmatrix},\ 3)\ P_i = \begin{bmatrix} \frac{\lambda_{ai}}{K_i} & \frac{\lambda_{bi}}{K_i} \\ 1 & 1 \end{bmatrix}. \qquad \square$$

Remark 4.3. GUAS of a system of the form (4.10) can alternatively be analyzed using a common Lyapunov function approach [73]. Due to typically large differences between A_1 and A_2 (resulting from a large difference between the contact stiffness k_e and the proportional feedback gain K_p of the motion controller), it is generally hard to find an analytic expression for a common Lyapunov function. Therefore, an analytical approach is developed to analyze GUAS of (4.10) using the theory for conewise linear systems presented in [16]. In doing so, analytical stability conditions are provided in terms of the system and controller parameters, which is beneficial for system design.

Theorem 4.2 can be interpreted as follows. If the system Σ^w does not have a visible eigenvector (case *ii*), the response spirals around the origin and visits the regions $\mathcal{S}_1$ and $\mathcal{S}_2$ infinitely many times. In such a case, the worst-case system Σ^w switches between free motion and contact, but if $\Lambda < 1$, defined in the proof of Theorem 4.2, the resulting bouncing behavior is asymptotically stable, implying

that the amplitude of the oscillation decays over time. Furthermore, since the trajectory leaves each cone in *finite* time (see Lemma A.3 in Appendix A.2), the time between two switches is fixed and finite, implying that Zeno behavior (infinitely many switches in finite time) of Σ^w is excluded. If Σ^w does have a visible eigenvector with $\lambda < 0$ (case i), the response converges to the origin exponentially without leaving the cone (see Lemma A.2 in Appendix A.2). Then, the system does not switch between free motion and contact and bouncing of the manipulator against the environment does not occur.

The following lemma states that GUAS of Σ^w implies GUES of Σ^u.

Lemma 4.3. *If Σ^w in (4.10) is GUAS, then the origin of Σ^u in (4.9) is GUES for arbitrary $x_d(t)$ satisfying Assumption 4.1.*

Proof. By Lemma 4.1, $\|\Phi_u(t, t_0; \sigma)z_0\| \leq \|\Phi_w(t, t_0)z_0\|$. So, if the origin of Σ^w is GUAS, then so is the origin of Σ^u for arbitrary $x_d(t)$ satisfying Assumption 4.1. Then, from Theorem 2.4 of [73] it follows that the origin of Σ^u is GUES for arbitrary $x_d(t)$ satisfying Assumption 4.1. □

From Lemma 4.3, Σ^u is GUES if Σ^w is GUAS, and this last fact is guaranteed when one of the conditions given in Theorem 4.2 holds true. The following theorem provides conditions for ISS of the perturbed system Σ^p in (4.7).

Theorem 4.4. *Consider the perturbed system Σ^p in (4.7), with piecewise-continuous, bounded input $w_i(t)$. If the origin of the unperturbed system Σ^u in (4.9) is GUES for arbitrary $x_d(t)$ satisfying Assumption 4.1, then Σ^p is ISS w.r.t. $x_d(t)$.*

Proof. For an arbitrary switching sequence $\sigma(t) : \mathbb{R} \to \{1, 2\}$, resulting from arbitrary $x_d(t)$ satisfying Assumption 4.1, the solution of Σ^p, with initial condition z_0 at t_0, can be expressed as (see [127], Chapter 1)

$$z(t) = \Phi_u(t, t_0; \sigma)z_0 + \int_{t_0}^{t} \Phi_u(t, \tau; \sigma)\ Nw_i(\tau)d\tau. \tag{4.15}$$

If the origin of Σ^u is GUES, which is guaranteed if the conditions in Lemma 4.3 are satisfied, $\|\Phi_u(t, t_0; \sigma)\| \leq ce^{-\lambda(t-t_0)}$, for some constants $c, \lambda > 0$. Then, it follows from (4.15) that

$$\begin{aligned}
\|z(t)\| &\leq \|\Phi_u(t, t_0; \sigma)z_0\| + \|\int_{t_0}^{t} \Phi_u(t, \tau; \sigma)Nw_i(\tau)d\tau\| \\
&\leq ce^{-\lambda(t-t_0)}\|z_0\| + c\int_{t_0}^{t} e^{-\lambda(t-\tau)}\ \|Nw_i(\tau)\|d\tau \\
&\leq \underbrace{ce^{-\lambda(t-t_0)}\|z_0\|}_{\beta(\|z_0\|, t-t_0)} + \underbrace{\frac{c}{\lambda}\sup_{t_0\leq\tau\leq t}\|Nw_i(\tau)\|}_{\gamma(\sup_{t_0\leq\tau\leq t}\|Nw_i(\tau)\|)}.
\end{aligned}$$

Since β is a class $\mathcal{KL}$ function and γ is a class $\mathcal{K}$ function, Σ^p is ISS for arbitrary $x_d(t)$ satisfying Assumption 4.1. □

This theorem can be interpreted as follows. If $Nw_i(t) \equiv 0$, the response of Σ^p is equivalent to the response of Σ^u, whose origin is GUES. Due to (4.5), $x_d(t)$ encodes the information of $F_d(t)$ during the contact phase, so $x \to x_d(t)$ and $F_e \to F_d(t)$ exponentially. If $Nw_i(t) \neq 0$, the response of Σ^p deviates from the response of Σ^u, (i.e. x and F_e will only converge to neighbourhoods of $x_d(t)$ and $F_d(t)$, respectively), but due to the ISS property the response of Σ^p is bounded and the bound on the error norm $\|z\|$, with z defined in (4.6), will depend on the norm of the perturbation Nw_i.

4.4 Example with a stiff environment

The use of the developed theory is illustrated by means of simulations and the implications of satisfying Theorem 4.4 on the controller design are shown. Consider a manipulator with $M = 1$ kg and $b = 0$ Ns/m (i.e. no viscous friction is present in the manipulator to help dissipate energy), interacting with an environment with $k_e = 10^6$ N/m and $b_e = 10$ Ns/m. The control parameters are selected as $M_a = 0.8$ kg, $k_p = 4000$, $k_d = 80$, $k_f = 1$ and $b_f = 5$. For this parameter set, the eigenvectors of A_2 in (4.7) are complex, such that no visible eigenvectors exist in the contact phase (see Definition 4.2). The eigenvectors of A_1 in (4.7) are real, but not visible. The response of the system is shown in Fig. 4.3. Although $x_d(t)$ and $F_d(t)$ used for the simulation in Fig. 4.3 are not necessarily worst-case inputs, the value $\Lambda = \Lambda_1^2\Lambda_2^2 = 10.16$ indicates that the system is *potentially* unstable (the conditions in case *ii* of Theorem 4.2 are *necessary and sufficient* for stability of Σ^w, since they are based on its exact solution). The controller tracks $x_d(t)$ in free motion, but due to the stiff environment and nonzero impact velocity, a large peak force occurs (see middle plot in Fig. 4.3). The manipulator bounces then back from the environment and breaks contact. During the 0.15 s of intended contact, the manipulator continues to bounce and the controller keeps switching between the motion and force controller. This results in high control forces (see bottom plot in Fig. 4.3) and the controller is not able to track the desired contact force $F_d(t)$, which has a maximum of 7 N. Around 0.27 s the *motion* controller is no longer able to bring the manipulator in contact with the environment due to the relatively large negative derivative term in (4.3a). The amplitude of the bouncing does decay over time, but Fig. 4.3 clearly illustrates an undesired response. The problem is the lack of damping in contact. Increasing the damping level in the force controller to $b_f = 9000$ results in $\Lambda = \Lambda_1^2\Lambda_2^2 = 0.98$, such that the origin of Σ^w is GUAS (see Theorem 4.2) and the system Σ^p is ISS, for *any* motion-force profile $x_d(t), F_d(t)$ satisfying Assumption 4.1 (see Theorem 4.4). With $b_f = 9000$, the manipulator does not

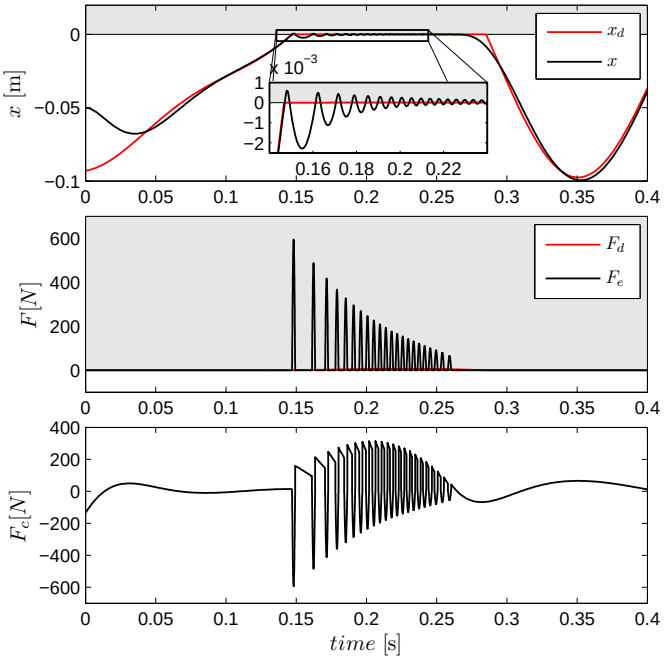

Fig. 4.3. Simulation results with $b_f = 5$. The grey area indicates the contact phase.

bounce against the environment (see Fig. 4.4) and, after the peak impact force, the contact force F_e approximately tracks $F_d(t)$.

However, such a high damping gain b_f in contact is probably not realizable in practice, so therefore a different solution is considered, namely the use of the switched motion-force controller in combination with a compliant manipulator. The results of Theorem 4.4 are then used as a systematic procedure to design the stiffness of the wrist. This solution is discussed in the next section.

4.5 Compliant manipulator design

This section discusses the motivation for the need of compliancy in the contact phase. In particular, for a compliant manipulator, it is shown how Theorem 4.4 can be used to tune the stiffness and damping properties of the introduced compliancy.

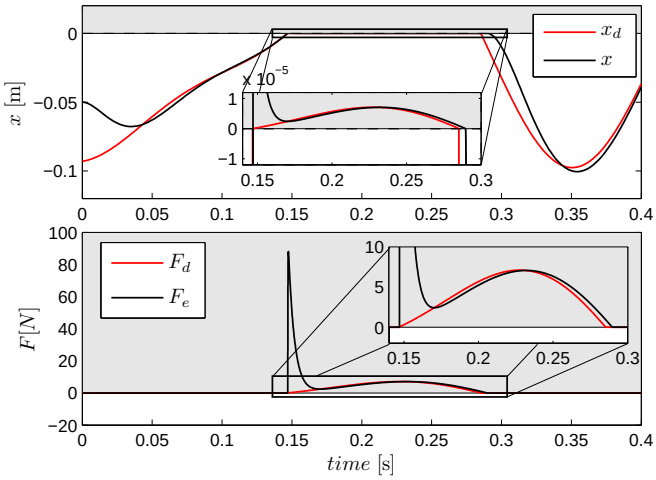

Fig. 4.4. Simulation results with $b_f = 9000$. The grey area indicates the contact phase.

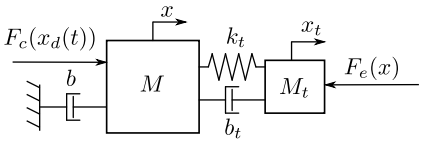

Fig. 4.5. Manipulator with compliant wrist.

4.5.1 Motivation and design

A drawback of the high damping gain b_f used in the simulation in Fig. 4.4 is that it results in a lag in tracking $F_d(t)$ for $t \in [0.17, 0.28]$ (sluggish response). Moreover, most manipulators are not equipped with velocity sensors. So typically, the velocity signal $\dot{x}$, used in (4.3b), must be obtained from the position measurements. Due to measurement noise, encoder quantization and a finite sample interval, realizing the damping force $-b_f\dot{x}$ appearing in (4.3b) is very hard, for not saying impossible, in practice, even if one would use a state observer to estimate $\dot{x}$.

To guarantee stable impacts without the need of high damping gains, many solutions in the literature aim at making the contact phase compliant. For example, the desired compliancy can be created using an impedance or admittance controller [24, 58, 142]. Alternatively, as sketched in Fig. 4.5, the compliancy could be implemented mechanically by designing the manipulator with a compliant connection between the arm and the end-effector (wrist) or a compliant cover, like the skin around a human finger. Unlike impedance or admittance

controllers, a mechanical compliance does not suffer from a noisy force sensor, encoder quantization or sampling-induced effects. In contrast, with mechanical compliance, a direct response to the fast impact phenomena is guaranteed. Therefore, to illustrate how the results for the rigid manipulator can be applied to a compliant manipulator, a manipulator with mechanical compliance, as depicted in Fig. 4.5, is considered for illustration purposes. Indicating with k_t and b_t, respectively, the stiffness and damping coefficient of the wrist and with x_t the position of the end-effector, the dynamics of the compliant manipulator is

$$M\ddot{x} + b\dot{x} = F_c - F_t, \tag{4.16a}$$

$$M_t\ddot{x}_t = F_t - F_e(x_t, \dot{x}_t), \tag{4.16b}$$

where the internal force F_t is given by

$$F_t = k_t(x - x_t) + b_t(\dot{x} - \dot{x}_t). \tag{4.17}$$

The environment model and controller are still given by (4.2) and (4.3), respectively, and (4.3) controls x to $x_d(t)$.

The compliant wrist and end-effector are designed to improve the response during and after the impact phase. So, a design is considered where the mass M_t is smaller than M to reduce the kinetic energy of M_t engaged at impact. The damping b_t is larger than b_e to help dissipate the impact energy and provide more damping in the contact phase. The stiffness k_t is designed smaller than k_e (k_e is much larger than all other parameters) to reduce the eigenfrequency and increase the damping ratio of the contact phase. In symbols, these assumptions can be written as

$$M_t \ll M,\ k_t \ll k_e,\ b_t \gg b_e,\ \text{and}\ \frac{b_t}{k_e} \ll 1\ \text{s}. \tag{4.18}$$

4.5.2 Reduced order model

The stability results of Section 4.3 only apply to two-dimensional systems. The dynamics of the 2-DOF compliant manipulator of (4.16) is 4-dimensional, so Theorem 4.2 cannot be applied directly. However, when (4.18) is satisfied, the compliant 2-DOF manipulator (4.16) exhibits a clear separation between fast and slow dynamics. In free motion, the fast dynamics are related to $x - x_t$, and, in contact, to the end-effector position x_t. The time-scale of the (exponentially stable) fast dynamics is very small compared to the time-scale of interest, so the slow dynamics can be considered as the dominant dynamics describing the response x of the compliant manipulator to the control input $F_c(t)$.

Consider the 2-DOF compliant manipulator (4.16), (4.2) with $M \sim 10^0$, $b \sim 10^0$, $M_t \sim 10^{-2}$, $k_t \sim 10^4$, $b_t \sim 10^2$, $k_e \sim 10^6$ and $b_e \sim 10^1$. The model reduction analysis in Appendix A.3 shows that the slow time-scale response of this system

in free motion and contact considered separately can be approximated by the following model of reduced (2^{nd}) order:

$$M\ddot{x} + b\dot{x} = F_c - \bar{F}_e(x, \dot{x}), \tag{4.19}$$

$$\bar{F}_e(x, \dot{x}) = \begin{cases} 0 & \text{for } x \leq 0 \\ \bar{b}_e\dot{x} + \bar{k}_e x & \text{for } x > 0 \end{cases} \tag{4.20}$$

with $\bar{b}_e := b_t \frac{k_e}{k_t + k_e}$ and $\bar{k}_e := k_t \frac{k_e}{k_t + k_e}$. The fraction $\frac{k_e}{k_t + k_e} \approx 1$ for $k_t \ll k_e$, so k_t and b_t directly influence the perceived environment damping and stiffness by the mass M.

The reduced-order dynamics (4.19), (4.20) are obtained separately for the free motion and contact case. During free motion to contact transitions, the high-frequency dynamics of (4.16), (4.2), which are not captured in (4.19), (4.20), might still be excited. However, the simulations provided in Section 4.5.4 indicate that the response of (4.19), (4.20) accurately approximates the response of (4.16), (4.2), subject to (4.18) and controlled by (4.3). Hence, it is claimed that the reduced-order model (4.19), (4.20) can be used to analyze stability of (4.16), (4.2), in closed loop with (4.3).

4.5.3 Stability of the reduced-order model

Since the reduced-order model (4.19), (4.20) has exactly the same structure as (4.1), (4.2), the stability analysis presented in Section 4.3 can be employed to design the parameters of the controller in (4.3). In contact, a similar expression is used to relate $F_d(t)$ to $x_d(t)$, namely

$$F_d(t) = \bar{k}_e x_d(t) + \bar{b}_e \dot{x}_d(t) + \bar{w}_f(t), \quad \text{for } F_d(t) > 0 \tag{4.21}$$

with $\bar{w}_f(t) := (\tilde{k}_e - \bar{k}_e)x_d(t) + (\tilde{b}_e - \bar{b}_e)\dot{x}_d(t)$, and $\tilde{k}_e$ and $\tilde{b}_e$ available estimates of $\bar{k}_e$ and $\bar{b}_e$, respectively. Note that compared to k_e and b_e, knowledge of $\bar{k}_e$ and $\bar{b}_e$ will be more accurate, since satisfying (4.18) results in $\bar{k}_e \approx k_t$ and $\bar{b}_e \approx b_t$. The design of the desired trajectories such that $x_d(t)$ is bounded and twice differentiable is discussed in Appendix A.1.

The system described by (4.19), (4.20), (4.3) and (4.21) can be expressed in the form Σ^p of (4.7), with (4.8a), (4.8c), (4.8d) and

$$K_2 := \frac{(1 + k_f)\bar{k}_e}{M}, \quad B_2 := \frac{(1 + k_f)\bar{b}_e + b_f + b}{M}. \tag{4.22}$$

As a result, ISS can be concluded from Theorem 4.4 for arbitrary $x_d(t)$ satisfying Assumption 4.1 if the conditions of Theorem 4.2 are satisfied. Compared to the system without compliant wrist, there is now more flexibility to tune the parameters for stability and performance. From Theorem 4.2, the required values of the design parameters k_t and b_t can be computed to meet design specifications

such as the existence of a visible eigenvector corresponding to a stable eigenvalue (implying bounceless impact) or an upper bound on $\Lambda = \Lambda_1^2\Lambda_2^2$ in Theorem 4.2. In case of a visible eigenvector corresponding to a stable eigenvalue, stable contact with the environment *without* bouncing can be achieved for *all* bounded signals $x_d(t), F_d(t)$.

Remark 4.4. The second-order closed-loop dynamics

$$M_d(\ddot{x}_d(t) - \ddot{x}) + B_d(\dot{x}_d(t) - x) + K_d(x_d(t) - x) = F_e, \tag{4.23}$$

obtained in, e.g., [142] after the implementation of an impedance controller, can also be expressed in the form Σ^p in (4.7). Therefore, even if the desired impedance parameters M_d, B_d and K_d switch for the free motion and contact phase (as done in [142]), Theorem 4.2 can be used to tune these parameters to guarantee stable and bounceless impacts. A reduction of the closed-loop model is in that case not required.

4.5.4 Compliant manipulator example

The following example illustrates how to design the compliant wrist parameters M_t, b_t and k_t to obtain satisfactory closed-loop performance. For the design of the end-effector, consider $M_t = 0.05$ kg and $k_t = 5 \cdot 10^4$ N/m ($k_t \ll k_e$, but still large to minimize the spring-travel in the wrist). With $b_f = 5$ Ns/m, it is required that $b_t > 170$ Ns/m to guarantee that $\Lambda < 1$, such that one of the conditions of Theorem 4.2 is satisfied. Fig. 4.6 shows the response of the *unreduced* compliant system (4.16), (4.3) and (4.2), with $b_t = 171$ Ns/m. Compared to Fig. 4.3, the peak impact force is reduced and the computed control force F_c is improved. During the first 20 ms of intended contact, the tip makes and breaks contact due to the fast dynamics of (4.16). After 20 ms the fast dynamics of (4.16) damp out, the slow dynamics become dominant and the response of (4.16) converges to that of (4.19). Hence, F_e tracks the desired trajectory $F_d(t)$ (without a sluggish response as in Fig. 4.4). Since stability is now obtained with a (more practical) passive implementation, there is more freedom in tuning the parameters of the controller in (4.3).

Finally, Fig. 4.7 shows a comparison of the response of the 4-dimensional compliant manipulator described by (4.16), (4.17), (4.2), controlled by (4.3), and the 2-dimensional model described by (4.19), (4.20), and controlled by (4.3). The peak impact force of the 2-dimensional model is 30 percent smaller, but the time of making and breaking contact is almost equal. The main difference between the two models is found between 0.155 s and 0.18 s, where the fast dynamics of the 4-dimensional model are excited due to bouncing of the tip against the environment. Here, the 2-dimensional model has a second peak around 0.16 s due to a larger impact velocity compared to the tip of the 4-dimensional model. After 0.18 s, the response of both models is similar, indicating that (4.19), (4.20) is indeed a good (slow time-scale) approximation of (4.16), (4.17), (4.2) and that

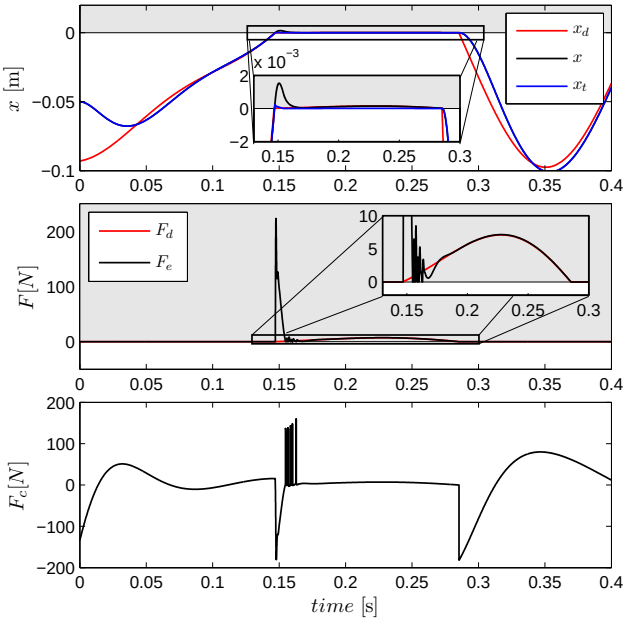

Fig. 4.6. Simulation results of compliant manipulator described by (4.16). The grey area indicates the contact phase.

Theorem 4.2 can be used as a guideline for the design of damping and stiffness parameters of the compliant wrist and of the switching controller (4.3).

4.5.5 Discussion

From the expressions $\bar{k}_e$ and $\bar{b}_e$ in (4.20) and the results in Fig. 4.6, it is found that the compliance in the manipulator can contribute to guaranteeing stability and improve the tracking performance during free motion to contact transitions. In fact, with $b_t \gg b_e$, the end-effector acts as a vibration-absorber, dissipating the kinetic energy present at impact. And due to the compliance, the stiffness can be lowered and the damping of the perceived manipulator-environment connection in contact can be increased. As a result, the controllers (4.3a) and (4.3b) can be tuned separately for optimal performance in free motion and contact, respectively, rather than a trade-off to guarantee stability during transitions in case of a rigid manipulator. Using a light end-effector and tuning of b_t and k_t to satisfy Theorem 4.2, stable contact with the environment can be made for arbitrary $x_d(t)$ and $F_d(t)$ satisfying Assumption 4.1. Moreover, if a visible eigenvector exists in the contact phase, even bouncing of the manipulator can

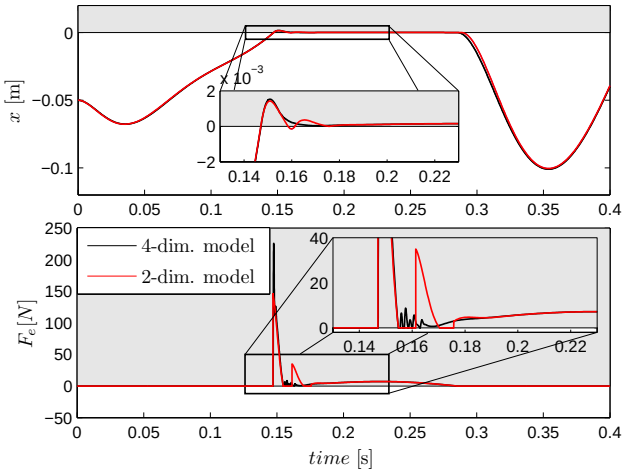

Fig. 4.7. Simulation results of the compliant manipulator described by (4.16), (4.17), (4.2) (black line), and the reduced-order model described by (4.19), (4.20) (blue line). The grey area indicates the contact phase, i.e. $x_t > 0$ for the 4-dimensional model (4.16), (4.17), (4.2) and $x > 0$ for the 2-dimensional model (4.19), (4.20).

be prevented for arbitrary $x_d(t)$ and $F_d(t)$.

4.6 Conclusion

This chapter considers the position-force control of a manipulator in contact with a stiff environment, focusing on a single direction of contact interaction. Using a novel analytical stability analysis, sufficient conditions are provided for the input-to-state stability (ISS) of the closed-loop switching tracking error dynamics with respect to perturbations related to desired time-varying trajectories. From this analysis, guidelines are obtained to ensure stable bounded tracking of *time-varying* motion and force profiles. For a rigid manipulator and realistic parameter values, a high level of controller damping is required during contact to guarantee stability of the closed-loop system. Such high-gain velocity feedback is undesirable for achieving satisfying tracking performance and, moreover, likely to be unrealizable in practice.

Based on the results of the investigation, the proposed switching controller is combined with a mechanical design of the manipulator that includes a compliant wrist. Together with a reduction of the compliant model, the proposed stability conditions are used as a guideline for the design of the damping and stiffness of this compliant wrist, as well as the controller parameters, to guarantee stability. Furthermore, those stability conditions can be used to shape the

closed-loop response to prevent persistent bouncing of the manipulator against the environment for arbitrary desired time-varying motion and force profiles.

An extension of the results towards nonlinear multiple-DOF systems where the constrained direction cannot be decoupled from the unconstrained directions is considered as future work. Furthermore, including more advanced controllers, such as PD or PI force control in contact, requires an extension to include switched systems with an increased state-space dimension.

In the context of teleoperation, this chapter was dedicated to guaranteeing stability of the local slave-environment interaction. The next chapter focuses on the design of a novel architecture to guarantee passivity of the teleoperator in the presence of delays, when interacting with stiff remote environments.

Chapter 5

A 2-layer architecture for direct force-reflection with time delays

5.1 Introduction

This chapter presents a novel two-layer architecture designed specifically for direct force-reflecting teleoperation with communication delays. In contrast to bilateral motion synchronization, direct force-reflection architectures do not suffer from delay-induced forces or a reflection of the slave dynamics (see Sections 2.2 and 2.3 for an elaborate discussion). When the slave is in free motion, the architecture is unilateral and therefore the stability and performance are not affected by the delays. On the other hand, when the slave makes contact with the environment, the scheme switches to a bilateral architecture. This switch in the dynamics could result in unstable impact behavior and/or a recoiling of the master device. If these issues are not analyzed and controlled properly, the operator might not be able to keep the slave in contact with the environment.

In free motion, the slave is commanded to follow the master position, whereas in contact the slave should apply the same force on the environment as the operator applied on the master. If not enough damping is present in the contact phase, the teleoperator might become unstable for specific operator inputs. But even if the local interaction between the slave and the environment is stable, the master might still recoil due to the delayed reflection of the environment force to the operator. Such a recoiling must be prevented when designing a bilateral teleoperator, but traditional approaches that use constant parameters inject either a lot of damping (see, e.g., [94] and the references therein), or reduce the coupling strength between the master and slave significantly [36, 62, 64]. This is not desired, since using high damping gains in free motion increases the

operator effort. Moreover, both high damping gains (see [15]) and a low coupling strength result in a softer perception of the environment.

In this chapter, an alternative approach is taken, in which performance is only sacrificed when stability is in danger. Inspired by online passivity approaches presented in Section 2.4, a novel architecture is designed, based on a separation of the control architecture in two layers, as proposed in [40]. In [40], Franken et al. achieve a passive teleoperator and use a variable damping gain on the master device to harvest the energy required to actuate both the master and slave. The harvested energy is then distributed over the two controllers by synchronizing the energy levels in so called energy tanks. The point of departure that differentiates the approach presented in this chapter from [40] is that synchronizing the energy seems to be a natural option for bilateral motion synchronization, but it is not necessary for direct force-reflection.

The proposed architecture consists of two layers, called the Performance Layer (PeL) and Passivity Layer (PaL). The controller is designed explicitly for the case where the master and slave have similar, but not necessarily identical, kinematics and dynamics. If this is not the case, or if scaling of either position and/or velocity is required, the proposed two-layer controller can still be used if the scaling and the difference in the devices are addressed in an outer loop of the controller, such that the dynamics appear similar to the inner loop. For these situations, the proposed two-layer controller can be implemented in the inner loop of the controller.

In the Pel, in principle any traditional controller can be implemented to achieve the desired performance. Based on the results of the experimental comparison presented in Chapter 3, a PF-F architectures seems a good choice for contact with stiff environments. The novelty of the approach lies in the PaL, where the two controllers use a duplicate of the energy applied by the operator and environment on the teleoperator. By monitoring the energy flows online, the damping gains of both controllers are adapted when active behavior is detected. Furthermore, when more energy is generated than allowed by the designer, the control force demanded by the PeL is gradually reduced to prevent a violent recoiling of the master device. Finally, passivity of the teleoperator is proven, even in the presence of delays and for bounded activity of the operator and environment.

Interestingly, delay-free simulations show that in free motion the controller synchronizes the master and slave by synchronizing their dynamics (identical friction and inertial forces). In the delayed case, stable operation without a violent recoiling of the master is achieved, but here the dynamics of master and slave are not synchronized. Instead, it is illustrated that the variable damping gains are low when the slave is in free motion and high when the slave is in contact. This results in a minimal additional operator effort to move the teleoperator as the velocity during contact is almost zero, while stability in the contact phase is guaranteed. Without the PaL, the direct force-reflecting architecture is

shown to perform rather poorly, as previously reported in, e.g., [36, 69, 78]. Finally, the proposed controller is implemented on an experimental 1-DOF setup. Despite nonlinear friction, noisy force signals and differentiation of position measurements to obtain velocity signals, the experimental results match rather well with the numerical simulation results.

This chapter is organized as follows. Section 5.2 explains the philosophy and the key details behind the proposed control scheme. The explicit controller design and model of the teleoperator are presented in Section 5.3. Passivity of the teleoperator is proven in Section 5.4. The simulation example in Section 5.5 illustrates the behavior of the controller in both the delay-free and delayed case. Section 5.6 presents the results of the experimental implementation. Conclusions are presented in Section 5.7.

5.2 A direct force-reflection 2-layer architecture

In this section, using Fig. 5.1, the foundations are presented of the novel two-layer architecture. In Fig. 5.1, the teleoperator is indicated with a light grey background color, and the Passivity Layer with a dark grey background color. As mentioned in the Introduction, a traditional control algorithm can be implemented in the Performance Layer to obtain optimal performance, without considering passivity or stability. Ideally, this can be any of the force-reflecting algorithms discussed in Section 2.3, such as a P-F or PF-F architecture. The PeL computes the desired forces $F_{mc} \in \mathbb{R}^n$ and $F_{sc} \in \mathbb{R}^n$, with n indicating the number of degrees of freedom, to actuate the master and slave, respectively. These forces are sent to the PaL. The PaL monitors the power flows between several components of the teleoperator and is presented in detail below.

The PeL used in the proposed controller plays the same role as the transparency layer in [40]. The proposed PaL, instead, is completely different, since it is based on the philosophy of a force-reflecting architecture: the slave and master controllers represent a *virtual* operator and environment. Seeing the master controller as a virtual environment leads to allow the PaL of the master controller to use a *duplicate* of the power $P_e := -F_e^\top \dot{x}_s$ applied by the slave on the environment, with $F_e \in \mathbb{R}^n$ the force applied by the slave on the environment and $\dot{x}_s \in \mathbb{R}^n$ the slave velocity. Similarly, seeing the slave controller as a virtual operator leads to allow the PaL of the slave controller to use a *duplicate* of the power $P_h := F_h^\top \dot{x}_m$ applied by the operator on the master, with $F_h \in \mathbb{R}^n$ the force applied by the operator and $\dot{x}_m \in \mathbb{R}^n$ the master velocity. Let P_h and P_e indicate the power inflow of the PaL and $P_{ic} := F_{ic}^\top \dot{x}_i$, $i \in \{m, s\}$, the power ideally applied by the controller on the master and slave, as the power outflow. Denote with $E_{m,diff}$ and $E_{s,diff}$ the difference in the energy inflow and outflow of the controllers. Then, the rate of change of $E_{m,diff}$ and $E_{s,diff}$ are given by

$$\frac{d}{dt} E_{m,diff} = P_e - P_{mc}, \tag{5.1a}$$

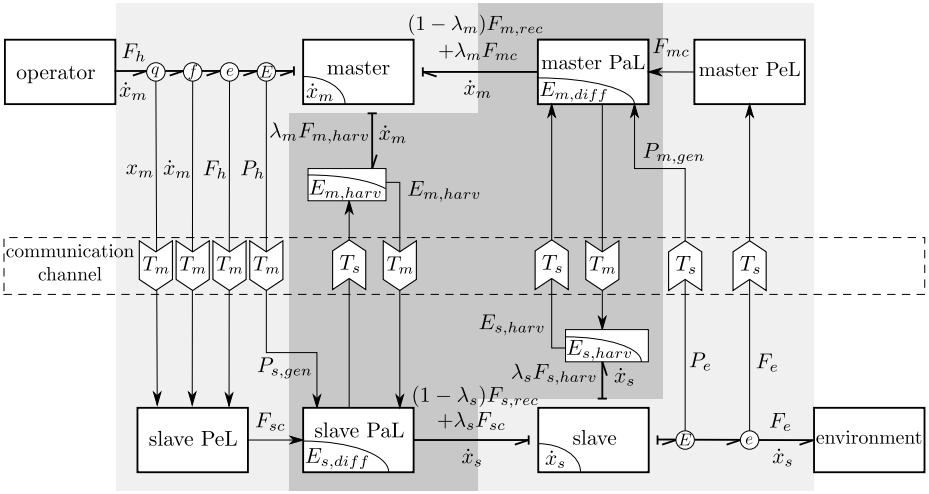

Fig. 5.1. Block diagram of the proposed 2-layer architecture. The teleoperator is indicated with a light grey background color, the Passivity Layer with a dark grey background color. Half arrows represent power flows and full arrows represent information flows. The symbols E, e, f and q represent, respectively, power-, effort-, flow- and momentum sensors.

$$\frac{d}{dt}E_{s,diff} = P_h - P_{sc}. \tag{5.1b}$$

Under ideal circumstances when the master and slave are identical (recall that the two-layer controller is designed for similar master and slave devices), they start at the exact same position and velocity, and the communication delays are zero, $P_{mc} = P_e$ and $P_{sc} = P_h$, such that $E_{i,diff}$ remains identically equal to zero when $F_{mc} = -F_e$ and $F_{sc} = F_h$ from the PeL are applied directly.

In practice, such an ideal situation occurs rarely due to differences in the master and slave dynamics and/or the existence of delays, so the control forces F_{mc} and F_{sc} will in general not result in $P_{mc} \equiv P_e$ and $P_{sc} \equiv P_h$. As a result, both $E_{m,diff}$ and $E_{s,diff}$ will diverge from zero, if left uncontrolled. Controlling $E_{i,diff}$ to zero is the novelty of the proposed controller and is the task assigned to the proposed PaL. The PaL is identical for both the master and slave controller, so for illustration purposes, this section focuses only on the description of the slave controller (virtual operator).

A positive value of $E_{s,diff}$ means that the slave controller applied *less* energy to actuate the slave than the operator applied to control the master, whereas a negative value of $E_{s,diff}$ implies that the slave controller used *more* energy. The latter, $E_{s,diff} < 0$, is associated with undesired active behavior of the controller. The PaL prevents unbounded active behavior by requesting extra power from

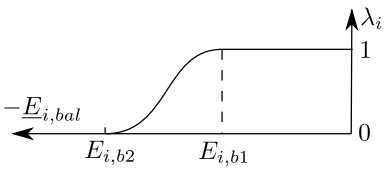

Fig. 5.2. The state-dependent variable gain λ_i as a function of $\underline{E}_{i,bal}$.

the master device, $P_{s,gen}$ in Fig. 5.1, to increase the energy level $E_{s,diff}$. The requested energy is *harvested* by injecting a variable amount of damping on the master device, indicated by $F_{m,harv}$. The variable damping gain increases as the magnitude of $E_{m,harv}$, the amount of energy that must still be harvested from the master, increases.

In case the amount of harvested energy is insufficient to compensate for the energy shortage in the slave controller, e.g., due to zero velocity of the master, and $E_{s,bal}$, the total energy balance of the slave PaL, introduced later on in (5.7), drops below a designed threshold $E_{s,b1} < 0$, the control force F_{sc} coming from the PeL is *gradually* decreased. This is done by modulating F_{sc} with a continuous and state-dependent variable gain $\lambda_s(\underline{E}_{s,bal}) \in [0,1]$. Here, $\underline{E}_{s,bal}$ is a lower bound of $E_{s,bal}$ that can be computed online and is defined later on in (5.14). The gain $\lambda_s(\underline{E}_{s,bal})$ is equal to one if $\underline{E}_{s,bal} \geq E_{s,b1}$. If $E_{s,b1} > \underline{E}_{s,bal} > E_{s,b2}$, $\lambda_s(\underline{E}_{s,bal}) \in (0,1)$ monotonically decreases to zero for decreasing values of $\underline{E}_{s,bal}$. An example of such a function is illustrated in Fig. 5.2. In the extreme case when $\underline{E}_{s,bal} \leq E_{s,b2}$, the variable gain λ_s is set to zero, such that the slave controller can no longer apply energy to the slave device. Additionally, when $\underline{E}_{s,bal} < E_{s,b1}$ the PaL *recovers* from the energy shortage by applying a force $(1-\lambda_s)F_{s,rec}$ with a variable amount of damping on the slave device.

The design of the bounds $0 > E_{s,b1} > E_{s,b2}$ affect how aggressively the PaL responds to an energy shortage in the controller. When $\underline{E}_{s,bal} > E_{s,b1}$, the variable gain λ_s is equal to one, such that the PeL force F_{sc} is applied without modification. A more negative value of $E_{s,b1}$ allows for a wider range of *temporarily* active behavior. A small difference between $E_{s,b1}$ and $E_{s,b2}$ implies an aggressive fluctuation of λ_s, while a larger difference creates a more gradual fluctuation.

Summarizing, the PaL of the slave controller monitors and regulates the use of a duplicate of the energy applied by the operator in order to apply a force F_{sc} coming from the PeL. When a mismatch in the energy consumption of the slave controller is detected, two possibilities exist. First, if the controller uses less energy than the operator, part of the excess energy is discarded, because the slave does not need it. Second, if the PeL force requires more energy than the operator, more energy is asked from the operator by injecting a variable amount

of damping on the master. If insufficient energy is harvested from the master, e.g., because the master is moving slowly, energy is harvested from the slave and the PeL force F_{sc} is modulated.

The same design is used for the PaL of the master controller. The only difference is that the master controller represents the virtual environment, so the PaL of the master controller uses a duplicate of the energy applied by the environment. If there is insufficient energy to apply the PeL force F_{mc}, extra energy is harvested by injecting a variable amount of damping on the slave. If not enough energy can be harvested from the slave, the energy is harvested from the master and the PeL force F_{mc} is modulated.

5.3 System modeling and controller design

The considered teleoperator dynamics are presented in this section, together with the details of the novel PaL illustrated in Section 5.2.

5.3.1 Teleoperator model

It is assumed that gravity is compensated in the controllers, and that the master and slave dynamics, described in Cartesian space by

$$\bar{M}_m(x_m)\ddot{x}_m + \bar{C}_m(x_m, \dot{x}_m)\dot{x}_m + \bar{f}_m(x_m, \dot{x}_m) = F_h + F^*_{mc}, \tag{5.2}$$

$$\bar{M}_s(x_m)\ddot{x}_s + \bar{C}_s(x_s, \dot{x}_s)\dot{x}_s + \bar{f}_s(x_s, \dot{x}_s) = F^*_{sc} - F_e, \tag{5.3}$$

hold globally. The end-effector positions are denoted by $x_i \in \mathbb{R}^n$, $\bar{M}_i(x_i) > 0 \in \mathbb{R}^{n\times n}$ is the inertia matrix, $\bar{C}_i(x_i) > 0 \in \mathbb{R}^{n\times n}$ the Coriolis' matrix and $\bar{f}_i(x_i, \dot{x}_i) \in \mathbb{R}^n$ is the friction of device i. The inputs F_h and F_e, as mentioned in Section 5.2, are the operator and environment forces. The control forces F^*_{ic} of the PaL are addressed in the next subsection, after the introduction of the following two assumptions, required later on in Section 5.4 to prove passivity of the teleoperator.

Assumption 5.1. *The input forces F_h and F_e satisfy*

1. $\|F_h\| \leq \overline{F}_h$ *and* $\|F_e\| \leq \overline{F}_e$, *with* $\overline{F}_h, \overline{F}_e > 0$,
2. $F_h^\top \dot{x}_m \leq 0$, *if* $|\dot{x}_m| > \dot{x}^a_m > 0$, *and*
3. $F_e^\top \dot{x}_s \leq 0$, *if* $|\dot{x}_s| > \dot{x}^a_s > 0$.

Condition 1 of Assumption 5.1 implies that the forces applied by the operator and environment are bounded. Boundedness of F_h is plausible due to the operator's physical limitations. Conditions 2 and 3 allow for an active operator and environment as long as the master and slave velocities do not exceed $\dot{x}^a_i$. As a result, Assumption 5.1 allows for both passive and bounded active behavior and

is therefore less restrictive than the passive operators and environments that are typically required for bilateral teleoperation controller designs (see e.g. [94] and the references therein).

Assumption 5.2. *The control forces F_{ic} of the PeL satisfy*

1. $\|F_{ic}\| \leq \overline{F}_{ic}$, *with* $\overline{F}_{ic} > 0$, *and*
2. $F_{ic}^{\top}\dot{x}_i \leq 0$, *if* $|\dot{x}_i| > \dot{x}_i^b > 0$.

Assumption 5.2 implies that the PeL forces F_{ic} are bounded and do not inject energy in the master and slave device above a certain velocity $\dot{x}_i^b$, which can be selected arbitrarily large to not affect stable operation. Assumption 5.2 can be satisfied by using a (smooth) saturation function to modify F_{ic} whenever Assumption 5.2 would be violated otherwise.

5.3.2 Design of the Passivity Layer controller

As described in words in Section 5.2, the PaL control force F_{ic}^* applied on device i consists of the PeL force, F_{ic}, modulated by $\lambda_i \in [0,1]$, and the *harvesting* and *recovering* forces $F_{j,harv}$ and $F_{i,rec}$. Namely,

$$F_{ic}^* = \lambda_i F_{ic} - \lambda_i F_{i,harv} - (1-\lambda_i)F_{i,rec}. \tag{5.4}$$

The harvesting and recovery forces need to satisfy $\lambda_j F_{j,harv}^{\top}\dot{x}_j \geq 0$ and $(1-\lambda_i)F_{i,rec}^{\top}\dot{x}_i \geq 0$ (recall that $j \in \{m,s\}$, $j \neq i$). This work considers

$$F_{j,harv} = -\beta_j E_{j,harv}\dot{x}_j, \tag{5.5}$$
$$F_{i,rec} = -\gamma_i \underline{E}_{i,bal}\dot{x}_i, \tag{5.6}$$

but other choices are also possible. In (5.5) and (5.6), the gains β_j and γ_i are strictly positive, such that the terms $-\beta_j E_{j,harv} \geq 0$ and $-(1-\lambda_i)\gamma_i \underline{E}_{i,bal} \geq 0$ in (5.4) represent variable damping gains, which increase for decreasing values of $E_{j,harv} \leq 0$ and $\underline{E}_{i,bal}$, respectively. In (5.5), $E_{j,harv}$ represents the amount of energy that must still be *harvested* from device j (see Fig. 5.1), as explained in Section 5.2. Furthermore, $\underline{E}_{i,bal}$, defined later on in (5.14), is a conservative but online available lower bound of $E_{i,bal}$, the energy balance of the PaL controller. The balance $E_{i,bal}$ consists of $E_{i,diff}$ on the local side of the controller, the energy $E_{j,harv}$ on the remote side of the controller, and the energy stored in the communication channel obtained by integrating the power request $-P_{i,gen}$ over the delay interval:

$$E_{i,bal} := E_{i,diff} + E_{j,harv} - \int_{t-T_i}^{t} P_{i,gen}\, d\tau. \tag{5.7}$$

In (5.7), T_i represents, depending on the value of i, T_m and T_s, the delays from master to slave and from slave to master, respectively.

Using (5.4) and including the effect of the delays, the evolution of the energy levels $E_{i,diff}$, presented in a simplified form in (5.1), become

$$\begin{aligned}\dot{E}_{m,diff} &= P_e^{T_s} + P_{m,gen} - \lambda_m F_{mc}^{\top}\dot{x}_m - \lambda_m P_{m,diss} \\ &\quad + (1-\lambda_m)F_{m,rec}^{\top}\dot{x}_m, \qquad (5.8a)\\ \dot{E}_{s,diff} &= P_h^{T_m} + P_{s,gen} - \lambda_s F_{sc}^{\top}\dot{x}_s - \lambda_s P_{s,diss} \\ &\quad + (1-\lambda_s)F_{s,rec}^{\top}\dot{x}_s, \qquad (5.8b)\end{aligned}$$

where the dissipation $P_{i,diss}$, active for $E_{i,diff} > 0$, equals

$$P_{i,diss} = \begin{cases} 0, & \text{if } E_{i,diff} < 0, \\ \alpha_i E_{i,diff}, & \text{if } E_{i,diff} \geq 0 \end{cases} \qquad (5.9)$$

with $\alpha_i > 0$ a design parameter. Without $P_{i,diss}$, $E_{i,diff}$ might grow unbounded. In [42], this growth is denoted as an energy build-up in the controller, which could prevent an *immediate* reaction of the PaL to unstable behavior.

When $E_{i,diff} < 0$, power is *generated* immediately by

$$P_{i,gen} = \begin{cases} -\alpha_i E_{i,diff} & \text{if } E_{i,diff} < 0, \\ 0 & \text{if } E_{i,diff} \geq 0. \end{cases} \qquad (5.10)$$

Note that as $P_{i,diss} \geq 0$ and $P_{i,gen} \geq 0$, there is a persistent attempt to steer $E_{i,diff}$ towards zero, which is the key principle of the PaL.

The amount of generated power $P_{i,gen}$ on the local side is sent to the remote side, and used as the input for the harvesting dynamics

$$\dot{E}_{j,harv} = \lambda_j F_{j,harv}^{\top}\dot{x}_j - P_{i,gen}^{T_i} \qquad (5.11)$$

with $F_{j,harv}$ given in (5.5). Due to the first order dynamics (5.11), $E_{j,harv}$ is guaranteed to remain non positive for all time, since $P_{i,gen} \geq 0$ and by design the state-dependent term $\lambda_j F_{j,harv}^{\top}\dot{x}_j \geq 0$.

The time derivative of (5.7), using (5.8) and (5.11), is

$$\begin{aligned}\dot{E}_{m,bal} &= P_e^{T_s} - \lambda_m F_{mc}^{\top}\dot{x}_m - \lambda_m P_{m,diss} + \lambda_s F_{s,harv}^{\top}\dot{x}_s \\ &\quad + (1-\lambda_m)F_{m,rec}^{\top}\dot{x}_m, \qquad (5.12a)\\ \dot{E}_{s,bal} &= P_h^{T_m} - \lambda_s F_{sc}^{\top}\dot{x}_s - \lambda_s P_{s,diss} + \lambda_m F_{m,harv}^{\top}\dot{x}_m \\ &\quad + (1-\lambda_s)F_{s,rec}^{\top}\dot{x}_s. \qquad (5.12b)\end{aligned}$$

Due to the time delays, $E_{i,bal}$ in (5.12) cannot be computed online as $\lambda_j F_{j,harv}^{\top}\dot{x}_j$

at time t is not available for controller i. However,

$$\begin{aligned} E_{j,harv} &= E_{j,harv}^{T_j} + \int_{t-T_j}^{t} \lambda_j F_{j,harv}^{\top} \dot{x}_j d\tau - \int_{t-T_r}^{t-T_i} P_{i,gen} d\tau \\ &\geq E_{j,harv}^{T_j} - \int_{t-T_r}^{t-T_i} P_{i,gen} d\tau, \end{aligned} \tag{5.13}$$

where $T_r := T_m + T_s$ is the round-trip delay. Therefore, by defining

$$\underline{E}_{i,bal} := E_{i,diff} + E_{j,harv}^{T_j} - \int_{t-T}^{t} P_{i,gen} d\tau \leq E_{i,bal}, \tag{5.14}$$

a lower bound of $E_{i,bal}$ is obtained that can be computed online. Differentiating the equality in (5.14) with respect to time and using (5.8) and (5.11) gives

$$\begin{aligned} \dot{\underline{E}}_{m,bal} &= P_e^{T_s} - \lambda_m F_{mc}^{\top} \dot{x}_m + \lambda_s^{T_s} \left(F_{s,harv}^{T_s} \right)^{\top} \dot{x}_s^{T_s} - \lambda_m P_{m,diss} \\ &\quad + (1-\lambda_m) F_{m,rec}^{\top} \dot{x}_m, \end{aligned} \tag{5.15a}$$

$$\begin{aligned} \dot{\underline{E}}_{s,bal} &= P_h^{T_m} - \lambda_s F_{sc}^{\top} \dot{x}_s + \lambda_m^{T_m} \left(F_{m,harv}^{T_m} \right)^{\top} \dot{x}_m^{T_m} - \lambda_s P_{s,diss} \\ &\quad + (1-\lambda_s) F_{s,rec}^{\top} \dot{x}_s. \end{aligned} \tag{5.15b}$$

Summarizing, the teleoperator consists of the device dynamics (5.2)-(5.3) and the controller defined by (5.4)-(5.6), (5.9)-(5.11) and (5.15). Its inputs are F_h and $-F_e$ and its outputs $\dot{x}_m$ and $\dot{x}_s$. It is assumed that Assumptions 5.1 and 5.2 hold. In particular, the bound $\overline{F}_{ic}$ in condition 1 of Assumption 5.2 can be satisfied by using a smooth saturation function on the PeL force F_{ic}. In the following section it is proven that the proposed teleoperator is passive.

5.4 Passivity of the teleoperator

In this section, passivity is proven of the teleoperator introduced in the previous section. To this end, denote the total energy of the teleoperator (the light grey box in Fig. 5.1) by the storage functional V, which consists of the energy $E_i := \frac{1}{2} \dot{x}_i^{\top} \bar{M}_i(x_i) \dot{x}_i$ stored in the master and slave devices, the energy $E_{i,bal}$ present in the PaL, described by (5.7), and the energy $E_{h,com} := \int_{t-T_m}^{t} P_h d\tau$ and $E_{e,com} := -\int_{t-T_s}^{t} P_e d\tau$ present in the communication channel due to the power duplication:

$$V := E_m + E_s + E_{m,bal} + E_{s,bal} + E_{h,com} + E_{e,com}. \tag{5.16}$$

The energies E_m and E_s satisfy

$$\dot{E}_m = F_h^\top \dot{x}_m + \lambda_m F_{mc}^\top \dot{x}_m - \lambda_m F_{m,harv}^\top \dot{x}_m - (1-\lambda_m) F_{m,rec}^\top \dot{x}_m, \quad (5.17a)$$

$$\dot{E}_s = -F_e^\top \dot{x}_s + \lambda_s F_{sc}^\top \dot{x}_s - \lambda_s F_{s,harv}^\top \dot{x}_s - (1-\lambda_s) F_{s,rec}^\top \dot{x}_s. \quad (5.17b)$$

Assumptions 5.1 and 5.2 imply that E_i is bounded:

Property 5.1. *Given Assumptions 5.1 and 5.2, consider the closed loop dynamics of* (5.2)-(5.3) *using the controller* (5.4). *At the initial time t_0, let $|\dot{x}_i(t_0)| \leq \overline{\dot{x}}_i := \max(\dot{x}_i^a, \dot{x}_i^b) < \infty$. Then, the energy $E_i = \frac{1}{2}\dot{x}_i^\top \bar{M}_i(x_i)\dot{x}_i$ satisfies for all $t \geq t_0$*

$$0 \leq E_i \leq \overline{E}_i =: \frac{1}{2}\nu_i \overline{\dot{x}}_i^2 \quad (5.18)$$

with ν_i the largest eigenvalue of $\bar{M}_i(x_i)$.

Proof. At time t_0, $|\dot{x}_i(t_0)| \leq \overline{\dot{x}}_i$, and since $\bar{M}_i(x_i) \leq \nu_i I$ (see [125, Chapter 7]), with I the $n \times n$ identity matrix, it follows that $E_i(t_0) \leq \overline{E}_i$. Suppose that a time t^*, where $|\dot{x}_i| = \overline{\dot{x}}_i$, does not exist. Then $|\dot{x}_i| < \overline{\dot{x}}_i$ for all $t \geq t_0$ and it follows directly that $E_i < \frac{1}{2}\overline{\dot{x}}_i^\top \bar{M}_i(x_i)\overline{\dot{x}}_i \leq \frac{1}{2}\nu_i \overline{\dot{x}}_i^2 = \overline{E}_i$ for all $t \geq t_0$. If such a time t^*, where $|\dot{x}_i| = \overline{\dot{x}}_i$, does exist, then $E_i(t^*) = \frac{1}{2}\overline{\dot{x}}_i^\top \bar{M}_i(x_i)\overline{\dot{x}}_i \leq \frac{1}{2}\nu_i \overline{\dot{x}}_i^2 = \overline{E}_i$. The first two terms of (5.17) at t^* satisfy $F_h^\top \dot{x}_m \leq 0$ and $F_e^\top \dot{x}_s \leq 0$ due to Assumption 5.1, and $F_{ic}^\top \dot{x}_i \leq 0$ due to Assumption 5.2. The last two terms on the right hand side of (5.17) are nonpositive by design. As a result, $\dot{E}_i(t^*) \leq 0$, and due to the first order dynamics of (5.17) it follows that $E_i \leq \overline{E}_i$ is an invariant set, such that $E_i \leq \overline{E}_i$ for all $t \geq t_0$. Finally, the lower bound of E_i at 0 follows from $\bar{M}_i(x_i) > 0$, which completes the proof. □

The following theorem is one of the key results of this chapter.

Theorem 5.1. *Given Assumptions 5.1 and 5.2, consider the teleoperator described by* (5.2), (5.3), (5.4)-(5.6), (5.9)-(5.11), (5.15), *having input $u := \left[F_h^\top,\ -F_e^\top\right]^\top$ and output $y := \left[\dot{x}_m^\top,\ \dot{x}_s^\top\right]^\top$. At the initial time t_0, let $|\dot{x}_i(t_0)| \leq \overline{\dot{x}}_i$ and $\underline{E}_{i,bal}(t_0) > E_{i,b2}$, with $E_{i,b2}$ introduced in Section 5.2. Then, for all $t \in [t_0, \infty)$, the storage functional V, defined in* (5.16), *satisfies*

$$V > \underline{V} > -\infty, \quad (5.19)$$

$$\frac{dV}{dt} \leq 2u^\top y \quad (5.20)$$

with

$$\underline{V} := -\overline{E}_m - \overline{E}_s - \Delta\overline{E}_e - \Delta\overline{E}_h + E_{m,b2} + E_{s,b2} + H, \quad (5.21)$$

$H := \min(E_{m,b2} - E_{m,b3} - E_{m,diff}(t_0) - 2\Delta\overline{E}_e,\ E_{s,b2} - E_{s,b3} - E_{s,diff}(t_0) - 2\Delta\overline{E}_h)$, *$\overline{E}_i$ given in* (5.18), *and the constant*

$$E_{i,b3} := \frac{1}{\alpha_i}\left(\overline{F}_h + \overline{F}_e\right)\dot{x}_i^a, \quad (5.22)$$

$$\Delta\overline{E}_h := \int_{t-T_m}^{t} \overline{F}_h \dot{x}_m^a d\tau, \qquad \Delta\overline{E}_e := \int_{t-T_s}^{t} \overline{F}_e \dot{x}_s^a d\tau. \tag{5.23}$$

The bounds $\overline{F}_h$, $\overline{F}_e$ and $\dot{x}_i^a$ are given in Assumption 5.1.

Remark 5.1. Due to the presence of time delays, V is a functional defined in terms of the (infinite dimensional) state of the teleoperator, not explicitly indicated here. Equation (5.20) in Theorem 5.1 states that the power of the teleoperator is bounded from above by the power supplied by the operator and environment. The factor 2 in (5.20) is the result of the power duplication. Furthermore, equations (5.19) and (5.20) characterize V as a storage functional and allow to conclude that the teleoperator is passive.

Proof. Equation (5.19) follows directly from Lemma 5.3, which is presented at the end of this section. To prove (5.20), differentiate V in (5.16) with respect to time to obtain

$$\dot{V} = \dot{E}_m + \dot{E}_s + \dot{E}_{m,bal} + \dot{E}_{s,bal} + \dot{E}_{h,com} + \dot{E}_{e,com}, \tag{5.24}$$

where $\dot{E}_{h,com} := P_h - P_h^{T_m}$ and $\dot{E}_{e,com} := P_e - P_e^{T_s}$ represent the power present in the communication channel due to the duplication. Then, (5.20) is obtained by using (5.12), and (5.17) in (5.24). □

In the remainder of this section, it is proven that $V > \underline{V}$. This result is presented at the end of this section in Lemma 5.3.

Lemma 5.2. *Given Assumptions 5.1 and 5.2, the constant $E_{i,b3}$ defined in* (5.22) *and the constant $\overline{E}_i$ defined in* (5.18)*, it follows for all $t \geq t_0$ that*

$$\underline{E}_{i,bal}(t) + E_i(t) \leq E_{i,diff}(t_0) + E_{i,b3} + \overline{E}_i \tag{5.25}$$

Proof. Use (5.17) in (5.8) to obtain

$$\begin{aligned} \dot{E}_{m,diff} &= F_h^\top \dot{x}_m - (F_e^{T_s})^\top \dot{x}_s^{T_s} - \lambda_m F_{m,harv} \dot{x}_m + P_{m,gen} \\ &\quad - \lambda_m P_{m,diss} - \dot{E}_m \qquad (5.26a) \\ \dot{E}_{s,diff} &= (F_h^{T_m})^\top \dot{x}_m^{T_m} - F_e^\top \dot{x}_s - \lambda_s F_{s,harv} \dot{x}_s + P_{s,gen} \\ &\quad - \lambda_s P_{s,diss} - \dot{E}_s \qquad (5.26b) \end{aligned}$$

From Assumption 5.1 it follows that $F_h^\top \dot{x}_m \leq \overline{F}_h \dot{x}_m^a$ and $-F_e^\top \dot{x}_s \leq \overline{F}_e \dot{x}_s^a$. Moreover, using $0 \leq \lambda_i \leq 1$, it follows from (5.9), (5.10) that $P_{i,gen} - \lambda_i P_{i,diss} \leq -\alpha_i E_{i,diff}$. Then, together with $F_{i,harv} \dot{x}_i \geq 0$, (5.26) can be bounded as

$$\dot{E}_{i,diff} \leq -\alpha_i E_{i,diff} + \left(\overline{F}_h + \overline{F}_e\right) \dot{x}_i^a - \dot{E}_i(t) \tag{5.27}$$

Using the Comparison Lemma (see [59], Chapter 3), the following result is obtained

$$E_{i,diff}(t) \leq e^{-\alpha_i(t-t_0)}E_{i,diff}(t_0) - \int_{t_0}^{t} e^{-\alpha_i(t-\sigma)}\dot{E}_i(\sigma)d\sigma + \left(\overline{F}_h + \overline{F}_e\right)\dot{x}_i^a \int_{t_0}^{t} e^{-\alpha_i(t-\sigma)}d\sigma. \tag{5.28}$$

Since $\alpha_i > 0 \Rightarrow e^{-\alpha_i(t-t_0)} \leq 1$ and $E_i(t_0) \leq \overline{E}_i$ due to (5.18), it follows that

$$E_{i,diff}(t) \leq E_{i,diff}(t_0) + \frac{\dot{x}_i^a}{\alpha_i}\left(\overline{F}_h + \overline{F}_e\right) - E_i(t) + \overline{E}_i.$$

Then, since the last two terms in (5.14) are by design non positive, it follows that $\underline{E}_{i,bal} \leq E_{i,diff}$, such that using (5.22) gives

$$\underline{E}_{i,bal}(t) \leq E_{i,diff}(t_0) + E_{i,b3} - E_i(t) + \overline{E}_i. \tag{5.29}$$

Finally, adding $E_i(t)$ to both sides of (5.29) yields (5.25). □

Lemma 5.3. *Given Assumptions 5.1 and 5.2, consider the teleoperator described by* (5.2), (5.3), (5.4)-(5.6), (5.9)-(5.11) *and* (5.15). *At the initial time* t_0, *let* $|\dot{x}_i(t_0)| \leq \overline{\dot{x}}_i$ *and* $\underline{E}_{i,bal}(t_0) > E_{i,b2}$, *with* $E_{i,b2}$ *introduced in Section 5.2. Then, the storage functional* V, *defined by* (5.16), *satisfies*

$$V > \underline{V} > -\infty, \tag{5.30}$$

for all time $t \geq t_0$, *with* $\underline{V}$ *defined in* (5.21).

Proof. The proof can be found in Appendix A.4. □

5.5 Illustrative numerical simulations

In this section, the stability and performance of the proposed controller are illustrated by means of numerical simulations. Similar to the experiments presented in Chapter 3 and in the next section, the 1-DOF master and slave devices, consisting of a lever mounted on an actuated revolute joint, are considered here. The dynamics (5.2)-(5.3) simplify to a 1-DOF mass-damper system, where the inertia M_i and viscous friction $f_i(x_i, \dot{x}_i) = b_i\dot{x}_i$ are identified as $M_m = 2 \cdot 10^{-3}$ kgm^2, $M_s = 2.2 \cdot 10^{-3}$ kgm^2, $b_m = 5 \cdot 10^{-3}$ Nms/rad and $b_s = 7 \cdot 10^{-3}$ Nms/rad. These represent the nominal parameter values used in the simulations. Both devices have a link length of 0.075 m. The operator is modeled as

$$F_h = m_h\ddot{x}_d(t) + b_h(\dot{x}_d(t) - \dot{x}_m) + k_h(x_d(t) - x_m), \tag{5.31}$$

where $x_d(t)$ represents the operator's intended trajectory, $k_h = 750$ N/m and $b_h = 10$ Ns/m (corresponding to $k_h = 4.22$ Nm/rad and $b_h = 0.056$ Nsm/rad) and $m_h = 1.8 \cdot 10^{-3}$ kgm^2. These values are taken from [76] and represent a relatively stiff grasp for this specific setup. The environment is located at $x_e = 0$ rad, and has a linear stiffness of $50,000$ N/m and a damping coefficient of 30 Ns/m (corresponding to $k_e = 282$ Nm/rad and $b_e = 0.28$ Nsm/rad).

In the experimental comparison presented in Chapter 3, the PF-F controller is identified as the most suitable architecture for both the free motion and contact phase in the presence of delays. Therefore, the PF-F controller is implemented in the PeL:

$$F_{mc} = -F_e^{T_s}, \tag{5.32a}$$

$$F_{sc} = F_h^{T_m} + k_p \left(x_m^{T_m} - x_s\right) + k_d \left(\dot{x}_m^{T_m} - \dot{x}_s\right) \tag{5.32b}$$

with controller gains $k_p = 16$ Nm/rad and $k_d = 0.15$ Nms/rad. Compared to a traditional P-F architecture, also the feedforward F_h is used in F_{sc} to reduce the motion error $x_m - x_s$ in both free motion and contact.

In the remainder of this section, the behavior of the teleoperator with the proposed two-layer controller is, subsequently, illustrated for the undelayed and the delayed situations.

5.5.1 Undelayed case

When the dynamics of the master and slave are not identical, the controller synchronizes in the delay-free case the master and slave on both motion and force level. The controller is robust for a mismatch in the dynamics, e.g., a different mass or friction coefficient. This robustness property is useful when the master and slave have different dynamics or kinematics, or in case motion and/or force scaling is required. A (close to) perfect compensation in the outer loop of the controller is not required when the proposed two-layer architecture is implemented in the inner loop of the controller, since it compensates this mismatch by injecting a variable amount of damping. This is illustrated below for situations where the master and slave have either a different viscous friction coefficient b_i, or a different inertia M_i. The PaL parameters are selected as $\alpha_i = 500$, $\beta_i = 5$, $\gamma_i = 100$, to provide a fast response of the variable damping gains in $F_{j,harv}$ and $F_{i,rec}$. Furthermore, $E_{i,b1} = -1 \cdot 10^{-3}$ and $E_{i,b2} = -3 \cdot 10^{-2}$ are selected large enough to not affect the free motion response.

Fig. 5.3 presents results where the master and slave inertia are equal ($M_m = M_s = 2 \cdot 10^{-3}$ kgm^2), but the slave has more viscous friction than the master ($b_m = 5 \cdot 10^{-3}$ Nms/rad and $b_s = 11 \cdot 10^{-3}$ Nms/rad). The intended operator motion $x_d(t)$ consists of a 1 Hz sinusoid. Due to the higher friction coefficient, the slave controller needs more energy to follow the motion of the master. This energy is requested from the master as $E_{m,harv}$ and results in the damping force $F_{mc}^* = -\lambda_m \beta_m E_{m,harv} \dot{x}_m$. After the initial transients, the variable damping

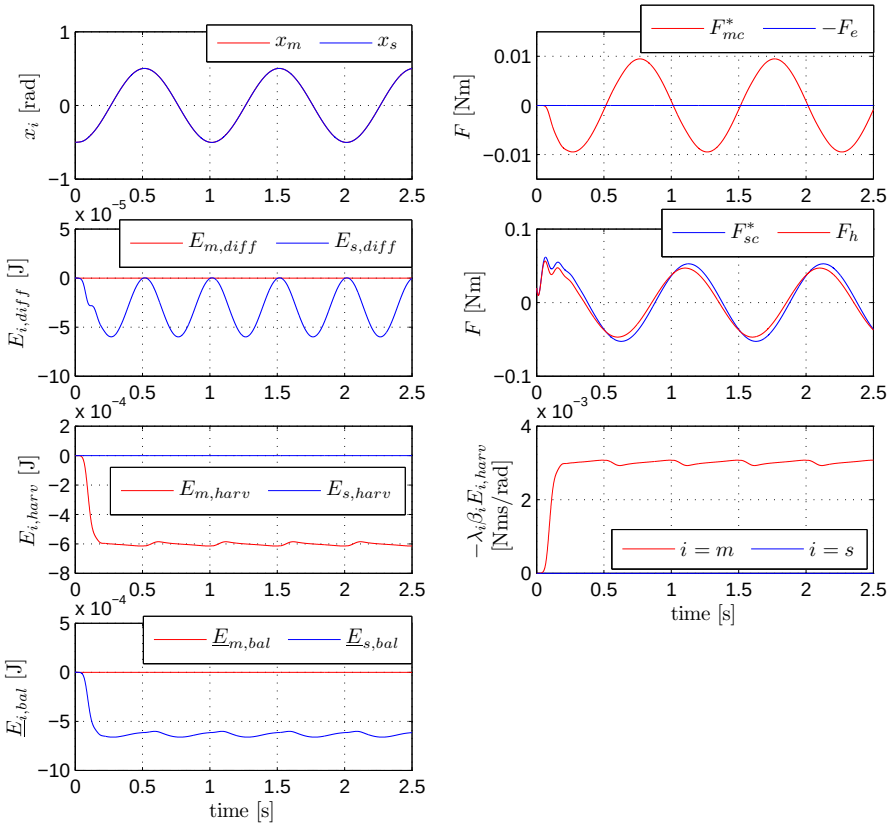

Fig. 5.3. Simulation results with PaL, no delay, $M_m = M_s = 2 \cdot 10^{-3}$ kgm^2, $b_m = 5 \cdot 10^{-3}$ Nsm/rad and $b_s = 11 \cdot 10^{-3}$ Nsm/rad. Since for all t $\underline{E}_{i,bal} > E_{i,b1}$, the force-reflection gains $\lambda_i = 1$ and the variable damping gains $-(1-\lambda_i)\gamma_i \underline{E}_{i,bal}$ in $F_{i,rec}$ remain equal to zero.

gain $-\lambda_m \beta_m E_{m,harv}$ settles around $3{\cdot}10^{-3}$ Nms/rad, i.e. half of the difference $b_s - b_m$. The factor two is the result of the energy duplication in the PaL.

When, instead, the master and slave have identical friction coefficients, but different inertias, this results in a different behavior of the controller. Fig. 5.4 shows results for $M_m = 2 \cdot 10^{-3}$ kgm^2, $M_s = 2.9 \cdot 10^{-3}$ kgm^2 and $b_m = b_s = 5 \cdot 10^{-3}$ Nsm/rad. Due to the higher inertia, the slave controller only requires more energy than it received from the operator during acceleration phases. The extra energy is requested from the master as $E_{m,harv}$ and results in the control force F^*_{mc} that opposes the motion of the master device only during the acceleration phases. During the deceleration phases, more energy is harvested by the

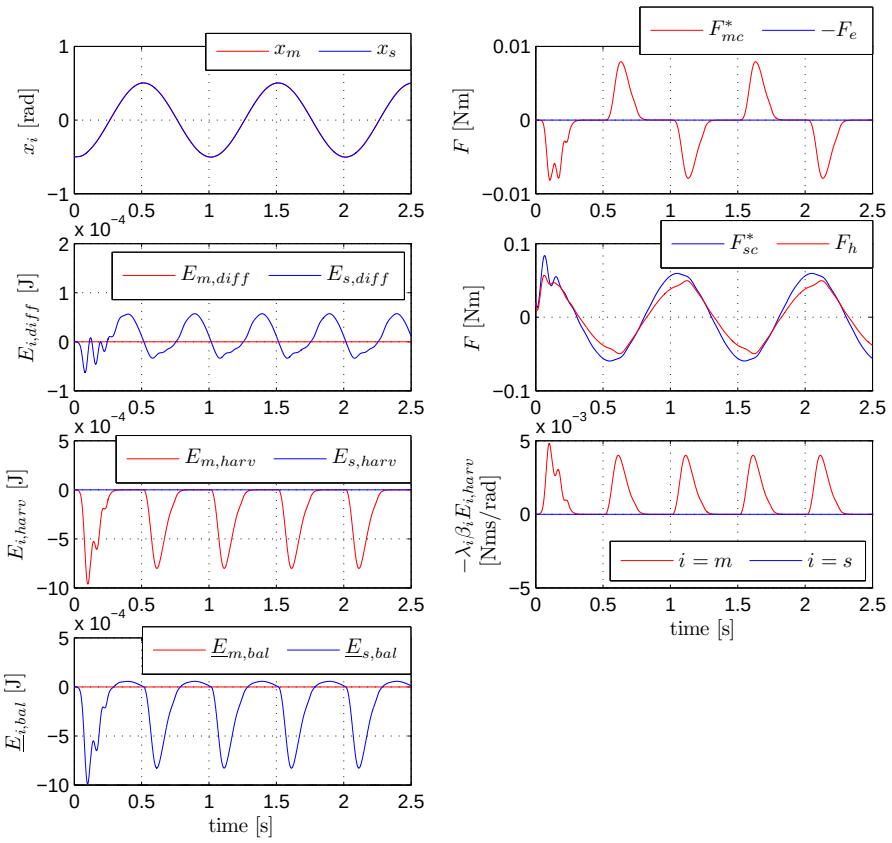

Fig. 5.4. Simulation results with PaL, no delay, $M_m = 2 \cdot 10^{-3}$ kgm^2, $M_s = 2.9 \cdot 10^{-3}$ kgm^2 and $b_m = b_s = 5 \cdot 10^{-3}$ Nsm/rad. Since for all t $\underline{E}_{i,bal} > E_{i,b1}$, the force-reflection gains $\lambda_i = 1$ and the variable damping gains $-(1-\lambda_i)\gamma_i \underline{E}_{i,bal}$ in $F_{i,rec}$ remain equal to zero.

slave controller from the slave than the operator harvests from the master. The resulting positive energy difference $E_{s,diff}$ is partly dissipated by $P_{s,diss}$ in (5.9).

Concluding, the PaL adjusts itself to compensate for (significant) differences in the dynamics of the master and slave. This feature is useful when the master and slave are not exactly identical. Without any knowledge regarding these dynamics, the dynamics of the slave are mimicked on the master side via a variable amount of damping.

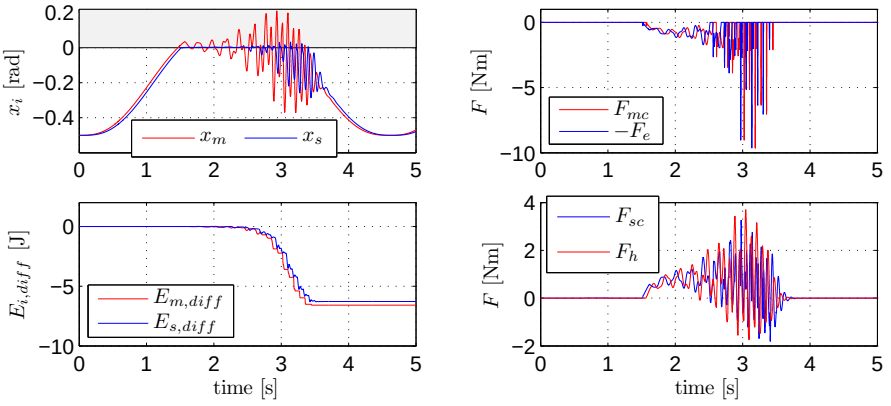

Fig. 5.5. Simulation results *without* PaL for $T_m = T_s = 0.05$ s and $E_{i,diff}$ given by (5.1).

5.5.2 100 ms round-trip delay

A major problem with direct force-reflecting architectures that suffer from communication delays is that the operator is not able to keep the slave in contact with the environment due to a violent recoiling of the master device. For the 1-DOF teleoperator, this is illustrated Fig. 5.5. The operator intends to move the teleoperator towards the environment, apply a force profile on the environment, and then detach again. The considered delays are $T_m = T_s = 0.05$ s, resulting in a round-trip delay of $T_r = 0.1$ s (a different distribution of T_r over T_m and T_s leads to the same response, apart from a shift in time of the slave motion). The PaL is *not* used and the PeL forces (5.32) are applied directly. During the intended contact phase the system oscillates and the slave bounces against the environment, creating high impact forces. This bouncing is *not* the result of the unstable local interaction of the slave and the environment, as considered in Chapter 4, because in this example the contact phase is sufficiently damped. Instead, the bouncing is the result of the delay in the closed loop of the controller and a detailed explanation for the occurrence of this bouncing is given in Section 2.3.1. Looking at $E_{i,diff}$ computed by (5.1), it is observed that the controllers generate energy.

Fig. 5.6 shows results of the same simulation, but this time *with* the proposed PaL. Due to the PaL, the teleoperator is stable in both free and constrained motion and bouncing or a violent recoiling does not occur. The PaL parameters are selected as $\alpha_i = 20$, $\beta_i = 40$, $\gamma_i = 100$, $E_{i,b1} = -1 \cdot 10^{-3}$, $E_{i,b2} = -3 \cdot 10^{-2}$ ($E_{i,b1} \neq E_{i,b2}$ to prevent chattering of F_{ic}^*). The tuning of the parameters α_i, β_i and γ_i is related to the expected kinetic energy of the manipulators. Here,

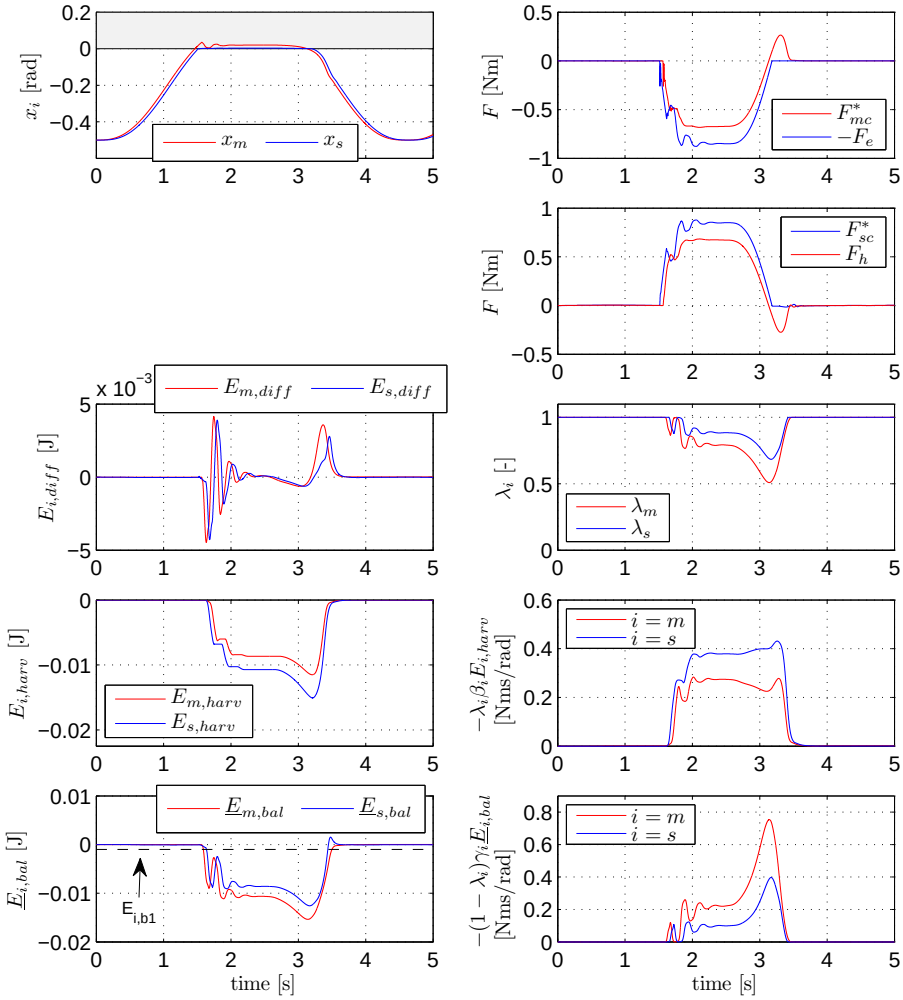

Fig. 5.6. Simulation results *with* PaL for $T_m = T_s = 0.05$ s.

they are tuned to provide a fast, but not too aggressive, response of the variable damping gains in $F_{j,harv}$ and $F_{i,rec}$. The bounds $E_{i,b1}$ and $E_{i,b2}$ are tuned such that λ_i does not fluctuate too fast and λ_i remains close to one during free motion. All energy levels, and thus the variable damping gains, are initialized at zero.

The working principle of the PaL is explained as follows. At the time of impact all kinetic energy of the slave is transferred to the environment. Due to the power duplication, T_s seconds later this energy is also subtracted from

$E_{m,diff}$. Since $F_{mc} = -F_e^{T_s}$, the master is first slowed down, increasing $E_{m,diff}$, and then pushed back, reversing its velocity and thus decreasing $E_{m,diff}$. The operator partially prevents that the master is pushed back by consuming part of its energy, i.e. $P_h < 0$. Due to duplication of P_h, $E_{s,diff}$ drops as well. When $E_{i,diff}$ drops, also $\underline{E}_{i,bal}$ drops, such that the variable damping gains of the *harvesting* and *recovery* forces increase, and λ_i is reduced slightly. The damping gains remain relatively high during contact, since the velocities are small and not much energy can be harvested. Note that during contact $F_{mc}^* \neq -F_e^{T_s}$ and $F_{sc}^* \neq F_h^{T_m}$, because $\lambda_i \neq 1$. However, this force-reflection gain is quite large compared to the recommendations in, e.g., [36, 139]. During the detachment phase, first the variable damping gains increase and λ_i reduces more to prevent that the master is pushed back violently as occurred in Fig. 5.5. After the detachment, when the velocities increase, energy is harvested, the variable damping gains quickly converge to zero and λ_i converges back to one.

Summarizing, the PaL prevents active behavior by increasing the damping gains *only* during the contact phase. The resulting damping forces are at least one order of magnitude smaller than F_e, since the velocities are low in contact. Moreover, the force-reflection gains λ_i are only *temporarily* smaller than one, but quite high compared to the constant values used in the previously mentioned literature.

5.6 Experiments

This section presents the experimental results of the proposed controller implemented on the same 1-DOF setup used in the previous section. Details of this setup were presented previously in Section 3.2. Compared to the ideal model used in the simulations, the velocity of the master and slave cannot be measured. Instead, the velocity is obtained from the position measurements and therefore suffers from encoder quantization and a finite sampling interval (1 kHz). The force sensor is located between the inner and outer segment of the setup and not at the end-effector. Apart from noise, also the effects of the dynamics between the force sensor and the end-effector are measured. In order to illustrate the robustness of the proposed controller, it is decided not to compensate the force measurements for these measured dynamics. Another difference with the simulation model of the master and slave is that the drive train is not infinitely stiff. Although the corresponding dynamics are typically of a high frequency, they can be exited during the crucial phase when the slave device makes contact with the environment.

Due to these imperfections, the proportional and derivative gains of the controller (5.32) are lowered to $k_p = 11.2$ Nm/rad and $k_d = 0.089$ Nsm/rad, compared to the simulations. The velocity signal is obtained by numerical differentiation of the position signal, in combination with a first-order lowpass filter with a cut-off frequency of 80 Hz. The force signals are filtered with a first-order

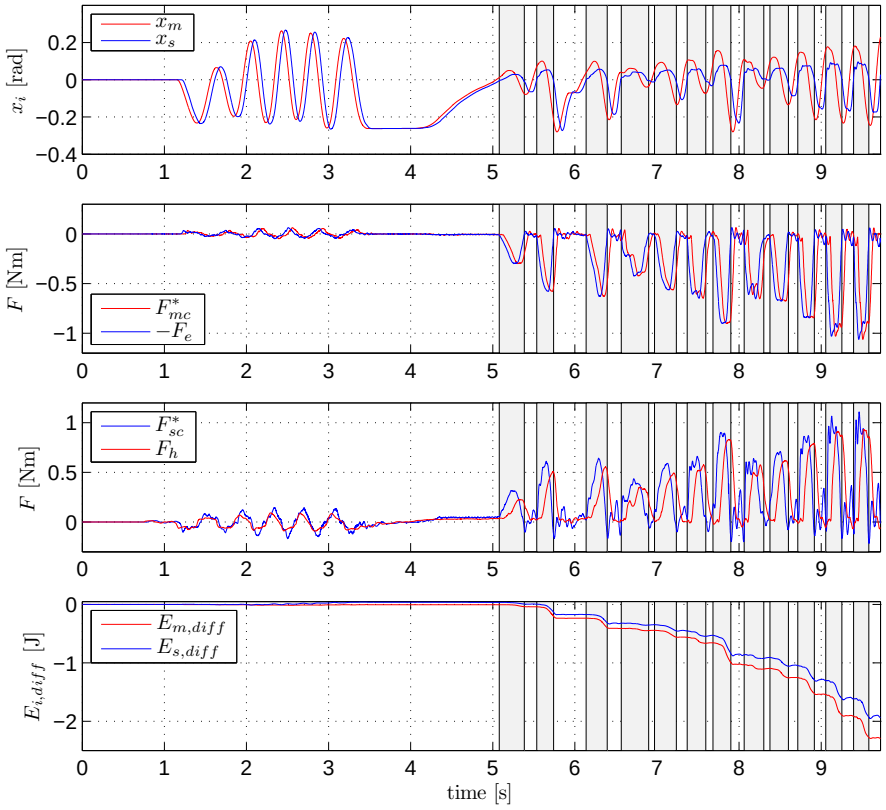

Fig. 5.7. Experimental results *without* PaL for $T_m = T_s = 0.05$ s: Positions, forces and the energy difference $E_{i,diff}$ computed by (5.1). In the light grey area the slave is in contact with the spring.

lowpass filter with a cut-off frequency of 15 Hz.

5.6.1 Without PaL

Fig. 5.7 presents results where the PaL of the proposed controller is not used. During the first four seconds the slave is in free motion and follows the master with a delay $T_m = 0.05$ s. After 5 s the operator attempts to keep the slave in contact with a spring, having stiffness $k_e \approx 2300$ N/m. The light grey areas indicate when the slave is in contact with the environment. The operator is not able to keep the slave in contact with the spring, despite the careful approach. The slave bounces several times, with increasing amplitude, against the envi-

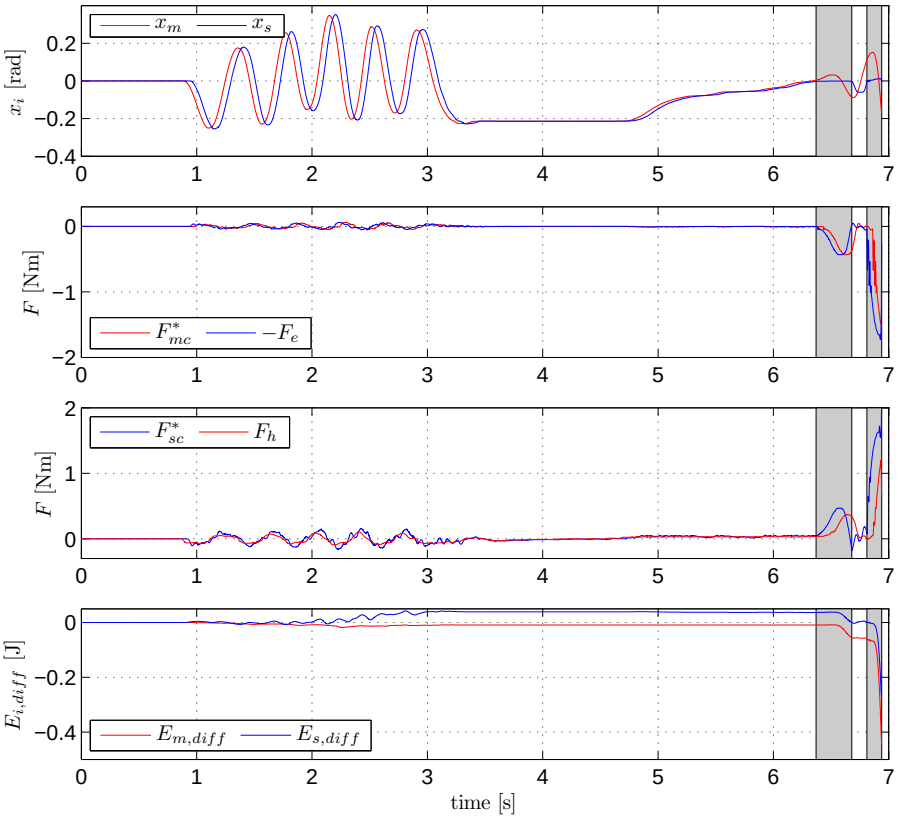

Fig. 5.8. Experimental results *without* PaL for $T_m = T_s = 0.05$ s: Positions, forces and the energy difference $E_{i,diff}$ computed by (5.1). In the dark grey area the slave is in contact with the aluminium cylinder.

ronment. Around 9.7 s the safety of the setup stops the experiment due to the high velocity of the master. Looking at the energy difference $E_{i,diff}$ computed by (5.1), it is observed that the controllers generate energy.

The violent recoiling of the master becomes more severe when the slave interacts with an aluminium cylinder. The results of this challenging task are shown in Fig. 5.8. The environment is approached carefully by the operator, but the slave bounces back from the cylinder. The master recoils twice before the safety of the setup stops the experiment due to the high master velocity. Again, the bouncing and recoiling are associated with active behavior of the controller (5.32), i.e. negative $E_{i,diff}$.

5.6.2 With PaL

Results for a combined free motion movement (first 4 s), contact with the spring (during the light grey area) and contact with the aluminium cylinder (during the dark grey area) with the controller proposed in this chapter are shown in Figs. 5.9 and 5.10. Due to the mentioned system imperfections, the PaL parameters are adjusted compared to the simulations of the previous section. They are selected as $\alpha_i = 5$, $\beta_i = 15$, $\gamma_i = 20$, $E_{i,b1} = -2 \cdot 10^{-3}$ and $E_{i,b2} = -6 \cdot 10^{-2}$ to barely affect the response in free motion, but rapidly react to the impact and detachment of the slave-environment interaction. Due to a limited actuator torque, the upper bound of the control forces F_{ic} in Assumption 5.2 is selected as $\overline{F}_{ic} = 1.5$ Nm, and the maximal allowed velocity is set to $\dot{x}_i^b = 7$ rad/s. The operator is instructed to satisfy the same bounds, i.e. in Assumption 5.1 $\overline{F}_h = 1.5$ Nm and $\dot{x}_m^a = 7$ rad/s. The environments considered here are passive and also satisfy these bounds.

During free motion, the slave follows the master with a delay of $T_m = 0.05$ s. The nonzero force F_e (due to the measured end-effector dynamics) is reflected and applied by the master PeL $T_s = 0.05$ s later. When F_e is applied, the master has a different velocity than the slave. Consequently, the energy levels presented in Fig. 5.10 are nonzero and the PaL is activated. The controller gains of the PaL are tuned such that the combined damping gains (two bottom plots of Fig. 5.9) remain smaller than 0.03 Nms/rad, therefore barely affecting the free motion response.

After the impact of the slave with the spring, a small transient is present in both the motion and force profiles. This transient is the start of the recoiling of the master device due to the phenomenon described in Section 2.3. Due to the PeL force $F_{mc} = -F_e^{T_s}$, the master is first slowed down and then pushed back, reversing its velocity. The associated active behavior is detected by the PaL. The variable damping gains increase and the variable force-reflection gains λ_i are reduced to prevent a recoiling of the master and damp out the transient. During the detachment phase, similar to the simulation results of Fig. 5.6, the variable damping gains first increase and λ_i decreases. Once the slave is in free motion, λ_i quickly converges to 1. The variable damping gains $-\lambda_i \beta_i E_{i,harv}$ are reduced, but remain nonzero since not enough energy was harvested from the master and slave during the short free motion period.

A similar response of the master, slave and controller is obtained during contact of the slave with the aluminium cylinder. Compared to the contact phase with the spring, the impact oscillation is more severe, but the PaL eliminates it after a few periods. The variable damping gains and λ_i ($\lambda_m = 0.76$ and $\lambda_m = 0.92$ during steady-state) are of the same order compared to the simulation results presented in Fig. 5.6, but quite higher compared to, e.g., [36, 139].

Summarizing, it is illustrated that the proposed controller is robust for the imperfect velocity- and force measurements of the setup. In free motion of the slave, the damping gains are low and λ_i is almost always equal to one. When the

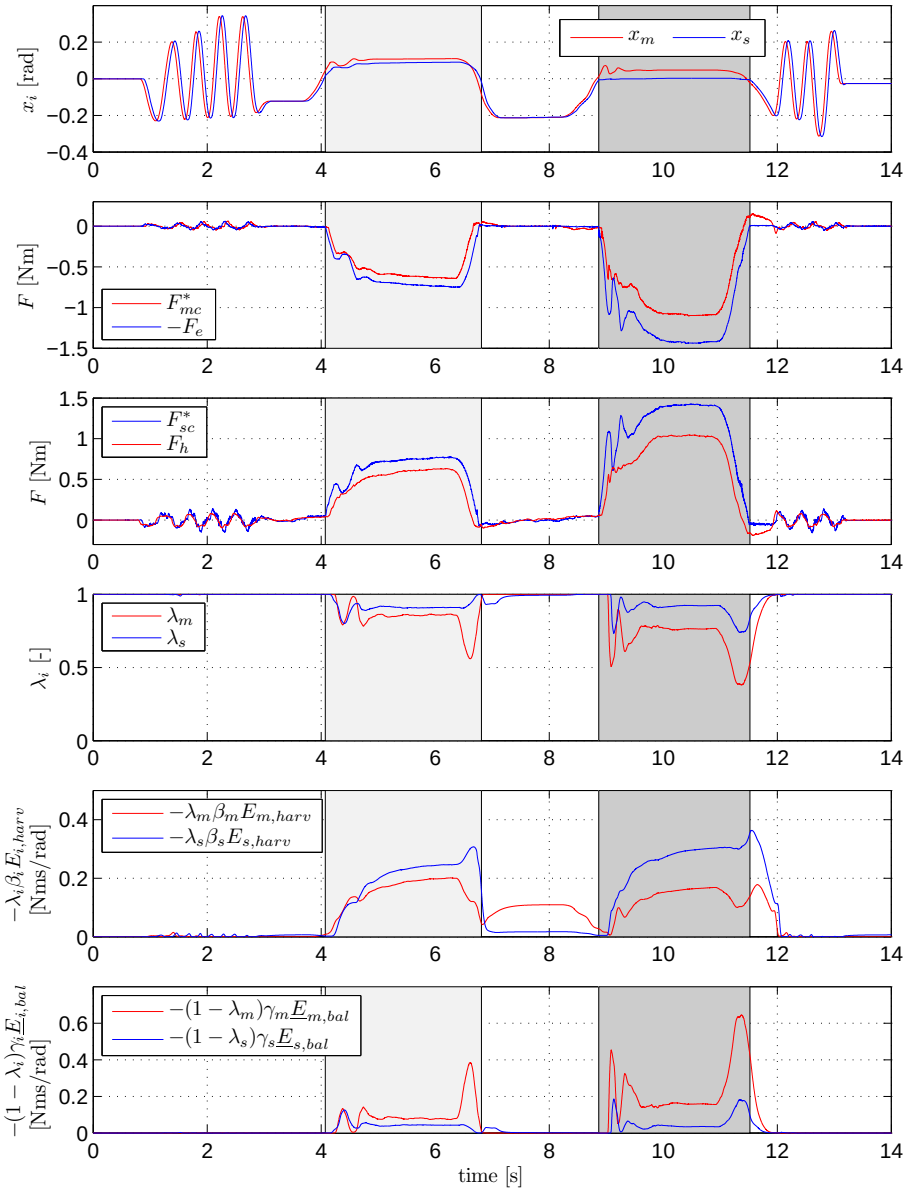

Fig. 5.9. Experimental results *with* PaL for $T_m = T_s = 0.05$ s: Positions, forces, variable damping gains and λ_i. In the light grey area the slave is in contact with the spring. In the dark grey area the slave is in contact with the aluminium cylinder.

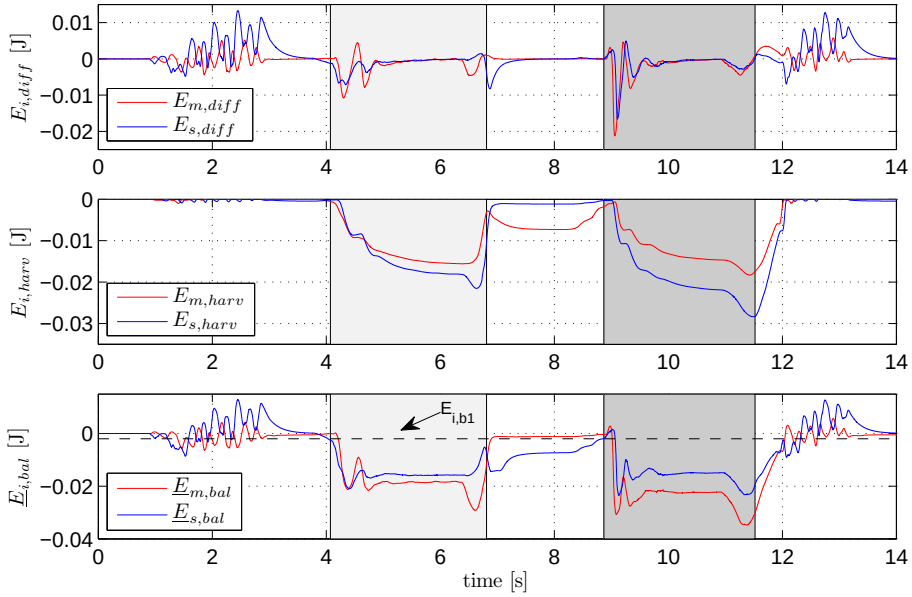

Fig. 5.10. Experimental results *with* PaL for $T_m = T_s = 0.05$ s: Energy levels. In the light grey area the slave is in contact with the spring. In the dark grey area the slave is in contact with the aluminium cylinder.

slave makes contact with the environment, the PaL prevents active behavior, and thus a recoiling of the master during the impact and detachment phase. This is achieved by temporarily increasing the variable damping gains and slightly reducing the force-reflection gains λ_i. Consequently, the performance loss during the free motion, impact, contact and detachment phases is rather minimal.

5.7 Conclusion

In this chapter, a novel two-layer control architecture is proposed for direct force-reflecting bilateral teleoperation systems subject to communication delays, having similar master and slave devices. In principle, any traditional controller can be implemented in the PeL, while the PaL guarantees a passive implementation by adapting the amount of damping injected on the master or slave device and modulating the PeL output when necessary. According to the *direct force-reflection* philosophy, the design of the PaL is based on a *duplication* of the power exchanged between the operator/environment and the teleoperator. Passivity of the teleoperator is analyzed and a formal proof is given. The behavior of the

controller in the delay-free situation is illustrated with numerical simulations. When the master and slave dynamics are different, the controller compensates for the mismatch and synchronizes the motion, forces and dynamics of the master and slave. Furthermore, the experimental results illustrate the performance that can be obtained for a rather large, but realistic, round-trip delay of 100 ms and different types of environment. The damping gains are low in free motion of the slave, whereas in contact the damping gains increase to stabilize the teleoperator. The force-reflection gains are also reduced during the impact and detachment phase to prevent a recoiling of the master, but their values are quite high compared to other recommendations found in the literature.

To improve the performance, especially in the contact phase, it is recommended to focus on how to increase the force-reflection gains even further to obtain the optimal performance computed by the PeL. This could be achieved by optimizing the tuning of the PeL and PaL parameters and investigating (nonlinear) alternatives to generate and harvest energy in the PaL. Furthermore, it is very interesting to extend the obtained results, both numerically and experimentally, to a multi-DOF teleoperator. An increase in the force-reflection gains could then be achieved by, e.g., harvesting energy from directions tangential to the direction of contact. Finally, to further improve impact transients with extremely stiff environments, it is suggested to exploit the compliancy in the slave device, as discussed in Chapter 4.

Chapter 6

Conclusions and Recommendations

6.1 Conclusions

In this thesis, the design of a control architecture for bilateral teleoperation is considered. In particular, the focus has been on applications where the communication is subject to communication delays and the slave device interacts with a stiff environment. It is observed that, partly due to the conservatism in most traditional approaches to analyze and guarantee stability of the teleoperator, the performance of existing control architectures is not always satisfactory. Typically, the reflected environment is perceived too soft and in free motion a high physical operator effort is required, thereby making the teleoperator rather heavy to operate. The goal of this thesis is to improve the performance of bilateral teleoperators in the presence of delays. In the introduction of this thesis, the main research objective is stated as follows:

Develop and experimentally validate a control architecture for bilateral teleoperation with communication delays, trading off stability and performance, but paying particular attention to low physical operator effort and high transparency when interacting with a stiff environment.

The main contributions of this thesis can be classified as performance-oriented and stability-related results. These contributions are summarized below.

Performance-related contributions

From the literature review, presented in Chapter 2, it follows that existing controllers proposed for delayed bilateral teleoperation can be separated in architectures that either aim at *bilateral motion synchronization* or *direct force-reflection*. In bilateral motion synchronization, both the master and slave controller are designed to synchronize the motion of the master and slave device. These architectures suffer from a reflection of the slave dynamics and, in the presence of delays, also from delay-induced forces. Typically, stability can only be guaranteed by reducing the coupling strength between the master and slave, using high damping gains, or applying both options at the same time. Consequently, the environment is perceived too soft and the operator requires a rather high effort to move the teleoperator. In direct force-reflection, only the slave controller is tasked with motion tracking and the master controller reflects the environment to the operator directly. These architectures do not suffer from a reflection of the slave dynamics or delay-induced forces due to the absence of motion feedback terms in the master controller.

The *first contribution* is the development of an experimental comparison method, presented in Chapter 3. Several existing bilateral motion synchronizing and direct force-reflecting architectures are applied on a real, physical setup and the performance is analyzed as a function of the communication delay. Carefully selected quantitative performance metrics are chosen to capture the motion tracking accuracy, the physical operator effort, and the quality of the force reflection and stiffness perception. A virtual human operator is used to make the comparison fair and repeatable.

The results obtained from the theoretical survey and the experimental comparison show that direct force-reflection architectures can achieve better performance than bilateral motion synchronizing controllers in terms of the considered metrics. Especially a Position/Force-Force architecture yields good motion tracking, a low operator effort and high reflected environment stiffness. In contrast, either motion tracking, stiffness reflection, or both are compromised in the bilateral motion synchronization architectures. Despite practical system imperfections like measurement noise, (nonlinear) friction and drive train flexibility, these results support the claim that direct force-reflection is more suitable than bilateral motion synchronization to achieve high performance bilateral teleoperators in the presence of communication delays.

Interestingly, most of the existing control approaches presented in the literature aim at improving the performance of bilateral motion synchronization architectures. However, the theoretical survey of Chapter 2 and experimental comparison of Chapter 3 clearly show that with direct force-reflecting architectures better performance can be obtained in both free motion and contact, since these architectures are less sensitive to communication delays. Therefore, from a performance point of view, a paradigm shift towards direct force-reflection is advised for the design of controllers for delayed bilateral teleoperation.

Stability-related contributions

In free motion, direct force-reflection architectures are unilateral, such that the stability is unaffected by delays. However, when the slave makes contact with the environment, these architectures switch from a unilateral to a bilateral structure and the stability of the closed-loop system depends on the size of the communication delay. Moreover, the operator is often not able to keep the slave in contact with the environment due to a recoiling of the master device. In order to exploit the full potential of direct force-reflection architectures for delayed bilateral teleoperation, this thesis specifically focuses on minimizing the performance loss while guaranteeing stable contact of the slave-environment interaction.

The *second contribution*, presented in Chapter 4, is the development of a novel technique to analyze stability of the local interaction between a single manipulator, for instance the slave, and a stiff environment, while tracking arbitrary time-varying motion and force profiles. Guaranteeing stable impact of the slave with the environment, while tracking these time-varying trajectories coming from the master side, is one of the key requirements to achieve successful teleoperation. For the single degree of freedom slave-environment interaction, sufficient conditions are presented to guarantee input-to-state stability of the switching closed-loop system with respect to perturbations related to the time-varying desired motion-force profile. The analysis shows that, with the proposed controller, guaranteeing closed-loop stability while tracking these arbitrary time-varying motion-force profiles requires injection of a considerable (and often unrealistic) amount of damping. As an alternative, it is proposed to mechanically redesign the manipulator by including a compliant wrist. Using the novel analysis method, guidelines are provided for the design of the compliant wrist, while employing the designed switching control strategy. Consequently, stable tracking of a motion-force reference trajectory can be achieved and bouncing of the slave, while making contact with the stiff environment, can be avoided.

The *last contribution*, presented in Chapter 5, is the development of a novel two-layer controller for delayed bilateral teleoperation. This controller is structured with an outer layer, called the performance layer, and an inner layer, called the passivity layer. In the performance layer, in principle any controller can be implemented to obtain high performance. In the passivity layer, the output of the performance layer is modified to guarantee that, from the operator and environment perspective, the overall teleoperator is passive. By modulating the performance layer outputs and by injecting a variable amount of damping via an innovative logic that follows a principle of energy duplication and takes into account the effects of the delays, passivity in ensured and also formally proven. In contrast to bilateral motion synchronizing controllers, which require an as-stiff-as-possible coupling between the master and slave devices, the proposed scheme is specifically designed for direct force-reflection. The tuning of the control parameters is elaborately discussed and the effectiveness of the proposed controller to obtain low operator effort and high transparency, while making and breaking

contact with a static environment, is demonstrated experimentally for a challenging round-trip communication delay of 100 ms.

Summarizing, a control architecture is designed for delayed bilateral teleoperation that requires low operator effort in free motion and has high transparency when interacting with stiff environments. This high performance teleoperator is obtained by separating in the controller the performance requirements from stability. Using a theoretical and experimental comparison it is shown that in the presence of delays direct force-reflection architectures, in particular a position/force-force controller, provide the best performance in terms of operator effort, motion tracking and stiffness reflection. Subsequently, a novel energy-based controller is developed specifically for direct force-reflection architectures, such that passivity is guaranteed while the performance loss during the free motion and contact phase is minimized. Finally, a method is developed to analyze stability of the slave-environment interaction, including the free motion, contact and transition phases, while tracking time-varying motion-force profiles. A compliant design of the slave device is proposed to achieve stable and even bounceless impact of the slave with the stiff environment for arbitrary motion-force profiles coming from the human operator.

6.2 Recommendations

In this final section, recommendations for future work are proposed to improve and extend the work presented in this thesis. Regarding the experimental comparison to evaluate the performance of existing architectures designed for delayed bilateral teleoperation, the following extensions are suggested:

- In this thesis, the focus has been on achieving high performance in the free motion and contact phases separately. The transitions between free motion and contact are included in the stability analysis, but not in the performance requirements. A crisp reflection of the impact between the slave and the stiff environment is key to provide a natural sensation of the impact. However, to the best of the author's knowledge, a clear metric to quantitatively analyze the performance during the impact phase does not yet exists. It is therefore recommended to develop such a metric and include the performance of the 'impact reflection' in future comparisons.
- The experimental comparison is performed with a modeled operator to achieve consistency and repeatability in the results. In this way, the relative *controller* performance is evaluated between several architectures, but an absolute evaluation to achieve high *operator* or *task* performance is not included in the current analysis. For instance, identifying per performance metric an absolute value or threshold of the required performance, or analyzing the sensitivity of the operator to an absolute change in performance,

is very useful for engineers to design, evaluate and optimize controllers to achieve high task performance.

As an alternative to evaluate and optimize operator and task performance, an experimental comparison with human operators could be performed. In such an experimental comparison, it is interesting to extend the evaluation of the operator and task performance to the case where the teleoperator has multiple degrees of freedom.

Concerning the stability of the interaction between the slave and the stiff environment and the stability of the teleoperator in the presence of communication delays, the following recommendations are provided:

- The technique proposed in Chapter 4 to analyze stability of a single manipulator interacting with a stiff environment, while tracking arbitrary motion-force signals, focuses on a one degree of freedom contact and assumes a linear contact model. In order to increase the range of applications, it is recommended to incorporate also nonlinear contact models in the analysis and extend the presented work to contacts in which multiple degrees of freedom are constrained.

- For the two-layer architecture, presented in Chapter 5, it is recommended to investigate how the force-reflection gains can be increased during the contact phase to achieve the desired performance computed in the performance layer. This could be achieved by optimizing the tuning of the proposed architecture, or by using nonlinear functions to, respectively, harvest and recover energy. Furthermore, to implement the architecture in a system with multiple degrees of freedom, it is recommended to investigate the optimal way to distribute the variable damping gains over the different degrees of freedom during the free motion, transition and contact phases.

Finally, the following general recommendations are proposed to improve the overall performance of bilateral teleoperators in the presence of communication delays:

- Integrate and experimentally validate the proposed compliancy of the slave with the presented two-layer architecture to optimize the trade-off between guaranteeing a stable or even bounceless impact and achieving high performance. In particular, optimizing the stiffness, damping and tip mass of the compliant slave is of interest, since, e.g., a low stiffness is preferable for stable impacts, but a high stiffness is required to reflect both a high environment stiffness and the crispness of the impact.

- In order to improve the crispness of the reflected impact between the slave and a stiff environment, it is important to haptically reflect the high frequencies of the impact. Due to the limited bandwidth of the controller and

the relatively heavy master device, these high frequencies are often filtered out. Consequently, the impact of the slave with the stiff environment feels more like contact with soft foam. In order to improve the perception of the impact, event-based high-frequency transient forces could be superimposed over the traditional feedback [63]. Alternatively, even a small actuator attached to the end-effector of the master device could be used to mimic these high frequency impact forces.

- Finally, as already mentioned in Chapter 2, achieving high transparency is not the only way to improve the task performance in bilateral teleoperation. If knowledge about the task or the intention of the operator is available, additional information to improve the task performance could be reflected to the operator haptically, for instance in the form of Haptic Shared Control. Furthermore, the provided haptic feedback must be integrated with the visual and acoustic feedback to optimize telepresence and consequently also the completion time and task accuracy.

Appendix A

Proofs and technical results

A.1 Design of continuous signals $x_d(t)$ and $\dot{x}_d(t)$

For Assumption 4.1 in Chapter 4, this appendix presents a method to obtain continuous signals $x_d(t)$ and $\dot{x}_d(t)$ (and corresponding $F_d(t)$), required as reference signals for the switched controller (4.3), from the continuous and bounded reference profiles $\tilde{x}_d(t)$ and $\tilde{F}_d(t)$ *specified by the user*.

Denote the i^{th} intended time of making contact by $t_{c,i}$ and the subsequent time of breaking contact by $t_{b,i}$ respectively, as indicated in Fig. A.1. Then, during the contact time interval $[t_{c,i}, t_{b,i}]$, $F_d(t)$ and $x_d(t)$ are obtained from

$$\ddot{y}_1 = -2\gamma_1\dot{y}_1 - \gamma_1^2(y_1 - \tilde{F}_d(t)), \tag{A.1a}$$
$$y_1(t_{c,i}) = \hat{k}_e x_d(t_{c,i}) + \hat{b}_e\dot{x}_d(t_{c,i}),$$
$$\dot{y}_1(t_{c,i}) = \hat{k}_e\dot{x}_d(t_{c,i}) + \hat{b}_e\ddot{x}_d(t_{c,i}),$$
$$\ddot{y}_2 = -\frac{\hat{k}_e}{\hat{b}_e}\dot{y}_2 + \frac{1}{\hat{b}_e}\dot{y}_1, \qquad y_2(t_{c,i}) = x_d(t_{c,i}), \tag{A.1b}$$
$$\dot{y}_2(t_{c,i}) = \dot{x}_d(t_{c,i})$$

with the outputs $F_d(t) = y_1$, $x_d(t) = y_2$ and $\dot{x}_d(t) = \dot{y}_2$ for $t \in [t_{c,i}, t_{b,i}]$. The y_2-dynamics follow from the time derivative of (4.4) and guarantee continuity of $x_d(t)$ and $\dot{x}_d(t)$ at $t = t_{c,i}$. The y_1-dynamics represent a critically damped second-order filter on $\tilde{F}_d(t)$ to guarantee continuity of $F_d(t)$ and $\dot{F}_d(t)$ at $t = t_{c,i}$. As a guideline, the time constant $\gamma_1 > 0$ in (A.1a) is chosen such that the 'bandwidth' of this filter is significantly higher than the frequencies present in $\tilde{F}_d(t)$.

Continuity of the profiles $x_d(t)$ and $\dot{x}_d(t)$ when breaking contact is guaranteed when these profiles during the free motion time interval $[t_{b,i}, t_{c,i+1}]$ are obtained

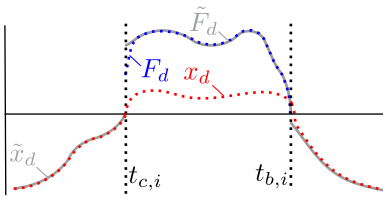

Fig. A.1. Example of a construction of $x_d(t)$ and $F_d(t)$ from $\tilde{x}_d(t)$ and $\tilde{F}_d(t)$.

from $\tilde{x}_d(t)$ filtered by the critically damped second-order filter

$$\begin{aligned} \ddot{y}_3 \;=\; -2\gamma_2\dot{y}_3 - \gamma_2^2(y_3 - \tilde{x}_d(t)),\; y_3(t_{b,i}) = x_d(t_{b,i}), \\ \dot{y}_3(t_{b,i}) = \dot{x}_d(t_{b,i}), \end{aligned} \tag{A.2}$$

with outputs $x_d(t) = y_3$ and $\dot{x}_d(t) = \dot{y}_3$ for $t \in [t_{b,i}, t_{c,i+1}]$. As for γ_1 in (A.1a), the time constant $\gamma_2 > 0$ in (A.2) is chosen such that the 'bandwidth' of (A.2) is significantly higher than the frequencies typically present in $\tilde{x}_d(t)$.

A.2 GUAS of a conewise linear system

The stability results of Chapter 4 are based on the results presented in [16] and ultimately lead to the statement of Theorem A.4, which is used in the proof of Theorem 4.2 in the main text of Chapter 4. The results in [16] apply to *continuous*, conewise linear systems. The conewise linear system Σ^w in (4.10) is, however, discontinuous. The continuity of the vector field is required in [16] to exclude the existence of unstable sliding modes at the switching surfaces of the conewise linear system. The following lemma shows that Σ^w has no sliding modes at the switching surfaces.

Lemma A.1. *For $K_1 - K_2 < 0$, the conewise linear system Σ^w has no sliding mode.*

Proof. The existence of a sliding mode at the two switching surfaces $z_2 = 0$ and $z_2 = -\frac{K_1 - K_2}{B_1 - B_2} z_1$ of Σ^w are considered sequentially:

- Consider the subspace $\{z \in \mathbb{R}^2 | z_1 \geq 0\}$. The normal $\mathcal{N}_1$ to the switching surface $z_2 = 0$ is given by $\mathcal{N}_1 = [0, 1]^T$. The inner product of the vector fields $A_i z$, $i \in \{1, 2\}$, with $\mathcal{N}_1$ at the switching surface $z_2 = 0$ reads $\lambda \mathcal{N}_1^T A_i \nu_1 = -\lambda K_i$, where $\nu_1 = [1, 0]^T$ and $\lambda \geq 0$. This inner product has the same sign for both vector fields associated with $i = 1$ and $i = 2$, such that no sliding mode exists at the switching surface $z_2 = 0$, see e.g. [72].

- Consider the subspace $\{z \in \mathbb{R}^2 | z_1 \geq 0\}$. The normal $\mathcal{N}_2$ to the switching surface $z_2 = -\frac{K_1-K_2}{B_1-B_2} z_1$ is given by $\mathcal{N}_2 = \frac{1}{L}[\Delta K, \Delta B]^T$, with $\Delta K := K_1 - K_2$, $\Delta B := B_1 - B_2$ and $L := \sqrt{(\Delta K)^2 + (\Delta B)^2}$. The projection of the vector fields $A_i z$, $i \in \{1, 2\}$, with $\mathcal{N}_2$ at the switching surface $z_2 = -\frac{K_1-K_2}{B_1-B_2} z_1$ read

$$\lambda \mathcal{N}_2^T A_1 \nu_2 = \frac{\lambda}{L^2}((\Delta K)^2 + K_1(\Delta B)^2 - B_1(\Delta K)(\Delta B)),$$
$$\lambda \mathcal{N}_2^T A_2 \nu_2 = \frac{\lambda}{L^2}((\Delta K)^2 + K_2(\Delta B)^2 - B_2(\Delta K)(\Delta B)),$$

  where $\nu_2 = \frac{1}{L}[-\Delta B, \Delta K]^T$ and $\lambda \geq 0$. It can be shown that $\lambda \mathcal{N}_2^T A_1 \nu_2 - \lambda \mathcal{N}_2^T A_2 \nu_2 = 0$, $\forall K_i, B_i > 0$, hence, the inner products $\lambda \mathcal{N}_2^T A_1 \nu_2$ and $\lambda \mathcal{N}_2^T A_2 \nu_2$ have the same sign, such that no sliding mode exists on the switching surface $z_2 = -\frac{K_1-K_2}{B_1-B_2} z_1$, see e.g. [72].

With a similar analysis, the same results can be obtained for the subspace $\{z \in \mathbb{R}^2 | z_1 \leq 0\}$. □

The following lemma holds for continuous conewise linear systems Σ^w *with* visible eigenvectors.

Lemma A.2 ([16]). *Consider a continuous, conewise linear system of the form Σ^w. When this system contains one or more visible eigenvectors, then $z = 0$ is an asymptotically stable equilibrium of Σ^w if and only if all visible eigenvectors correspond to eigenvalues $\lambda < 0$.*

This lemma can also be shown to be valid for discontinuous conewise systems Σ^w in the absence of a sliding mode. The following lemma is useful in the analysis of the behavior of Σ^w in the absence of visible eigenvectors.

Lemma A.3 ([16]). *Let $\bar{\mathcal{S}}_i$ be a closed cone in $\mathbb{R}^2$. Suppose no eigenvectors of $A_i \in \mathbb{R}^{2\times 2}$ are visible in $\bar{\mathcal{S}}_i$. Then for any initial condition $z_0 \in \bar{\mathcal{S}}_i$, with $z_0 \neq 0$, there exists a time $t \geq 0$ such that $e^{A_i t} z_0 \notin \bar{\mathcal{S}}_i$.*

If Lemma A.3 holds for all cones, the trajectories exhibit a spiralling response, visiting each region i once per rotation, as indicated in Fig. A.2. Stability for a spiraling motion can be analyzed by the computation of a return map. Suppose the trajectory of (4.10) enters a region $\mathcal{S}_i$ at t_{i-1} at position $z(t_{i-1})$, which is located on the boundary $E_{i-1,i}$ between cones $\mathcal{S}_{i-1}$ and $\mathcal{S}_i$, such that $z(t_{i-1})$ can be expressed as $z(t_{i-1}) = p^i \rho_{i-1,i}$. Here, p^i represents the radial distance from the origin at time t_{i-1} and $\rho_{i-1,i}$ is the unit vector parallel to the boundary $E_{i-1,i}$. The trajectory crosses the next boundary $E_{i,i+1}$ at finite time t_i (Lemma A.3), and the position of this crossing is given by $z(t_i) = p^{i+1} \rho_{i,i+1}$, such that $z(t_i)$ is parallel to $\rho_{i,i+1}$. Since the dynamics in each cone are linear, the time t_i can be computed explicitly. The crossing positions are linear in p^i, so expressions for a scalar Λ_i, such that $p^{i+1} = \Lambda_i p^i$, can be obtained.

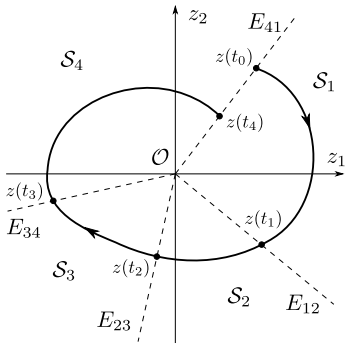

Fig. A.2. Example of a trajectory of (4.10) that traverses each cone once per rotation.

In order to construct the return map, consider for each cone the following coordinate transformation

$$\tilde{z}^i = P_i^{-1} z, \text{for } \tilde{z}^i \in \tilde{\mathcal{S}}_i := \{\tilde{z}^i \in \mathbb{R}^2 \mid \tilde{z}^i = P_i^{-1} z \mid z \in \bar{\mathcal{S}}_i\},$$

where P_i is given by the real Jordan decomposition of A_i, yielding $A_i = P_i J_i P_i^{-1}$. Depending on the eigenvalues of A_i, three different cases can be distinguished.

1. A_i has complex eigenvalues denoted by $a_i \pm \omega_i$, where a_i and ω_i are real constants and $\omega_i > 0$. Then, $J_i = \left[\begin{smallmatrix} a_i & -\omega_i \\ \omega_i & a_i \end{smallmatrix}\right]$. Define $\phi(r_1, r_2)$ to be the angle in counter clockwise direction from vector r_1 to vector r_2. Then,

$$\Lambda_i = \frac{\|\tilde{\rho}^i_{i-1,i}\|}{\|\tilde{\rho}^i_{i,i+1}\|} e^{\frac{a_i}{\omega_i}\phi(\tilde{\rho}^i_{i-1,i}\ ,\ \tilde{\rho}^i_{i,i+1})}, \tag{A.3}$$

   with $\tilde{\rho}^i_{i-1,i} := P_i^{-1}\rho_{i-1,i}$ and $\tilde{\rho}^i_{i,i+1} := P_i^{-1}\rho_{i,i+1}$

2. A_i has two equal real eigenvalues λ_{ai} with geometric multiplicity 1. Then, $J_i = \left[\begin{smallmatrix} \lambda_{ai} & 1 \\ 0 & \lambda_{ai} \end{smallmatrix}\right]$ and

$$\Lambda_i = \left|\frac{e_2^T\tilde{\rho}^i_{i-1,i}}{e_2^T\tilde{\rho}^i_{i,i+1}}\right| e^{\lambda_{ai}\left(\frac{e_1^T\tilde{\rho}^i_{i,i+1}}{e_2^T\tilde{\rho}^i_{i,i+1}} - \frac{e_1^T\tilde{\rho}^i_{i-1,i}}{e_2^T\tilde{\rho}^i_{i-1,i}}\right)}, \tag{A.4}$$

   where $e_1 := [1, 0]^T$ and $e_2 := [0, 1]^T$.

3. A_i has two distinct real eigenvalues λ_{ai} and λ_{bi}. Then, $J_i = \left[\begin{smallmatrix} \lambda_{ai} & 0 \\ 0 & \lambda_{bi} \end{smallmatrix}\right]$ and

$$\Lambda_i = \left|\frac{e_2^T\tilde{\rho}^i_{i,i+1}}{e_2^T\tilde{\rho}^i_{i-1,i}}\right|^{\frac{\lambda a_i}{\lambda b_i - \lambda a_i}} \left|\frac{e_1^T\tilde{\rho}^i_{i,i+1}}{e_1^T\tilde{\rho}^i_{i-1,i}}\right|^{\frac{\lambda b_i}{\lambda a_i - \lambda b_i}}. \tag{A.5}$$

From the scalars Λ_i for each cone $\mathcal{S}_i$, $i = 1, \ldots, m$, the return map between the positions z_k and z_{k+1} of two consecutive crossings of the trajectory $z(t)$ with the boundary E_{m1} can be computed as $z_{k+1} = \Lambda z_k$, where

$$\Lambda = \prod_{i=1}^{m} \Lambda_i.$$

Theorem A.4 below is an extension of Theorem 6 in [16] and provides necessary and sufficient conditions for GUAS of the origin of the discontinuous, conewise linear system Σ^w.

Theorem A.4. *Under the assumption that no sliding modes exist, the origin of the discontinuous, conewise linear system Σ^w in (4.10) is GUAS if and only if at least one of the following conditions is satisfied:*

(i) In each cone $\mathcal{S}_i$, $i = 1, ..., m$, all visible eigenvectors are associated with eigenvalues $\lambda < 0$.

(ii) In case there exists no visible eigenvector, it holds that $\Lambda < 1$.

Proof. If no sliding modes exist on the switching surfaces, GUAS of the origin of the discontinuous system Σ^w can be proven similarly to the proof of Theorem 6 in [16] for continuous, conewise linear systems. □

From Lemma A.1 it follows that Σ^w in (4.10) has no sliding modes on the switching surfaces, so Theorem A.4 can indeed be applied to conclude GUAS of the origin of Σ^w.

A.3 Model reduction compliant manipulator

The model (4.19)-(4.20) in Chapter 4 describes the slow dynamics of (4.16), (4.17), (4.2) and is obtained by employing Theorem 11.2 of [59]. With this theorem, the slow dynamics are obtained for an infinite time horizon $t \in [t_0, \infty]$. This theorem will be referred to as *Tikhonov's extended theorem*, since the original theorem of Tikhonov, see e.g. Chapter 7 of [132], only applies on a finite time horizon $t \in [t_0, t_f]$.

Tikhonov's extended theorem is applicable to systems described by (non)linear continuous, possibly time varying, dynamics. The dynamics of (4.16), (4.17), (4.2) are not continuous due to the switch between free motion and contact. Therefore, the model reduction of the free motion ($x_t \leq 0$) and contact ($x_t > 0$) phases are considered separately. The simulation results presented in Section 4.5 indicate that for the considered parameter values the response of the original compliant manipulator dynamics (4.16), (4.17), (4.2), *including* the transitions between free motion and contact, can be approximated by the dynamics of the reduced-order model (4.19)-(4.20).

Below, for both free motion and contact, the reduction of the 4^{th}-order model (4.16), (4.17), (4.2) to the second-order model (4.19)-(4.20) is performed in two steps, where in each step the model is reduced with one order.

Free motion

Consider the following states

$$e := x - x_t$$
$$\dot{e} := \dot{x} - \dot{x}_t.$$

The following parameters are used as an example to illustrate the separation of the two distinct time-scales of the system described by (4.16), (4.17), (4.2): $M \sim 10^0$, $b \sim 10^0$, $M_t \sim 10^{-2}$, $k_t \sim 10^4$, $b_t \sim 10^2$, $k_e \sim 10^6$ and $b_e \sim 10^1$. For these parameter values, the dynamics (4.16), (4.17), (4.2) in free motion can be written as

$$\ddot{x} = \underbrace{\frac{1}{M}}_{\sim 10^0} F_c(t) - \underbrace{\frac{b}{M}}_{\sim 10^0} \dot{x} - \underbrace{\frac{k_t}{M}}_{\sim 10^4} e - \underbrace{\frac{b_t}{M}}_{\sim 10^2} \dot{e}$$
$$\underbrace{\frac{M_t}{(1+M_t/M)k_t}}_{\sim 10^{-6}} \ddot{e} = \underbrace{\frac{M_t}{M(1+M_t/M)k_t}}_{\sim 10^{-6}} F_c(t) - e - \underbrace{\frac{b_t}{k_t}}_{\sim 10^{-2}} \dot{e} - \underbrace{\frac{M_t b}{M(1+M_t/M)k_t}}_{\sim 10^{-6}} \dot{x}.$$

Define $\mu_1 := \frac{M_t}{(1+M_t/M)k_t} \approx \frac{M_t}{M(1+M_t/M)k_t} \approx \frac{M_t b}{M(1+M_t/M)k_t}$ and $\mu_2 := \frac{b_t}{k_t}$. With these parameters, it follows that $\mu_1 \ll \mu_2$, and the following dynamics are obtained

$$\ddot{x} = \frac{1}{M}(F_c(t) - b\dot{x} - k_t e - b_t \dot{e}) \tag{A.7a}$$
$$\mu_1 \ddot{e} = \mu_1 F_c(t) - \mu_1 \dot{x} - e - \mu_2 \dot{e}. \tag{A.7b}$$

Note that x does not appear directly in the right-hand side of (A.7). Therefore, the dynamics of (A.7) are described by the three states $(\dot{x}, e, \dot{e})$ only.

In the analysis that follows, μ_1 and μ_2 are considered as *singular perturbations* and Tikhonov's extended theorem is used twice (once for μ_1 and once for μ_2) to obtain a model of reduced order.

Before proceeding, first the free response of (A.7) is decoupled from the forced response (due to $F_c(t)$). To this end, consider the coordinate transformation $\dot{\tilde{x}} := \dot{x} - \dot{\bar{x}}_{F_c}(t)$, where $\bar{x}_{F_c}(t)$ is defined as the forced response of the slow dynamics of (A.7) (i.e. for $\mu_1 = \mu_2 = 0$) to the continuous and bounded input $F_c(t)$, such that

$$M\ddot{\bar{x}}_{F_c}(t) + b\dot{\bar{x}}_{F_c}(t) = F_c(t). \tag{A.8}$$

Note that $\dot{\bar{x}}_{F_c}(t)$ and $\ddot{\bar{x}}_{F_c}(t)$ are continuous and bounded since $F_c(t)$ is continuous and bounded. By employing (A.8), the unforced dynamics of (A.7) can be

expressed as

$$\ddot{\tilde{x}} = \frac{1}{M}(-b\dot{\tilde{x}} - k_t e - b_t \dot{e}) \tag{A.9a}$$

$$\mu_1 \ddot{e} = \mu_1 F_c(t) - \mu_1(\dot{\tilde{x}} + \dot{\tilde{x}}_{F_c}(t)) - e - \mu_2 \dot{e}. \tag{A.9b}$$

Since μ_1 is much smaller than all other parameters, it is treated as the vanishing perturbation parameter and Tikhonov's extended theorem is used to obtain a model of reduced order that describes the slow dynamics of this system. Consider $y = [y_1, y_2]^T := [\dot{\tilde{x}}, e]^T$ as the states of the slow dynamics $f_1(y, \zeta)$ and $\zeta := \dot{e}$ as the state of the fast dynamics $g_1(t, y, \zeta, \mu_1)$ of (A.9) according to

$$\begin{bmatrix} \dot{y}_1 \\ \dot{y}_2 \end{bmatrix} = \begin{bmatrix} \frac{1}{M}(-by_1 - k_t y_2 - b_t \zeta) \\ \zeta \end{bmatrix} =: f_1(y, \zeta) \tag{A.10a}$$

$$\mu_1 \dot{\zeta} = \mu_1 F_c(t) - \mu_1(y_1 + \dot{\tilde{x}}_{F_c}(t)) - y_2 - \mu_2 \zeta \ =: g_1(t, y, \zeta, \mu_1). \tag{A.10b}$$

For $\mu_1 = 0$, $\zeta = h_1(y) := -\frac{1}{\mu_2} y_2$ is the solution of $0 = g_1(t, y, \zeta, 0)$ for $y \in D_y = \mathbb{R}^2$ and $v_1 := \zeta - h_1(y) \in D_{v1} = \mathbb{R}$. The three conditions of Tikhonov's extended theorem are analyzed sequentially:

C1. The functions f_1, g_1, their first partial derivatives with respect to (y, ζ, μ_1), and the first partial derivative of g_1 with respect to t are continuous and bounded on any compact subset $D_y \times D_{v1}$, since $F_c(t)$ is continuous and bounded. Furthermore, $h_1(y)$ and $[\partial g_1(t, y, \zeta, 0)/\partial \zeta]$ have bounded first partial derivatives and $[\partial f_1(y, h_1(t, y), 0)/\partial y]$ is Lipschitz in y.

C2. The slow dynamics of (A.10)

$$\begin{aligned} \dot{y} = f_1(y, h_1(y)) &= \begin{bmatrix} \frac{1}{M}(-by_1 - k_t y_2 + \frac{b_t}{\mu_2} y_2) \\ -\frac{1}{\mu_2} y_2 \end{bmatrix} \\ &= \begin{bmatrix} -\frac{b}{M} & \frac{b_t}{\mu_2 M} - \frac{k_t}{M} \\ 0 & -\frac{1}{\mu_2} \end{bmatrix} \begin{bmatrix} y_1 \\ y_2 \end{bmatrix} \end{aligned} \tag{A.11}$$

have a *globally* exponentially stable equilibrium point $y = 0$, since $-\frac{b}{M}$ and $-\frac{1}{\mu_2}$, representing the eigenvalues of the system matrix of the linear dynamics in (A.11), are both negative.

C3. With $\mu_1 \frac{dv_1}{dt} = \frac{dv_1}{d\tau_1}$ (i.e. $\tau_1 := \frac{1}{\mu_1} t$) the (linear) boundary-layer system

$$\begin{aligned} \frac{\partial v_1}{\partial \tau_1} = g_1(t, y, v_1 + h_1(y), 0) &= -y_2 - \mu_2(v_1 - \frac{1}{\mu_2} y_2) \\ &= -\mu_2 v_1 \end{aligned} \tag{A.12}$$

has a *globally* exponentially stable equilibrium point at the origin (since $\mu_2 > 0$), uniformly in (t, y) with region of attraction $\mathcal{R}_{v1} = D_{v1} = \mathbb{R}$.

From the conditions above, Tikhonov's extended theorem allows us to conclude that for all $t_0 \geq 0$, initial conditions $y_0 \in D_y$, $\zeta_0 \in D_\zeta := \mathbb{R}$, and sufficiently small $0 < \mu_1 < \mu_1^*$, the singular perturbation problem of (A.10) has a unique solution $y(t, \mu_1)$, $\zeta(t, \mu_1)$ on $[t_0, \infty)$, and

$$\begin{aligned} y(t, \mu_1) - \bar{y}(t) &= \mathcal{O}(\mu_1) \\ \zeta(t, \mu_1) - h_1(\bar{y}(t)) - \hat{v}_1(t/\mu_1) &= \mathcal{O}(\mu_1) \end{aligned}$$

holds uniformly for $t \in [t_0, \infty)$, with initial time t_0, where $\bar{y}(t)$ and $\hat{v}_1(\tau)$ are the solutions of (A.11) and (A.12), with $\bar{y}(t_0) = y(t_0)$ and $\hat{v}_1(t_0) = \zeta(t_0) + \frac{1}{\mu_2} y_2(t_0)$ respectively. Moreover, given any $t_b > t_0$, there is $\mu_1^{**} \leq \mu_1^*$ such that

$$\zeta_1(t, \mu_1) - h_1(\bar{y}(t)) = \mathcal{O}(\mu_1)$$

holds uniformly for $t \in [t_b, \infty)$ whenever $\mu_1 < \mu_1^{**}$. Hence, on the domain $t \in [t_b, \infty)$, (A.10) can be approximated by (A.11). Rewriting the reduced-order model (A.11) as the time-invariant system

$$\dot{y}_1 = \frac{1}{M}(-by_1 - k_t y_2 + \frac{b_t}{\mu_2} y_2) \quad := f_2(y_1, y_2, \mu_2) \tag{A.13a}$$

$$\mu_2 \dot{y}_2 = -y_2 \quad := g_2(y_2, \mu_2), \tag{A.13b}$$

it becomes clear that $\mu_2 = \frac{b_t}{k_t} \sim 10^{-2}$ is much smaller than all other parameters in (A.13). Hence, Tikhonov's extended theorem can be applied once more with μ_2 considered as the singular perturbation parameter, y_1 the slow dynamics and y_2 the fast dynamics.

The details regarding the reduction step with μ_2 considered as the singular perturbation is performed in a similar fashion as the first reduction step and is therefore omitted here for the sake of brevity. With $y_2 = h_2(y_1) := 0$ the solution of $0 = g_2(y_2, 0)$, the following globally exponentially stable slow dynamics of (A.13) are obtained

$$\dot{y}_1 = f_2(y_1, h_2(y_1), 0) = -\frac{b}{M} y_1. \tag{A.14}$$

With $v_2 := y_2 - h_2(y_1)$ and $\tau_2 := \frac{1}{\mu_2} t$, the boundary-layer system $\frac{\partial v_2}{\partial \tau_2} = g_2(y_1, v_2 + h_2(y_1), 0) = -v_2$ is globally exponentially stable. Hence, the three conditions of Tikhonov's extended theorem are satisfied, such that it can be concluded that (A.14) is an approximation of (A.13). After reversing the coordinate transformation, i.e. $y_1 = \dot{x} - \dot{\tilde{x}}_{F_c}(t)$, and using (A.8),

$$M\ddot{x} + b\dot{x} = F_c(t) \tag{A.15}$$

is obtained as the approximation of (4.16) in free motion.

Contact

Similar as for the free motion case, the model reduction for the contact case is performed in two steps. Due to the relatively high environmental contact stiffness k_e in (4.16), it is expected that x_t (and time derivatives) is approximately equal to zero (the nominal position of the environment). Therefore, the motion x_t of the tip can be considered as the fast dynamics, and the motion x of the manipulator can be considered as the slow dynamics. The dynamics (4.16), (4.17), (4.2) for $x_t > 0$ can be rewritten as

$$\ddot{x} = \underbrace{\frac{1}{M}}_{\sim 10^0} F_c(t) - \underbrace{\frac{(b+b_t)}{M}}_{\sim 10^2} \dot{x} + \underbrace{\frac{b_t}{M}}_{\sim 10^2} \dot{x}_t - \underbrace{\frac{k_t}{M}}_{\sim 10^4} (x - x_t) \tag{A.16a}$$

$$\underbrace{\mu_3}_{\sim 10^{-8}} \ddot{x}_t = \underbrace{\frac{k_t}{k_t + k_e}}_{\sim 10^{-2}} x + \underbrace{\frac{b_t}{k_t + k_e}}_{\sim 10^{-4}} \dot{x} - x_t - \underbrace{\frac{b_t + b_e}{k_t + k_e}}_{\sim 10^{-4}} \dot{x}_t, \tag{A.16b}$$

where $\mu_3 := \frac{M_t}{k_t + k_e}$. Consider the coordinate transformation

$$\begin{aligned} y_1 &:= x - \bar{x}_{F_c}(t), \\ y_2 &:= \dot{x} - \dot{\bar{x}}_{F_c}(t), \qquad\qquad \zeta_1 := \dot{x}_t - \dot{\bar{x}}_{t,F_c}(t), \\ y_3 &:= x_t - \bar{x}_{t,F_c}(t), \end{aligned} \tag{A.17}$$

such that $y = [y_1, y_2, y_3]^T = 0$ and $\zeta_1 = 0$ is the equilibrium of (A.16) in the new coordinates. In (A.17), $\bar{x}_{t,F_c}(t)$ and $\bar{x}_{F_c}(t)$ are defined as the forced response of (A.16) for $\mu_3 = 0$, to the continuous and bounded input $F_c(t)$, i.e.

$$\dot{\bar{x}}_{t,F_c}(t) = \frac{1}{b_t + b_e}\Big(k_t \bar{x}_{F_c}(t) + b_t \dot{\bar{x}}_{F_c}(t) - (k_t + k_e)\bar{x}_{t,F_c}(t)\Big), \tag{A.18}$$

$$\begin{aligned} M\ddot{\bar{x}}_{F_c}(t) + (b + b_t)\dot{\bar{x}}_{F_c}(t) - b_t \dot{\bar{x}}_{t,F_c}(t) \\ + k_t(\bar{x}_{F_c}(t) - \bar{x}_{t,F_c}(t)) = F_c(t). \end{aligned} \tag{A.19}$$

Using the coordinate transformation (A.17) and the expressions (A.18) and (A.19), (A.16) can be rewritten as

$$\begin{bmatrix} \dot{y}_1 \\ \dot{y}_2 \\ \dot{y}_3 \end{bmatrix} = \begin{bmatrix} y_2 \\ \frac{1}{M}(-(b+b_t)y_2 + b_t\zeta_1 - k_t(y_1 - y_3)) \\ \zeta_1 \end{bmatrix} =: f_3(y, \zeta_1) \tag{A.20a}$$

$$\begin{aligned} \mu_3 \dot{\zeta}_1 &= \frac{1}{k_t + k_e}\Big(k_t y_1 + b_t y_2 - (k_t + k_e)y_3 - (b_t + b_e)\zeta_1\Big) - \mu_3 \dddot{\bar{x}}_{t,F_c}(t) \\ &=: g_3(t, y, \zeta_1, \mu_3). \end{aligned} \tag{A.20b}$$

Since μ_3 is much smaller than all other parameters, see (A.16b), it is treated as the vanishing perturbation and Tikhonov's extended theorem is used to obtain a model of reduced order.

The details regarding the reduction step with singular perturbation parameter μ_3 follows similar to the reduction step for the free motion case with μ_1 considered as the singular perturbation parameter and is therefore omitted for the sake of brevity. With

$$\zeta_1 = \frac{1}{b_t + b_e}\left(k_t y_1 + b_t y_2 - (k_t + k_e) y_3\right) =: h_3(y)$$

the solution of $0 = g_3(t, y, \zeta_1, 0)$, the following globally exponentially stable slow dynamics of (A.20) are obtained

$$\dot{y} = f_3(y, h_3(y)) = \left[\begin{array}{c} y_2 \\ \hdashline \frac{1}{M}(-(b + b_t) y_2 + \frac{b_t}{b_t + b_e}(k_t y_1 + b_t y_2 \\ \qquad - (k_t + k_e) y_3) - k_t y_1 + k_t y_3) \\ \hdashline \frac{1}{b_t + b_e}(k_t y_1 + b_t y_2 - (k_t + k_e) y_3) \end{array}\right] \tag{A.21}$$

With $v_3 := \zeta_1 - h_3(y) \in D_{v3} = \mathbb{R}$ and $\mu_3 \frac{dv_3}{dt} = \frac{dv_3}{d\tau_3}$ (i.e. $\tau_3 := \frac{1}{\mu_3} t$), the boundary-layer system

$$\frac{\partial v_3}{\partial \tau_3} = g_3(t, y, v_3 + h_3(y), 0) = -\frac{b_t + b_e}{k_t + k_e} v_3$$

is globally exponentially stable, and the conditions of Tikhonov's extended theorem are satisfied, such that it can be concluded that (A.21) is an approximation of (A.20). Using (A.18), (A.19) and inverting the coordinate transformation (A.17), the (intermediate) slow dynamics (A.21) can be written in the original coordinates as

$$\begin{aligned} M\ddot{x} &= F_c(t) - (b + b_t)\dot{x} - k_t x + k_t x_t \\ &\quad + \frac{b_t}{b_t + b_e}\Big(k_t x + b_t \dot{x} - (k_t + k_e) x_t\Big) && \text{(A.22a)} \\ (b_t + b_e)\dot{x}_t &= k_t x + b_t \dot{x} - (k_t + k_e) x_t. && \text{(A.22b)} \end{aligned}$$

This third-order system is further approximated to a system of order 2 by considering $\mu_4 := \frac{b_t + b_e}{k_t + k_e}$ as a singular perturbation parameter. To this end, consider the state transformation

$$\begin{aligned} y_1 &:= x - \bar{r}(t), \\ y_2 &:= \dot{x} - \dot{\bar{r}}(t), \\ \zeta_2 &:= (k_t + k_e)(x_t - \bar{r}_t(t)), \end{aligned} \tag{A.23}$$

such that $y = [y_1, y_2]^T = 0$ and $\zeta_2 = 0$ is the equilibrium of (A.22) in the new coordinates. Here, $\bar{r}_t(t)$ is defined as the forced response of the fast dynamics of

(A.22) for $\mu_4 = 0$, and $\bar{r}(t)$ is defined as the forced response of the slow dynamics of (A.22) to the input $F_c(t)$, with $\mu_4 = 0$, i.e.

$$\bar{r}_t(t) = k_t\bar{r}(t) + b_t\dot{\bar{r}}(t) \tag{A.24}$$

$$M\ddot{\bar{r}}(t) + (b + b_t\frac{k_e}{k_t+k_e})\dot{\bar{r}}(t) + k_t\frac{k_e}{k_t+k_e}\bar{r}(t) = F_c(t). \tag{A.25}$$

Rewriting (A.22) in terms of the coordinates y_1, y_2 and ζ_2, given in (A.23), and using (A.24), (A.25), gives

$$\begin{aligned}\begin{bmatrix}\dot{y}_1\\ \dot{y}_2\end{bmatrix} &= \left[\begin{array}{l} y_2 \\ \hdashline \frac{1}{M}\Big(-(b+b_t)y_2 - k_t y_1 + \frac{k_t}{k_t+k_e}\zeta_2 \\ \qquad\qquad + \frac{b_t}{b_t+b_e}\big(k_t y_1 + b_t y_2 - \zeta_2\big)\Big)\end{array}\right] \\ &=: f_4(y,\zeta_2) \end{aligned} \tag{A.26a}$$

$$\begin{aligned}\underbrace{\mu_4}_{\sim 10^{-4}}\dot{\zeta}_2 &= \underbrace{k_t}_{\sim 10^4}y_1 + \underbrace{b_t}_{\sim 10^2}y_2 - \zeta_2 - \underbrace{\mu_4}_{\sim 10^{-4}}\dot{\bar{r}}_t(t) \\ &:= g_4(t,y,\zeta_2,\mu_4).\end{aligned} \tag{A.26b}$$

Since μ_4 is small compared to the other parameters, it is considered a singular perturbation parameter for the system (A.26) and Tikhonov's extended theorem is used once more to obtain a model of reduced order. Again, the proof of the reduction step with μ_4 considered as the singular perturbation follows similar to the previous reduction steps and is therefore omitted.

For $\mu_4 = 0$, $\zeta_2 = k_t y_1 + b_t y_2 := h_4(y)$ is the root of $0 = g_4(t,y,\zeta_2,0)$ and the following slow dynamics of (A.26) are obtained

$$\begin{aligned}\dot{y} &= f_4(y, h_4(y)) \\ &= \left[\begin{array}{l} y_2 \\ \frac{1}{M}\Big(-\big(b + b_t\frac{k_e}{k_t+k_e}\big)y_2 - k_t\frac{k_e}{k_t+k_e}y_1\Big)\end{array}\right].\end{aligned} \tag{A.27}$$

With $v_4 := \zeta_2 - h_4(y) \in D_{v4} = \mathbb{R}$ and $\mu_4\frac{dv_4}{dt} = \frac{dv_4}{d\tau_4}$ (i.e. $\tau_4 := \frac{1}{\mu_4}t$), the boundary-layer system $\frac{\partial v_4}{\partial \tau_4} = g_4(t,y,v_4 + h_4(y),0) = -v_4$ is globally exponentially stable, and the conditions of Tikhonov's extended theorem are satisfied, such that the theorem allows us to conclude that (A.27) is an approximation of (A.26). Using the inverse of the coordinate transformation (A.23), we get

$$M(\ddot{x} - \ddot{\bar{r}}(t)) = -k_t\frac{k_e}{k_t+k_e}(x - \bar{r}(t)) - (b + b_t\frac{k_e}{k_t+k_e})(\dot{x} - \dot{\bar{r}}(t)).$$

Using (A.25), the slow dynamics of (A.22) (and thus of (A.16)) are given by

$$M\ddot{x} + b\dot{x} = F_c(t) - k_t\frac{k_e}{k_t+k_e}x - b_t\frac{k_e}{k_t+k_e}\dot{x}. \tag{A.28}$$

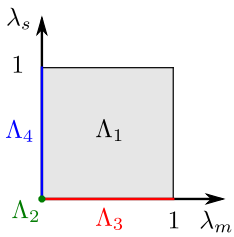

Fig. A.3. Relation between Λ_k, $k \in \{1,2,3,4\}$ and the state-dependent, continuously varying gains λ_m and λ_s.

Finally, by combining the results (A.15) and (A.28), for free motion and contact, the model of reduced order described by (4.19)-(4.20) is obtained.

A.4 Proof of Lemma 5.3

From Assumption 5.1 and (5.23) it follows that

$$E_{h,com} \geq -\Delta\overline{E}_h, \quad \forall t \in \mathcal{T}, \tag{A.29a}$$
$$E_{e,com} \geq -\Delta\overline{E}_e, \quad \forall t \in \mathcal{T} \tag{A.29b}$$

with $\mathcal{T} := [t_0, \infty)$. Split $\mathcal{T}$ in the intervals

$$\mathcal{T}_1 := \{t \in \mathcal{T} | \underline{E}_{m,bal} > E_{m,b2} \wedge \underline{E}_{s,bal} > E_{s,b2}\}, \tag{A.30a}$$
$$\mathcal{T}_2 := \{t \in \mathcal{T} | \underline{E}_{m,bal} \leq E_{m,b2} \wedge \underline{E}_{s,bal} \leq E_{s,b2}\}, \tag{A.30b}$$
$$\mathcal{T}_3 := \{t \in \mathcal{T} | \underline{E}_{m,bal} > E_{m,b2} \wedge \underline{E}_{s,bal} \leq E_{s,b2}\}, \tag{A.30c}$$
$$\mathcal{T}_4 := \{t \in \mathcal{T} | \underline{E}_{m,bal} \leq E_{m,b2} \wedge \underline{E}_{s,bal} > E_{s,b2}\}, \tag{A.30d}$$

such that $\mathcal{T}_1 \cup \mathcal{T}_2 \cup \mathcal{T}_3 \cup \mathcal{T}_4 = \mathcal{T}$. By hypothesis, $t_0 \in \mathcal{T}_1$. Due to the design of λ_i in Fig. 5.2, $t \in \mathcal{T}_k \iff (\lambda_m(t), \lambda_s(t)) \in \Lambda_k$, with $k \in \{1,2,3,4\}$ and Λ_k given in Fig. A.3. To prove equation (5.30), the intervals $\mathcal{T}_k$ are considered sequentially.

Interval $\mathcal{T}_1$: In this region, $\underline{E}_{i,bal} > E_{i,b2}$. From (5.16), using (5.14), (A.29), and $E_i \geq 0$, it follows that

$$V > E_{m,b2} + E_{s,b2} - \Delta\overline{E}_h - \Delta\overline{E}_e, \quad \forall t \in \mathcal{T}_1. \tag{A.31}$$

Interval $\mathcal{T}_2$: Denote an arbitrary time of entering $\mathcal{T}_2$ by $t_2 > t_0$, such that $\underline{E}_{i,bal}(t_2) = E_{i,b2}$. Then, with $\underline{E}_{i,bal} \leq E_{i,b2}$, $\forall t \in \mathcal{T}_2$, it follows that $\lambda_i = 0$, such that (5.15) reduces to

$$\dot{\underline{E}}_{m,bal} + \dot{E}_{e,com} = -F_e^\top \dot{x}_s + F_{m,rec}^\top \dot{x}_m, \tag{A.32a}$$
$$\dot{\underline{E}}_{s,bal} + \dot{E}_{h,com} = F_h^\top \dot{x}_m + F_{s,rec}^\top \dot{x}_s. \tag{A.32b}$$

Summing up (A.32a) and (A.32b), using (5.17) with $\lambda_i = 0$, yields

$$\begin{aligned}&\underline{\dot{E}}_{m,bal} + \underline{\dot{E}}_{s,bal} + \dot{E}_{h,com} + \dot{E}_{e,com} = \\ &\dot{E}_m + \dot{E}_s + 2F_{m,rec}^{\top}\dot{x}_m + 2F_{s,rec}^{\top}\dot{x}_s \geq \dot{E}_m + \dot{E}_s,\end{aligned} \tag{A.33}$$

since $F_{i,rec}^{\top}\dot{x}_i \geq 0$. Time integration of both sides of (A.33) from t_2 to t, recalling that $\underline{E}_{i,bal}(t_2) = E_{i,b2}$, yields

$$\begin{aligned}&\underline{E}_{m,bal}(t) + \underline{E}_{s,bal}(t) + E_{h,com}(t) + E_{e,com}(t) \\ &\quad\geq\ E_{m,b2} + E_{s,b2} + E_{h,com}(t_2) + E_{e,com}(t_2) + E_m(t) - E_m(t_2) \\ &\qquad +E_s(t) - E_s(t_2) \\ &\quad\geq\ E_{m,b2} + E_{s,b2} - \Delta\overline{E}_h - \Delta\overline{E}_e - \overline{E}_m - \overline{E}_s,\end{aligned}$$

where for the last step the bounds (5.18) and (A.29) are used. Using the above inequality in (5.16), recalling that $E_{i,bal} \geq \underline{E}_{i,bal}$ due to (5.14) and $E_i \geq 0$ due to (5.18), gives

$$V \geq E_{m,b2} + E_{s,b2} - \Delta\overline{E}_h - \Delta\overline{E}_e - \overline{E}_m - \overline{E}_s, \qquad \forall t \in \mathcal{T}_2. \tag{A.34}$$

Interval $\mathcal{T}_3$: Denote an arbitrary time of entering $\mathcal{T}_3$ by $t_3 > t_0$, such that $\underline{E}_{s,bal}(t_3) = E_{s,b2}$ and $\underline{E}_{m,bal}(t_3) > E_{m,b2}$. Since in this region $\underline{E}_{s,bal} \leq E_{s,b2}$ and $\underline{E}_{m,bal} > E_{m,b2}$ for all $t \in \mathcal{T}_3$, it follows that $\lambda_s = 0$ and $\lambda_m > 0$ for all $t \in \mathcal{T}_3$, such that (5.15) reduces to

$$\underline{\dot{E}}_{s,bal} + \dot{E}_{h,com} = F_h^{\top}\dot{x}_m + F_{s,rec}^{\top}\dot{x}_s + \lambda_m^{T_m}\left(F_{m,harv}^{T_m}\right)^{\top}\dot{x}_m^{T_m} \tag{A.35}$$

$$\begin{aligned}\underline{\dot{E}}_{m,bal} + \dot{E}_{e,com} &= -F_e^{\top}\dot{x}_s + (1-\lambda_m)F_{m,rec}^{\top}\dot{x}_m - \lambda_m F_{mc}^{\top}\dot{x}_m \\ &\quad -\lambda_m P_{m,diss}\end{aligned} \tag{A.36}$$

To obtain a lower bound on $\underline{E}_{s,bal} + E_{h,com}$, solve (5.17b) for $F_e^{\top}\dot{x}_s$ and use it in (A.36). Solve the resulting expression for $\lambda_m F_{mc}^{\top}\dot{x}_m$ and use it in (5.17a). Then, solve the newly obtained expression for $F_h^{\top}\dot{x}_m$ and use it in (A.35) to obtain

$$\begin{aligned}\underline{\dot{E}}_{s,bal} + \dot{E}_{h,com} &= \lambda_m F_{m,harv}^{\top}\dot{x}_m + \lambda_m^{T_m}\Big(F_{m,harv}^{T_m}\Big)^{\top}\dot{x}_m^{T_m} + \dot{E}_m - \dot{E}_s \\ &\quad + \underline{\dot{E}}_{m,bal} + \dot{E}_{e,com} + \lambda_m P_{m,diss}, \\ &\geq \dot{E}_m - \dot{E}_s + \underline{\dot{E}}_{m,bal} + \dot{E}_{e,com}\end{aligned} \tag{A.37}$$

since by design $P_{m,diss} \geq 0$ and $\lambda_m F_{m,harv}^{\top}\dot{x}_m \geq 0$. Time integration of (A.37) from t_3 to t, together with (5.25) of Lemma 5.2, (5.18), (5.23) and (A.29), gives

$$\begin{aligned}&\underline{E}_{s,bal}(t) + E_{h,com}(t) \\ &\quad\geq \underline{E}_{s,bal}(t_3) + E_{h,com}(t_3) + E_m(t) - E_m(t_3) - E_s(t) + E_s(t_3) \\ &\qquad + \underline{E}_{m,bal}(t) - \underline{E}_{m,bal}(t_3) + E_{e,com}(t) - E_{e,com}(t_3) \\ &\quad\geq -\overline{E}_m - \overline{E}_s + E_{m,b2} + E_{s,b2} - E_{m,b3} - E_{m,diff}(t_0) - 2\Delta\overline{E}_e - \Delta\overline{E}_h.\end{aligned}$$

Using this expression in (5.16), together with $\underline{E}_{m,bal} > E_{m,b2}$, $E_{i,bal} \geq \underline{E}_{i,bal}$ due to (5.14), and $E_i \geq 0$ due to (5.18), results in

$$V > -\overline{E}_m - \overline{E}_s + 2E_{m,b2} + E_{s,b2} - E_{m,b3} - E_{m,diff}(t_0) - 3\Delta\overline{E}_e - \Delta\overline{E}_h, \quad \forall t \in \mathcal{T}_3. \quad \text{(A.38)}$$

Interval $\mathcal{T}_4$: By using a similar approach as for region $\mathcal{T}_3$, the following result is obtained due to the symmetric design of the PaL

$$V > -\overline{E}_m - \overline{E}_s + E_{m,b2} + 2E_{s,b2} - E_{s,b3} - E_{s,diff}(t_0) - 3\Delta\overline{E}_h - \Delta\overline{E}_e, \quad \forall t \in \mathcal{T}_4. \quad \text{(A.39)}$$

Equation (5.30) follows directly from the lower bounds (A.31), (A.34), (A.38) and (A.39) of regions $\mathcal{T}_1$, $\mathcal{T}_2$, $\mathcal{T}_3$ and $\mathcal{T}_4$.

Bibliography

[1] D.A. Abbink and M. Mulder. Exploring the dimensions of haptic feedback support in manual control. *Journal of Computing and Information Science in Engineering*, 9:011006, 2009.

[2] J.J. Abbott, P. Marayong, and A. Okamura. *Robotics Research*, chapter Haptic virtual fixtures for robot-assisted manipulation, pages 49–64. Springer Berlin Heidelberg, 2007.

[3] J.J. Abbott and A.M. Okamura. Stable forbidden-region virtual fixtures for bilateral telemanipulation. *Journal of Dynamic Systems, Measurement, and Control*, 128:53–64, 2006.

[4] J.J. Abbott and A.M. Okamura. Pseudo-admittance bilateral telemanipulation with guidance virtual fixtures. *The International Journal of Robotics Research*, 26:865–664, 2007.

[5] A. Albakri, C. Liu, and P. Poignet. Stability and performance analysis of three-channel teleoperation control architectures for medical applications. In *2013 IEEE/RSJ International Conference on Intelligent Robots and Systems*, pages 456–462, Tokyo, Japan, 2013.

[6] A. Albu-Schäffer, C. Ott, and G. Hirzinger. A unified passivity-based control framework for position, torque and impedance control of flexible joint robots. *Int. J. Robotics Research*, 26:23–39, 2007.

[7] I. Aliaga, A. Rubio, and Sánchez. Experimental quantitative comparison of different control architectures for master-slave teleoperation. *IEEE Transactions on Control Systems Technology*, 12:2–11, 2004.

[8] M. Alise, R.G. Roberts, and D.W. Repperger. The wave variable method for multiple degree of freedom teleoperation systems with time delay. In *Proceedings of the 2006 IEEE International Conference on Robotics and Automation*, pages 2908–2913, Orlando, Florida, USA, 2006.

[9] A. Alvarez Aguire. *Remote control and motion coordination of mobile robots*. PhD thesis, Technische Universiteit Eindhoven, 2011.

[10] R. J. Anderson and M. W. Spong. Bilateral control of teleoperators with time delay. *IEEE Transactions on Automatic Control*, 34(5):494–501, May 1989.

[11] P. Arcara and C. Melchiorri. Control schemes for teleoperation with time delay: A comparative study. *Robotics and Autonomous Systems*, 38:49–64, 2002.

[12] J. Artigas, C. Preusche, and G. Hirzinger. Time domain passivity for delayed haptic telepresence with energy reference. In *Proceedings of the 2007 IEEE/RSJ International Conference on Intelligent Robots and Systems*, pages 1612–1617, San Diego, CA, USA, 2007.

[13] J. Artigas, C. Preusche, G. Hirzinger, G. Borgeshan, and C. Melchiorri. Bilateral energy transfer in delayed teleoperation on the time domain. In *Proceedings of the IEEE International Conference on Robotics and Automation*, pages 671–676, Pasadena, CA, USA, 2008.

[14] A. Aziminejad, M. Tavakoli, R.V. Patel, and M. Moallem. Transparent time-delayed bilateral teleoperation using wave variables. *IEEE Transactions on Control Systems Technology*, 16:548–555, 2008.

[15] F.E. van Beek, D.J.F. Heck, H. Nijmeijer, W.M. Bergmann Tiest, and A.M.L. Kappers. The effect of damping on the perception of hardness. In *IEEE World Haptics Conference, 2015*, pages 82–87, Evanston, IL, USA, 2015.

[16] J.J.B. Biemond, N. van de Wouw, and H. Nijmeijer. Nonsmooth bifurcations of equilibria in planar continuous systems. *Nonlinear analysis: Hybrid Systems*, 4:451–474, 2010.

[17] H. Boessenkool, D.A. Abbink, C.J.M. Heemskerk, and F.C.T. van der Helm. Haptic shared control improves tele-operated task performance towards performance in direct control. In *Proceedings of the IEEE World Haptics Conference*, pages 433–438, Istanbul, Turkey, 2011.

[18] H. Boessenkool, D.A. Abbink, C.J.M. Heemskerk, F.C.T. van der Helm, and J. Wildenbeest. A task-specific analysis of the benefit of haptic shared control during telemanipulation. *IEEE Transactions on Haptics*, 6:2–12, 2013.

[19] J.-M. Bourgeot and B. Brogliato. Tracking control of complementary Lagrangian systems. *International Journal of Bifurcations and Chaos*, 15:1839–1866, 2005.

[20] B. Brogliato. *Nonsmooth Mechanics*. Springer-Verlag London, 1999.

[21] B. Brogliato, S.-I. Niculescu, and P. Orhant. On the control of finite-dimensional mechanical systems with unilateral constraints. *IEEE Transactions on Automatic Control*, 42:200–215, 1997.

[22] T.L. Brooks. Telerobotic response requirements. In *Proceedings of the IEEE International Conference on Systems, Man and Cybernetics*, page 113120, Los Angeles, CA, USA, 1990.

[23] E. Burdet, R. Osu, D.W. Franklin, T.E. Milner, and M. Kawato. The central nervous system stabilizes unstable dynamics by learning optimal impedance. *Nature*, 414:446–449, 2001.

[24] C. Canudas de Wit and B. Brogliato. Direct adaptive impedance control including transition phases. *Automatica*, 33:643–649, 1997.

[25] R. Carloni, R.G. Sanfelice, A.R. Teel, and C. Melchiorri. A hybrid control strategy for robust contact detection and force regulation. In *Proceedings of the 2007 American Control Conference*, pages 1461 – 1466, New York City, USA, 2007.

[26] M.C. Çavuşoğlu, A. Sherman, and F. Tendrick. Design of bilateral teleoperation controllers for haptic exploration and telemanipulation of soft environments. *Transactions on Robotics and Automation*, 18:641–647, 2002.

[27] S. Chiaverini and L. Sciavicco. The parallel approach to force/position control of robotic manipulators. *IEEE Transactions on Robotics and Automation*, 9:361–373, 1993.

[28] H. Ching and W.J. Book. Internet-based bilateral teleoperation based on wave variable with adaptive predictor and drift control. *Journal of Dynamic Systems, Measurement, and Control*, 128:86–93, 2006.

[29] N. Chopra and M.W. Spong. On synchronization of networked passive systems with time delays and application to bilateral teleoperation. In *Annual Conference of Society of Instrument and Control Engineers of Japan*, Okayama, Japan, 2005.

[30] N. Chopra, M.W. Spong, and R. Lozano. Synchronization of bilateral teleoperators with time delay. *Automatica*, 44:2142–2148, 2008.

[31] N. Chopra, M.W. Spong, and R. Lozano. Adaptive coordination control of bilateral teleoperators with time delay. In *43rd IEEE Conference on Decision and Control*, pages 4540–4547, Atlantis, Paradise Island, Bahamas, 2004.

[32] N. Chopra, M.W. Spong, R. Ortega, and N. E. Barabanov. On tracking performance in bilateral teleoperation. *IEEE Transactions on Robotics*, 22:861–866, 2006.

[33] N. Chopra, M.W. Spong, R. Ortega, and N. E. Barabanov. On position tracking in bilateral teleopetation. In 5244-5249, editor, *Proceedings of the 2004 American Control Conference*, Boston, Ma, USA, 2004.

[34] J.E. Colgate and J.M. Brown. Factors affecting the Z-width of a haptic display. In *Proceedings of the IEEE 1994 International Conference on Robotics and Automation*, pages 3205–3210, San Diego, CA, USA, 1994.

[35] J.E. Colgate and N. Hogan. Robust control of dynamically interacting systems. *International journal of control*, 48:65–88, 1988.

[36] R.W. Daniel and P.R. McAree. Fundamental limits of performance for force reflecting teleoperation. *International Journal of Robotics Research*, 17:811–830, 1998.

[37] Z. Doulgeri and G. Iliadis. Contact stability analysis of a one degree-of-freedom robot using hybrid system stability theory. *Robotica*, 23:607–614, 2005.

[38] 1954 ElectroMechanical Manipulator Ray Goertz (American). `http://cyberneticzoo.com/`, 2015.

[39] T. Flash and N. Hogan. The coordination of arm movements: an experimentally confirmed mathematical model. *Journal of Neuroscience*, 5:1688–1703, 1985.

[40] M. Franken, S. Stramigioli, S. Misra, C. Secchi, and A. Macchelli. Bilateral telemanipulation with time delays: a two-layer approach combining passivity and transparency. *IEEE Transactions on Robotics*, 27(4):741–756, 2011.

[41] M. Franken, S. Stramigioli, R Reilink, C. Secchi, and A. Macchelli. Bridging the gap between passivity and transparency. In *Proceedings of Robotics: Science and Systems*, Seattle, USA, 2009.

[42] M. Franken, B. Willaert, S. Misra, and S. Stramigioli. Bilateral telemanipulation: improving the complementarity of the frequency- and time-domain passivity approaches. In *2011 IEEE International Conference on Robotics and Automation*, pages 2104–2110, Shanghai, China, 2011.

[43] S.S. Ge, W. Li, and C. Wang. Impedance adaptation for optimal robotenvironment interaction. *International Journal of Control*, 87:249–263, 2014.

[44] G. Gilardi and I. Sharf. Literature survey of contact dynamics modeling. *Mechanism and Machine Theory*, 37:1213–1239, 2002.

[45] R.C. Goertz. Fundamentals of general-purpose remote manipulators. *Nucleonics, ceased publication*, 10:36–45, 1952.

[46] R.C. Goertz and Thompson W.M. Electronically controlled manipulator. *Nucleonics, ceased publication*, 12:46–47, 1954.

[47] B. Hannaford and J.-H. Ryu. Time domain passivity control of haptic interfaces. *IEEE Transactions on Robotics and Automation*, 18(1):1–10, 2002.

[48] K. Hashtrudi-Zaad and S.E. Salcudean. Analysis of control architectures for teleoperation systems with impedance/admittance master and slave manipulators. *The International Journal of Robotics Research*, 20:419–445, 2001.

[49] K. Hashtrudi-Zaad and S.E. Salcudean. Transparency in time-delayed systems and the effect of local force feedback for transparent teleoperation. *IEEE Transactions on Robotics and Automation*, 18:108–114, 2002.

[50] Ron Hendrix. *Robotically assisted eye surgery: A haptic master console*. PhD thesis, Technische Universitiet Eindhoven, 2011.

[51] S. Hirche and M. Buss. Human-oriented control for haptic teleoperation. *Proceedings of the IEEE*, 100:623 – 647, 2012.

[52] S. Hirche, T. Matiakis, and M. Buss. A distributed controller approach for delay-independent stability of networked control systems. *Automatica*, 45:1828–1836, 2009.

[53] N. Hogan. On the stability of manipulators performing contact tasks. *IEEE Journal of Robotics and Automation*, 4:677–686, 1988.

[54] N. Hogan. Controlling impedance at the man/machine interface. In *Proceedings of the 1989 IEEE Conference on Robotics and Automation*, pages 1626 – 1631, Scottsdale, AZ, USA 1989.

[55] P.F. Hokayem and M.W. Spong. Bilateral teleoperation: An historical survey. *Automatica*, 42:2035–2057, 2006.

[56] K.H. Hunt and F.R.E. Crossley. Coefficient of restitution interpreted as damping in vibroimpact. *ASME Journal of Applied Mechanics*, 43:440–445, 1975.

[57] International Energy Agency Tokamaks. `http://www.iea.org/techinitiatives/fusionpower/tokamaks/`, 2015.

[58] S. Jung, T.C. Hsia, and R.G. Bonitz. Force tracking impedance control of robot manipulator under unknown environment. *IEEE Transactions on Control Systems Technology*, 12(3):474–483, May 2004.

[59] Hassan K. Khalil. *Nonlinear Systems*. Prentice Hall, 2002.

[60] O. Khatib. A unified approach for motion and force control of manipulators: The operational space formulation. *IEEE Journal of Robotics and Automation*, 3:43–53, 1987.

[61] J. Kim, P.H. Chan, and H.-S. Park. Two-channel transparency-optimized control architectures in bilateral teleoperation with time delay. *IEEE Transactions on Control Systems Technology*, 21:40–51, 2013.

[62] W.S. Kim. Developments of new force-reflecting control schemes and an application to a teleoperation training simulator. In *Proceedings of the 1992 IEEE International conference on Robotics and Automation*, pages 1412–1419, Nice, France, 1992.

[63] K. Kuchenbecker, J. Fiene, and G. Niemeyer. Improving contact realism through event-based haptic feedback. *IEEE Transactions on Visualization and Computer Graphics*, 12:219–230, 2006.

[64] K.J. Kuchenbecker and G. Niemeyer. Induced master motion in force-reflecting teleoperation. *ASME Journal of Dynamic Systems, Measurement and Control*, 128:800–810, 2006.

[65] K.J. Kuchenbecker and G. Niemeyer. Modeling induced master motion in force-reflecting teleoperation. In *IEEE International Conference on Robotics and Automation*, pages 348–353, Barcelona, Spain, 2005.

[66] R. Kuiper, J.C.L. Frumau, F. van der Helm, and D.A. Abbink. Haptic support for bi-manual control of a suspended grab for deep-sea excavation. In *IEEE International Conference on Systems, Man and Cybernetics*, pages 1822–1827, Manchester, UK, 2013.

[67] R.J. Kuiper, D.J.F. Heck, I.A. Kuling, and D.A. Abbink. Haptic guidance improves nonholonomic steering due to added information of kinematics and suggested path. *IEEE Transactions on Human-Machine Systems*, 2015, submitted.

[68] Y.P. Lai, Y.L. anf Li, N.D. Vuong, T.M. Lim, C.Y. Ma, and C.W. Lim. Nonlinear damping for improved transient performance in robotics force control. In *IEEE/ASME International Conference on Advanced Intelligent Mechatronics*, pages 134–139, Kaohsiung, Taiwan, July 2012.

[69] D.A. Lawrence. Stability and transparency in bilateral teleoperation. *IEEE Transactions on Robotics and Automation*, 9:624–637, 1993.

[70] D. Lee and M.W. Spong. Passive bilateral control of teleoperators under constant time-delay. In *Proceedings of the 16th IFAC World Congress*, pages 1287–1287, Prague, Czech Republic, 2005.

[71] R. Leine and N. van de Wouw. *Stability and Convergence of Mechanical Systems with Unilateral Constraints*. Springer-Verlag Berlin Heidelberg, 2008.

[72] R.I. Leine and H. Nijmeijer. *Dynamics and bifurcations of non-smooth mechanical systems*. Springer-Verlag Berlin Heidelberg, 2004.

[73] D. Liberzon. *Switching in Systems and Control*. Birkhäuser Boston, 2003.

[74] Y.-C. Liu and N. Chopra. Controlled synchronization of heterogenous robotic manipulators in the task space. *IEEE Transactions on Robotics*, 28:268–275, 2012.

[75] F.B. Llewellyn. Some fundamental properties of transmission systems. *Proceedings of the IRE*, 40:271–283, 1952.

[76] C.A. López Martínez, Í. Polat, R. van de Molengraft, and M. Steinbuch. Robust high performance bilateral teleoperation under bounded time-varying dynamics. *IEEE Transcations on Control Systems Technology*, 23:206–218, 2015.

[77] C.A. López Martínez, R. van de Molengraft, and M. Steinbuch. High performance teleoperation using switching robust control. In *IEEE World Haptics Conference 2013*, pages 383–388, Daejeon, Korea, 2013.

[78] J.L. Love and W.J. Book. Force reflecting teleoperation with adaptive impdance control. *IEEE Transactions on Systems, Man and Cybernetics*, 34:159–165, 2004.

[79] M. Margaliot. Stability analysis of switched systems using variational priciples: an introduction. *Automatica*, 42:2059–2077, 2006.

[80] C. Melchiorri. Robotic telemanipulation systems: An overview on control aspects. In *Proceedings of the 7th IFAC Symposium on Robot Control*, pages 707–716, 2003.

[81] P. Mitra and G. Niemeyer. Model-mediated teleoperation. *The International Journal of Robotics Research*, 27:253262, 2008.

[82] I.C. Morărescu and B. Brogliato. Trajectory tracking control of multiconstraint complementary Lagrangian systems. *IEEE Transactions on Automatic Control*, 55:1300–1313, 2010.

[83] S. Munir and W.J. Book. Internet-based teleoperation using wave variables with prediction. *IEEE/ASME Transactions on Mechatronics*, 7:124–135, 2002.

[84] S. Munir and W.J. Book. Wave-based teleoperation with prediction. In *Proceedings of the American Control Conference*, pages 4605–4611, Arlington, VA, USA, 2001.

[85] T. Namerikawa and H. Kawada. Symmetric impedance matched teleoperation with position tracking. In *Proceedings of the 45th IEEE Conference on Decision and Control*, pages 4496–4501, San Diego, CA, USA, 2006.

[86] National Aeronautics and Space Administration Robonaut 1. `http://robonaut.jsc.nasa.gov/R1`, 2008.

[87] K. Natori, T. Tsuji, K. Ohnishi, A. Hace, and K. Jezernik. Time-delay compensation by communication disturbance observer for bilateral teleoperation under time-varying delay. *IEEE Transaction on Industrial Electronics*, 57:1050–1062, 2010.

[88] L. Ni and D.W.L. Wang. A gain-switching control scheme for position-error-based bilateral teleoperation: contact stability analysis and controller design. *The International Journal of Robotics Research*, 23:255–274, 2004.

[89] L. Ni and D.W.L. Wang. Contact transition stability analysis for a bilateral teleoperation system. In *Proceedings of the 2002 IEEE International Conference on Robotics and Automation*, pages 3272–3277, Washington, DC, USA, 2002.

[90] G. Niemeyer, C. Preusche, and G. Hirzinger. *Springer Handbook of Robotics*, chapter 31, pages 741–757. Springer-Verlag Berlin Heidelberg, 2008.

[91] G. Niemeyer and J.-J. E. Slotine. Stable adaptive teleoperation. *IEEE Journal of Oceanic Engineering*, 16:152–162, 1991.

[92] G. Niemeyer and J.-J. E. Slotine. Telemanipulation with time delays. *International Journal of Robotics Research*, 23(9):873–890, September 2004.

[93] G. Niemeyer and J.-J. E. Slotine. Towards force-reflecting teleoperation over the internet. In *Proceedings of the 1998 IEEE Conference on Robotics and Automation*, Leuven, Belgium, 1998.

[94] E. Nuño, L. Basañez, and R. Ortega. Passivity-based control for bilateral teleoperation: A tutorial. *Automatica*, 47:485–495, 2011.

[95] E. Nuño, L. Basañez, and R. Ortega. Passive bilateral teleoperation framework for assisted robotic tasks. In *2007 IEEE International Conference on Robotics and Automation*, pages 1645–1650, Rome, Italy, 2007.

[96] E. Nuño, L. Basañez, R. Ortega, and M.W. Spong. Position tracking for nonlinear teleoperators with variable time delay. *The International Journal of Robotics Research*, 28:895–910, 2009.

[97] E. Nuño, L. Basañez, and M. Prada. Asymptotic stability of teleoperators with variable time-delays. In *2009 IEEE International Conference on Robotics and Automation*, pages 4332–4337, Kobe, Japan, 2009.

[98] E. Nuño, R. Ortega, N.E. Barabanov, and L. Basañez. A globally stable PD controller for bilateral teleoperators. *IEEE Transactions on Robotics*, 24:753–758, 2008.

[99] E. Nuño, R. Ortega, and L. Basañez. An adaptive controller for nonlinear teleoperators. *Automatica*, 46:155–159, 2010.

[100] H. Okuda, S. Hayakawa, T. Suzuki, and N. Tsuchida. Modeling of human behavior in man-machine cooperative system based on hybrid system framework. In *IEEE International Conference on Robotics and Automation*, pages 2534–2539, Rome, Italy, 2007.

[101] M.K. O'Malley, A. Gupta, M. Gen, and Y. Li. Shared control in haptic systems for performance enhancement and training. *Journal of Dynamic Systems, Measurement, and Control*, 128:75–85, 2006.

[102] P.R. Pagilla. Control of contact problem in constrained Euler-Lagrange systems. *IEEE Transactions on Automatic Control*, 46:1595–1599, 2001.

[103] P.R. Pagilla and B. Yu. A stable transition controller for constrained robots. *IEEE/ASME Transactions on Mechatronics*, 6:65–74, 2001.

[104] Y.-J. Pan, C. Canudas-de Wit, and O. Sename. Predictive controller design for bilateral teleoperation systems with time varying delays. In *43rd IEEE Conference on Decision and Control*, pages 3521–3526, Atlantis, Paradise Island, Bahamas, 2004.

[105] C. Passenberg, A. Peer, and M. Buss. A survey of environment-, operator-, and task-adapted controllers for teleoperation systems. *Mechatronics*, 20:787–801, 2010.

[106] Í Polat. *Robustness analysis and controller synthesis for bilateral teleoperation systems via IQCs*. PhD thesis, Technische Universiteit Eindhoven, 2014.

[107] I.G. Polushin, P.X. Liu, and C.-H. Lung. A force-reflection algorithm for improved transparency in bilateral teleoperation with communcation delay. *IEEE/ASME Transactions on Mechatronics*, 12:361–374, 2007.

[108] I.G. Polushin, P.X. Liu, and C.-H. Lung. Stability of bilateral teleoperators with generalized projection-based force reflection algorithms. *Automatica*, 48:1005–1016, 2012.

[109] I.G. Polushin, P.X. Liu, and C.-H. Lung. Stability of bilateral teleoperators with projection-based force reflection algorithms. In *IEEE International Conference on Robotics and Automation*, pages 677–682, Pasadena, CA, USA, 2008.

[110] M.H. Raibert and J.J. Craig. Hybrid position/force control of manipulators. *ASME Journal of Dynamic Systems, Measurement and Control*, 103:126–133, 1981.

[111] J. Rebelo and A. Schiele. Time domain passivity controller for 4-channel time-delay bilateral teleoperation. *IEEE Transcations on Haptics*, 2014.

[112] E.J. Rodríguez-Seda. Transparency compensation for bilateral teleoperators with time-varying communication delays. In *IEEE/RSJ International Conference on Intelligent Robots and Systems*, Chicago, IL, USA, 2014.

[113] E.J. Rodríguez-Seda, D. Lee, and M.W. Spong. Experimental comparison study of control architectures for bilateral teleoperation. *IEEE Transactions on Robotics*, 25:1304–1318, 2009.

[114] E.J. Rodríguez-Seda and M.W. Spong. A time-varying wave impedance approach for transparency compensation in bilateral teleoperation. In *The 2009 IEEE/RSJ International Conference on Intelligent Robots and Systems*, pages 4609–4615, St Louis, USA, 2009.

[115] L.B. Rosenberg. Virtual fixtures: perceptual tools for telerobotic manipulation. In 76-82, editor, *IEEE Virtual Reality Annual International Symposium*, Seattle, WA, USA, 1993.

[116] J.-H. Ryu, J. Artigas, and C. Preusche. A passive bilateral control scheme for a teleoperator with time-varying communication delay. *Mechatronics*, 20:812–823, 2010.

[117] J.-H. Ryu, D.-S. Kwon, and B. Hannaford. Stable teleoperation with time-domain passivity control. *IEEE. Transactions on Robotics and Automation*, 20(2):365–373, 2004.

[118] J.-H. Ryu and C. Preusche. Stable bilateral control of teleoperators under time-varying communication delay: time domain passivity approach. In *2007 IEEE International Conference on Robotics and Automation*, pages 3508–3513, Roma, Italy, 2007.

[119] A. van der Schaft. *L_2-Gain and passivity techniques in nonlinear control*. Springer Verlag London, 2000.

[120] T.B. Sheridan. Space teleoperation through time delay: review and prognosis. *IEEE Transactions on Robotcs and Automation*, 9:592–606, 1993.

[121] A. Sherman, M.C. Çavuşoğlu, and F. Tendik. Comparison of teleoperator control architectures for palpation task. In *Proceedings of IMECE'00 Symp. on Haptic Interfaces for Virtual Environment and Teleoperator Systems*, 2000.

[122] B. Siciliano and O. Khatib, editors. *Springer Handbook of Robotics*. Springer-Verlag Berlin, 2008. Ch. 7. Force Control.

[123] B. Siciliano, L. Sciavicco, L. Villani, and G. Oriolo. *Robotics, Modeling, Planning and Control*. Springer-Verlag London, 2009.

[124] C.S. Smith and K. Hashtrudi-Zaad. Smith predictor type control architectures for time delayed teleoperation. *The International Journal of Robotics Research*, 25:797–818, 2006.

[125] M.W. Spong, S. Hutchinson, and M. Vidyasagar. *Robot modeling and control*. John Wiley & Sons, 2006.

[126] D. Sun, F. Naghdy, and H. Du. Application of wave-variable control to bilateral teleoperation systems: A survey. *Annual Reviews in Control*, 38:12–31, 2014.

[127] Z. Sun and S.S. Ge. *Switched Linear Systems, Control and Design*. Springer-Verlag London, 2005.

[128] N.A. Tanner and G. Niemeyer. Improving perception in time-delayed telerobotics. *The International Journal of Robotics Research*, 24:631–644, 2005.

[129] N.A. Tanner and G. Niemeyer. Online tuning of wave impedance in telerobotics. In *Proceedings of the 2004 IEEE Conference on Robotics, Automation and Mechatronics*, pages 7–12, Singapore, 2004.

[130] N.A. Tanner and G. Niemeyer. Practical limitations of wave variable controllers in teleoperation. In *Proceedings of the 2004 IEEE Conference on Robotics, Automation and Mechatronics*, pages 25–30, Singapore, 2004.

[131] T.-J. Tarn, Y. Wu, N. Xi, and A. Isidori. Force regulation and contact transition control. *IEEE Control Systems Magazine*, 16:32–40, 1996.

[132] A.N. Tikhonov, A.B. Vasil'eva, and A.G. Sveshnikov. *Differential equations*. Springer-Verlag Berlin Heidelberg, 1985.

[133] B. Vanderborght et al. Variable impedance actuators: A review. *Robotics and Autonomous Systems*, 61:1601–1614, 2013.

[134] I. Vittorias and S. Hirche. Stable teleoperation with communication unreliabilities and approximate human/environment dynamics knowledge. In *American Control Conference*, pages 2791 – 2796, 2010.

[135] R. Volpe and P. Khosla. A theoretical and experimental investigation of impact control for manipulators. *Int. Journal of Robotics Research*, 12:351–365, 1993.

[136] H. Wang and Y. Xie. Task-space framework for bilateral teleoperation with time delays. *Journal of Dynamic Systems, Measurement, and Control*, 134, 2012.

[137] J. Wildenbeest, D.A. Abbink, C.J.M. Heemskerk, and F. van der Helm. The impact of haptic feedback quality on the performance of teleoperated assembly tasks. *IEEE Transaction on Haptics*, 6:242 – 252, 2013.

[138] B. Willaert, D. Corteville, D. Reynaerts, H. van Brussel, and E.B. Vander Poorten. Bounded environment passivity of the classical position-force teleoperation controller. In *The 2009 IEEE/RSJ International Conference on Intelligent robots and systems*, St. Louis, Missouri, USA, 2009.

[139] B. Willaert, D. Corteville, D. Reynaerts, H. van Brussel, and E.B. Vander Poorten. Transparency trade-offs for a 3-channel controller revealed by the bounded environment passivity method. In *Thrid International Conference on Advances in Computer-Human Interactions*, pages 66–72, St. Maarten, Netherlands Antilles, 2010.

[140] N. Yamada, S. Inagaki, T. Suzuki, H. Okuda, S. Hayakawa, and N. Tsuchida. Behavior modeling in manmachine cooperative system based on stochastic switched dynamics. In *IEEE International Conference on Robotics and Automation*, page 36183623, Orlando, Florida, USA, 2006.

[141] K. Yoshida, T. Namerikawa, and O. Sawodny. A state predictor for bilateral teleoperation with communication time delay. In *Proceedings of the 47th IEEE Conference on Decision and Control*, pages 4590–4595, Cancun, Mexico, 2008.

[142] R. Zotovic Stanisic and Á Valera Fernández. Adjusting the parameters of the mechanical impedance for velocity, impact and force control. *Robotica*, 30:583–597, 2012.

Dankwoord

Na 4 jaar zit de weg van ir. naar dr.ir. er dan bijna op. Vier jaar lang werken aan mijn eigen onderzoek. Voor twee extra letters en puntje voor mijn naam... Gelukkig dekt deze droge observatie niet mijn eigen beleving van de afgelopen jaren. Voor mijn gevoel is het allemaal veel te snel voorbij gegaan. Niet alleen is de tijd te kort gebleken om alle ideeën vóór het verschijnen van dit proefschrift uit te werken, maar ik zal net zo goed de gezellige, losse sfeer gaan missen in de 'D&C/CST' groep. En ondanks dat alleen mijn naam op voorkant staat, had dit proefschrift er zonder de hulp en steun van collega's, vrienden en familie niet zo uitgezien. Daarom wil ik iedereen bedanken voor de geweldige jaren.

Allereerst mijn begeleiders. Henk, bedankt dat je me de kans geboden hebt om na mijn afstuderen aan de slag te gaan op een zeer uitdagend project. Ik heb veel geleerd en erg genoten van onze discussies, zowel tijdens de 'serieuzere' vergaderingen als een van de vele borrels. Bedankt dat je af en toe tijd hebt vrijgemaakt als ik weer eens zonder afspraak jouw kantoor binnen liep. Of zoals je zelf zegt: "Is het hek weer van de dam?" Ale, I really enjoyed the two years you were my copromotor and sparring partner. Since our first discussions you often surprised me in a positive way by always asking the right questions to help me continue in the right direction. I especially enjoyed the brainstorm sessions, where we used all the space on the wall-wide white boards in your office. Ammiro la dedizione con la quale ti applichi nell' apprendere l'olandese, una lingua divertente con parole dal significato sorprendente. Spero che di me non rimanga solamente il ricordo della canzone 'Hansje Pansje Kevertje '... Nathan, jou wil ik ook bedanken voor de zeer leervolle discussies, je uitgebreide feedback en je duidelijkheid qua planning. Ook al was je niet mijn directe begeleider, zonder jou zou de samenhang van de wiskunde in hoofdstuk 4 waarschijnlijk niet te begrijpen zijn geweest.

César, as my closest haptics-colleague I want to thank you for all the help with the setup, for being a great sparring partner and for sharing my enthusiasm. I always enjoyed the lively discussions we had. Thanks also to all the students

I supervised during the past years for providing helpful results. Araz, Anna, Rik and Ruud, thank you for all the interesting discussions. Ruud, jij vooral bedankt voor het voorbereiden en opzetten van de experimenten. Zonder jou had ik hoofdstuk 3 nooit op tijd af gekregen.

Vervolgens wil ik mijn collega's(/vrienden) van vloer -1 bedanken voor de gezellige tijd, zowel tijdens de 'korte' koffiepauzes als de verschillende conferenties, concerten, borrels en andere uitjes. Maarten, Elise, Joris, Thijs, Jiquan, Bert en Debyjoti, jullie waren geweldige kantoorgenoten! Thijs, bedankt dat ik ook af en toe mocht winnen tijdens een van de kantoorspelletjes. Bert, sorry voor de propjes die soms jouw kant op vlogen. Jiquan said I would score bonus points if I hit you, so you can blame him... Thijs en Tom, bedankt voor de vele discussies, suggesties en jullie luisterend oor als ik weer eens vast liep. Volgens mij zijn jullie bijna net zo goed als ik op de hoogte van mijn onderzoek. Tom, hartstikke bedankt dat je me hebt overgehaald om een racefiets te kopen. De duizenden kilometers en drie fietsvakanties in de afgelopen twee jaar verraden wel dat de aanschaf geen miskoop was. Voor mij is fietsen synoniem komen te staan voor vrijheid; even weg van alle drukte en chaos. Daarbij worden je ongezouten meningen tijdens de vele tochtjes net zo gewaardeerd als je competitieve karakter. Bas, Niek, Benjamin, Rob, Michiel, Lennart, Robert, jullie ook bedankt voor de vele gezamenlijke tochtjes. Jullie hebben me goed uit de wind gehouden!

Naast mijn Eindhovense collega's heb ik ook het genoegen gehad om onderdeel uit te maken van het H-Haptics project. In dit project staat de 'H' voor 'Human-centered'. Tijdens vrijwel alle bijeenkomsten, symposia en Autumn Schools is wel gebleken dat de gezelligheid niet beperkt bleef tot de werkuren. Ik wil met name David, Femke, Irene, Jeroen, Bram, Arvid, Roel, Jan en Stefan bedanken voor hun enthousiasme en de vele late avonden en vroege ochtenden! Als iemand van onder de rivieren had ik niet gedacht dat het daarboven zo gezellig kon zijn! Ik baal er dan ook van dat ik niet mee kon naar de WHC.

Vanzelfsprekend wil ik mijn ouders, broertjes en familie bedanken voor de gezelligheid, de Brabantse nuchterheid, steun, interesse, adviezen en afleiding van de dagelijkse sleur. Pa, ma, bedankt voor de gastvrijheid, houvast,... en dat mijn fiets weer eens in de woonkamer mocht staan als de schuur nog opgeruimd moest worden. Tom, bedankt voor de updates over alles wat er in de sportwereld gebeurt. Zo hoef ik het sportnieuws niet meer te volgen! Frank, groot, klein broertje. Onder andere bedankt dat je het Bachelor vak van Alessandro gevolgd hebt. Daardoor hoefde ik het tentamen zelf niet te maken en heb ik de tijd gehad om dit dankwoord te schrijven.

Cheers!

List of Publications

Peer-reviewed journal articles

- R.J. Kuiper, D.J.F. Heck, I.A. Kuling, and D.A. Abbink. Haptic guidance improves nonholonomic steering due to added information of kinematics and suggested path, *IEEE Transactions on Human-Machine Systems*, *submitted*.
- D.J.F Heck, A. Saccon, N. van de Wouw and H. Nijmeijer. Switching control for tracking of a hybrid position-force trajectory, *Automatica*, *under review*.
- D.J.F Heck, C.J.M. Heemskerk, J.F. Koning, A. Abbasi, and H. Nijmeijer. Robust haptic large distance telemanipulation for ITER, *Fusion Engineering and Design*, 88:1997-2000, 2013.

Peer-reviewed articles in conference proceedings

- D.J.F Heck, A. Saccon and H. Nijmeijer. A 2-layer architecture for force-reflecting bilateral teleoperation with time delays, *54th Conference on Decision and Control*, Tokyo, Japan, 2015, *submitted*.
- D.J.F Heck, A. Saccon, N. van de Wouw and H. Nijmeijer. Switched position-force tracking control of a 1-DOF manipulator interacting with a stiff environment, *Proceedings of the American Control Conference*, pages 4832-4837, Chicago, IL, USA, 2015.
- F.E. van Beek, D.J.F. Heck, H. Nijmeijer, W.M. Bergmann Tiest, and A.M.L. Kappers. The effect of damping on the perception of hardness, In *IEEE World Haptics Conference*, pages 82-87, Evanston, IL, USA, 2015.
- D.J.F Heck, D. Kostić, A. Denasi and H. Nijmeijer. Internal and external force-based impedance control for cooperative manipulation., In *Proceedings of the European Control Conference*, pages 2299-2304, Zürich, Switzerland, 2013.

Journal articles in preparation

- R. Beerens, D.J.F Heck, A. Saccon and H. Nijmeijer. How to design the control architecture for delayed bilateral teleoperation? An experimental comparison of the performance (Chapter 3).
- D.J.F Heck, A. Saccon and H. Nijmeijer. Bilateral teleoperation with time delays: A direct force-reflecting 2-layer control approach (Chapter 5).

Curriculum Vitae

Dennis J.F. Heck was born in Roosendaal, the Netherlands in 1987. He received his B.Sc. (*with great appreciation*) and M.Sc degree (*cum laude*) in Mechanical Engineering at the Eindhoven University of Technology, the Netherlands. As part of his education he carried out an internship at the University of Southampton in the United Kingdom, where he combined Functional Electrical Stimulation with Iterative Learning Control for 3D rehabilitation robotics. His master thesis research focussed on motion and force control for cooperative manipulation.

In August 2011, Dennis started his PhD research in the Dynamics and Control group at the department of Mechanical Engineering of the Eindhoven University of Technology, under the supervision of prof.dr. H. Nijmeijer and dr. A. Saccon. His work was part of the H-Haptics project and focussed on the design of control architectures for delayed bilateral teleoperators interacting with stiff environments. During his PhD he completed the educational program of the graduate school DISC. In the academic year 2012-2013 he joined the Tech United Humanoid team as a control engineer.